INTENS

VTT

beyond
the obvious

Integrated Energy Solutions to Smart And Green Shipping

2020 Edition

Zou Guangrong | Saara Hänninen (Editors)

VTT TECHNOLOGY 380

VTT TECHNOLOGY 380

Integrated Energy Solutions to Smart And Green Shipping

2020 Edition

Zou Guangrong | Saara Hänninen (Editors)

VTT Technical Research Centre of Finland Ltd

ISBN 978-951-38-8740-7

VTT Technology 380

ISSN-L 2242-1211
ISSN 2242-122X (Online)
DOI: 10.32040/2242-122X.2020.T380

JULKAISIJA – PUBLISHER

VTT
PL 1000
02044 VTT
Puh. 020 722 111
https://www.vtt.fi

VTT
P.O. Box 1000
FI-02044 VTT, Finland
Tel. +358 20 722 111
https://www.vttresearch.com


Smart & Green
Shipping Together!
Innovation
Business
Platform

INTENS

co-funded by

BUSINESS FINLAND

Arctic Seas

Industrial partners

3D Studio BLOMBERG

DELTAMARIN®

dinex

Jeppo Biogas Ab
Jepuan Biokaasu Oy

JTK Power

MEYER TURKU
SHIPYARD 1737

NAPA

Parker

PINJA

TALLINK

SILJA LINE

VAHTERUS

VISORC

wasaline

WÄRTSILÄ

Research partners

Aalto University

LUT University

University of Vaasa

Åbo Akademi

VTT

Preface

The second INTENS project[1] public dissemination event, i.e. the 2020 Finnish maritime energy symposium on smart and green shipping, is finally ready for the interested maritime colleagues across the world. Due to the COVID-19 pandemic situation, this year it is exceptionally organized as the online INTENS WEEK public seminars to be held on October 5-9, 2020, instead of the originally planned public seminar.

The INTENS WEEK public webinar series are scheduled as four daily webinars. Each session includes 4-5 technical talks to address one dedicated topic on the decarbonization or digitalization of maritime shipping, specifically including (*Day 1) Novel solutions to digital shipping, (Day 2) Novel technologies for low-emission shipping, (Day 3) Novel technologies for energy-efficient shipping* and *(Day 4) Data-driven solutions to smart shipping*.

This book is a selected collection of extended abstracts of the aforementioned technical talks given at the webinars, also acting as the proceedings of the 2020 INTENS WEEK public webinar series. It aims to give the readers a brief update on some of the major results that have been achieved by the INTENS project partners during the second project year, and also showcase the latest Finnish maritime activities, research and innovation practices, and on-going research and industrial efforts towards the decarbonization, digitalization and automation of maritime shipping.

Acknowledgement

We gratefully acknowledge the great support of Business Finland, nineteen INTENS consortium partners, including fourteen industrial partners (3D Studio Blomberg Ltd, Deltamarin Ltd, Dinex Finland Oy, Jeppo Biogas Ab, JTK Power Oy, Meyer Turku Oy, NAPA Oy, Parker Hannifin Manufacturing Finland Oy, Pinja Oy (formerly Protacon technologies Oy), Tallink Silja Oy, Vahterus Oy, Visorc Oy, NLC Ferry Ab Oy and Wärtsilä Finland Oy) and five research institutions (Aalto University, LUT

[1] INTENS - Integrated energy solutions to smart and green shipping (2018 - 2021) is a national industry-wide collaborative research and development project jointly funded by the Business Finland's (formerly Tekes) Arctic Seas programme and the INTENS consortium. http://intens.vtt.fi

University, University of Vaasa, Åbo Akademi University, and VTT Technical Research Centre of Finland Ltd), and other INTENS consortium supporting partners.

Special thanks are due to the INTENS steering group, advisory group and project group, especially to all the authors contributing to the proceedings of the public webinars. Besides, the INTENS WEEK public webinar series also received high interest and great support from all the participants across the Finnish and global maritime communities, which are greatly appreciated!

Zou Guangrong
guangrong.zou@vtt.fi
VTT Technical Research Centre of Finland Ltd.

List of Contributors

(in the order of surnames)

Aalto University: Janne Huotari, Ossi Kaario, Armin Narimanzadeh, Antti Ritari, Kari Tammi, Bulut Tekgül, Ville Vuorinen,

Deltamarin Ltd: Jyri-Pekka Arjava, Mia Elg, Esa Jokioinen, Bogdan Molchanov, Matti Tammero, Lien Tran

Dinex Finland Oy: Kauko Kallinen, Teuvo Maunula

LUT University: Jurii Demidov, Radheesh Dhanasegaran, Paula Immonen, Andrey Lana, Tuomo Lindh, Henri Montonen, Pasi Peltoniemi, Olli Pyrhönen, Teemu Turunen-Saaresti, Antti Uusitalo

Meyer Turku Oy: Wilhelm Gustafsson

NAPA Oy: Ossi Mettälä

Parker Hannifin Manufacturing Finland Oy: Jagan Gorle

Semantum Ltd: Jari Lappalainen

Vahterus Oy: Valtteri Haavisto, Kerttu Kupiainen

University of Vaasa: Saana Hautala, Seppo Niemi, Kirsi Spoof-Tuomi, Emma Söderäng

Wärtsilä Finland Oy: Jari Hyvönen, Heikki Korpi, Juha Kortelainen, Eric Lendormy

Åbo Akademi University: Jerker Björkqvist, Joachim Hammarström, Wictor Lund, Mikael Manngård

VTT Technical Research Centre of Finland Ltd: Antti Hynninen, Päivi Koponen, Juha Kortelainen, Timo Korvola, Kati Lehtoranta, Hannu Rummukainen, Hannu Vesala

Contents

1. Data driven ship design for digitalizing maritime industry

Mia Elg[1], Jyri-Pekka Arjava[1], Matti Tammero[1], Esa Jokioinen[1],
Bogdan Molchanov[1], Lien Tran[1]
Deltamarin Ltd

1.1 Introduction

Digitalisation is a hot topic today in ship design and operation. For ship owners and operators, monitoring ship performance and learning from past behaviour can result in direct savings in fuel costs or anywhere else in the logistics chain. Nevertheless, the available data of ship operations and related processes has the possibility to make even larger impact once it is utilized for various optimization tasks on fleet level and during the entire lifetime of a vessel. In addition, the future targets for greenhouse gas (GHG) reductions on global fleet level, presented by IMO, are emphasizing that the reductions in emissions must be made compared to absolute emissions during a reference year in the past. Current rules existing for reducing ship CO2 emissions, such as the energy efficiency design index (EEDI), demand technically that the ship should achieve certain level of emissions at one single design point. Nevertheless, the future vision clearly emphasizes the actual impact the ships are making, instead of single point values. Therefore, it is fair to assume that, from operational energy efficiency, fuel saving and legislation points of view, the focus in new ship design should be on considering the ship operational profile from the beginning.

At this point of time, we have no clear map in front of us, i.e. which technical solutions or shipping fuels will prove to be superior, regarding both shipping GHG footprint reduction and providing profitable business case for the vessel considering the related costs. Most likely, there will not be single winners, but the optimal solution is always dependent on the unique factors for each ship and fleet regarding operational profile, surrounding climate, available infrastructure and so on. This

[1] Contact: firstname.lastname@deltamarin.com

means that, for both future ship design and operational optimization, it is wise to focus on identifying a set of most likely and most impactful scenarios and analysing the design based on the majority or combinations of them. The analysis will reveal direction which leads with the largest probability to the desired future result.

Therefore, the digitalizing maritime industry needs also a ship design process, which is natively able to adapt to the possibilities that the available data has. In practice, we need to be able to design the ship from the start with a “toolbox” where we can digest the available data for the ship and analyse the variations efficiently and quickly. Interactivity with the customer is a very important aspect since we should together decide on the design basis and the most relevant focus areas, such as the fuel and technology choices for the ship. Another key area to keep control over is the total costs of a ship. For example, preparing for future fuels or operating scenarios does not have to generate great additional costs during shipbuilding, but evaluating this is an important part of the process.

To work with various possible and probable scenarios during any ship design task is a part of a big entity known as “future-proof ship design”. Future-proof design provides resilience against the most probable future challenges and the capability of adapting to the identified opportunities that will be enabled in the years to come. This article presents in brief Deltamarin’s approach and newly developed methods for designing future-proof ships in practice with certain relevant examples. The methods are explained more in the Deltamarin’s blog series on digital design.

1.2 Data driven, digital ship

When designing a new ship, everything starts with understanding the requirements set for the new ship project, which are usually related to maximising the number of cargo units to be transported within the operating area. This very first step of the design process is also the starting point where the digitalisation comes into the picture: any measured operational data of suitable reference ships, other business-related data or data of the surrounding environment can be utilized as background for describing to certain extent the expected future operational field. We call this the extended operation profile of the ship. The traditional design process and methods, where the entire ship operational profile should be simplified for being able to focus on certain optimization points, would be major restriction for the utilization of the extended operation profile.

The clear benefit of understanding the various operational conditions is that the designer has the opportunity to optimize ship performance to the most relevant conditions, even though the ship and her main systems still have to be dimensioned for the extreme conditions. Moreover, any additional equipment, such as energy saving devices for reducing ship carbon footprint, should be fully dimensioned according to the expected operational conditions to ensure maximum performance with minimum investment.

What does a digital ship look like once she is at the “drawing board”? The answer is that the deliverable material is quite case-specific, focusing on reviewing and

highlighting the items that are crucial to the specific case. During INTENS project, we created an example of interactive, digital design portal, which shows a “sneak peek“ at how we can evaluate certain KPIs of a ship which is still only a model but can already sail on digital waters.

One example ship in the digital design portal is an Aframax-sized tanker. We can evaluate the daily emission rate and fuel consumption, based on the chosen fuel and route for the ship. In our portal, we have also included as an example a very traditional way to present a ship design. This so-called “data sheet” includes the main particulars of the ship, such as ship main dimensions, capacities and description of the most relevant machinery components. For reference, the data sheet also includes a figure of main engine daily fuel consumption at a certain design speed, which is 14.5 knots in the example case, and, the daily LNG (liquefied natural gas) consumption is stated as 31.7 tons per day with 1 ton per day of pilot diesel fuel consumption for the main engine. If we compare this number to the actual daily average consumption estimate in Figure 1, we can see that the actual fuel consumption is much smaller. This is naturally partly due to the chosen operation profile, which also includes a considerable amount of time in port. In addition, the digital design portal includes the expected auxiliary engine fuel consumption for producing electricity for the ship. Thus, the digital design portal aims for estimating the actual performance of the ship. We can see how the daily figures change as a function of the example profiles uploaded in the portal.

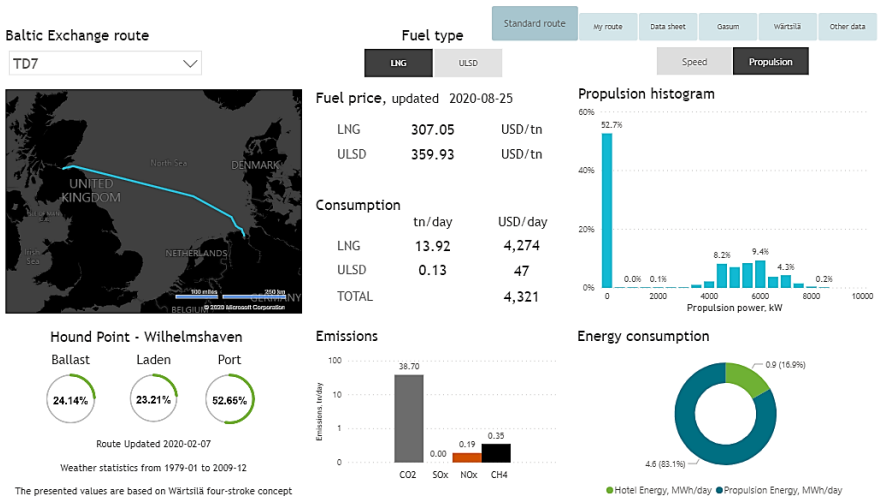

Figure 1. Digital ship design portal example.

1.3 Building blocks of the digital ship

At Deltamarin, we have focused lately on being able to start the entire ship design process genuinely from creating the ship digital prototype. The digital model of the ship must be able to be created fast during the early design process, which could ultimately evolve into a digital twin of a ship, once she is built and in operation. What we have found out is that an efficient process does not consist of one single program or tool but of layers. In our work, three specific “layers” or entities are utilized for forming the digital ship: energy and environmental performance simulations, the ship’s volume and structural model and the data layer where we combine the wind-, wave- and other measured data into the ship model to estimate its lifetime propulsion power profile. Each layer has interconnections with other ones, as with almost any ship design task, but the related tools and analysis methods are separate ones.

Our energy and environmental performance simulation entity is called DeltaKey. For every project, both new buildings and retrofit projects, we compile a system level model of the ship energy flows. The data for the energy model originates partly from the new technical data produced by the design team and partly from relevant reference data, both operational and technical. The important task of the energy modelling is to monitor the ship key performance indicator (KPI) or a set of indicators and recognize areas which could be improved for reaching the desired performance.

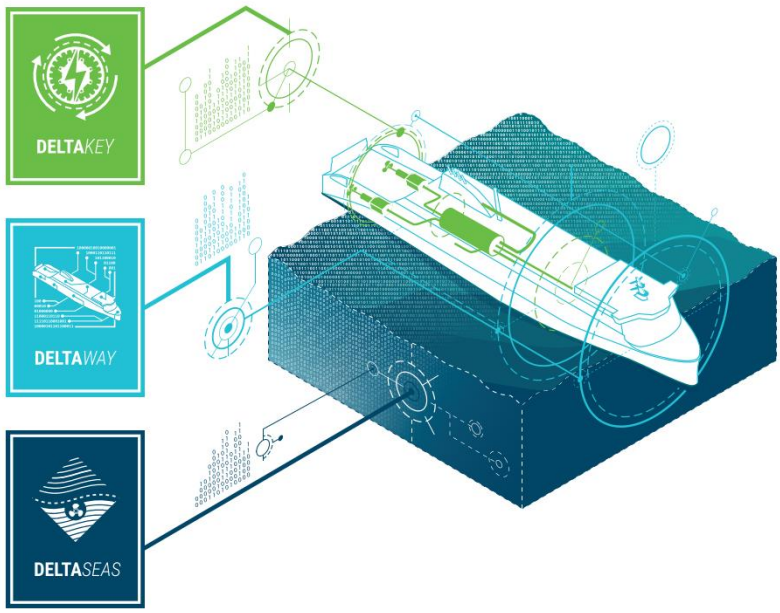

Figure 2. Digital ship design layers at Deltamarin.

The model of the ship energy and environmental performance in the intended operational conditions gives a highly valuable result for a newbuilding project. It shows for the entire project team “what good looks like”. This means, for example, a certain level of efficiency or expected fuel consumption. Keep in mind that the model can be utilized later for training the ship crew during ship building process. Especially, future new buildings most likely have new, complex technologies on board, for reaching the future performance targets. Even with a simplest ship, there is always a certain learning curve presented after the ship is commissioned before reaching a certain level of efficiency. Simulation models and the results from this work can help make this learning curve as steep as possible. The learning and operational optimization can be continued long after this, verified by actual measurement data from the current operations, which can suggest alternative targets for operational efficiency.

Refining the ship operational profile to describe as correctly as possible the intended ship operation is always the most important step of the process. Therefore, in the INTENS project, Deltamarin has worked with large amount of measured operational data from a customer. The data is first cleaned before it can be utilized for describing the ship average expected operation profile in an energy model. Secondly, the data can be analysed in various ways. During the project, Deltamarin has studied various machine learning methods for filtering out certain external condition and ship operation related factors, such as choosing a speed profile for a given schedule. The results can be utilized both for recognizing operational patterns that ship operators may improve in an existing ship and for creating new generation ships for the similar type of route with new technologies on board, for considerably lower carbon footprint. Figure 3 presents an example of the propulsion energy breakdown during a longer period of operation.

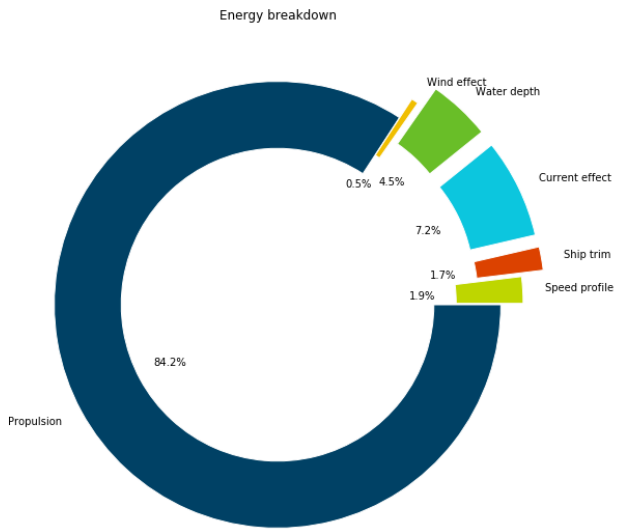

Figure 3. Propulsion energy break down in an example case.

DeltaSeas, our data layer, approaches the ship operational profile from even broader scope: no matter what kind of measurement data from existing ships we have for use at the start of a new building project, we must be able to always determine the ship propulsion power. Whereas the traditional methods rely on determining single speed calm water resistance with adding a fixed “sea margin” on top of that, DeltaSeas aims for determining ship life time propulsion power. DeltaSeas method was also presented in the previous publication for INTENS-project in Deltamarin’s article “Trashing design margins with smart data”.

The method requires the understanding of the ship itself, the speed and draft profile, the routes and weather. In a new build, Deltamarin is normally the designer of the hull and knows best how it behaves. In a conversion, some part or all the ship properties may come from previous reports or other sources. Normally, we would take responsibility for everything related to this. Our digital design portal includes small examples of the propulsion power profile that is calculated for an expected distribution of speed and loading condition of a ship at a specific sea area. The weather impact was considered with 30 years of statistical data from this area. Figure 4 presents the speed profile on the left and the resulting power profile on the right. Utilizing the left-most profile only for determining the ship energy consumption with a fixed weather margin would lead to very different energy consumption breakdown than the one on the right, followed by fuel consumption including all other related ship systems, such as waste heat recovery.

Nevertheless, for the DeltaSeas method, one starting point is to have available the model of the ship hull. This brings forward to our third, and probably most concrete, and visual layer of the digital ship: the ship volume and structural model. We call this layer DeltaWay, which is a unique method to start a ship concept. At the start, we define ship main dimensions, such as length, beam, draft and displacement. DeltaWay method was first developed for RoPAX ships, where this step includes an optimization routine, relying both on reference ship data and general ship design expertise at Deltamarin.

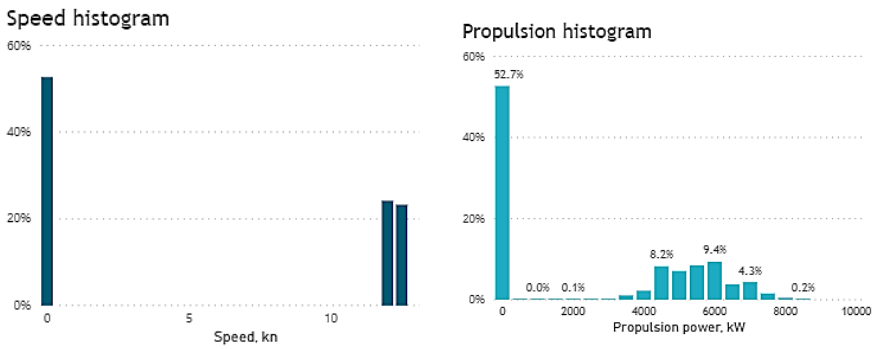

Figure 4. Example speed profile of a tanker (on the left) converted to a propulsion power profile including the expected ship loading condition and surrounding statistical weather data.

Once the main dimensions are defined, a tailor-made hull form will be created by our hydrodynamic team. The tailor-made hull form will be the basis for engine room development. Main engines will be fitted into hull form and engine room location and compartment layout development will be based on that. This will give a good basis for vessel development. The report from the arrangement model gives us the areas, volumes and center of gravity of each space of the vessel, which provides very accurate weight information of technical, interior and outfitting areas. This is also the natural stage for creating the ship energy model with DeltaKey for this specific project after performing the operational analysis using DeltaSeas with the new hull form. These tools and the related analysis can give valuable feedback so as to pay more attention or perform modifications in certain parts of the ship.

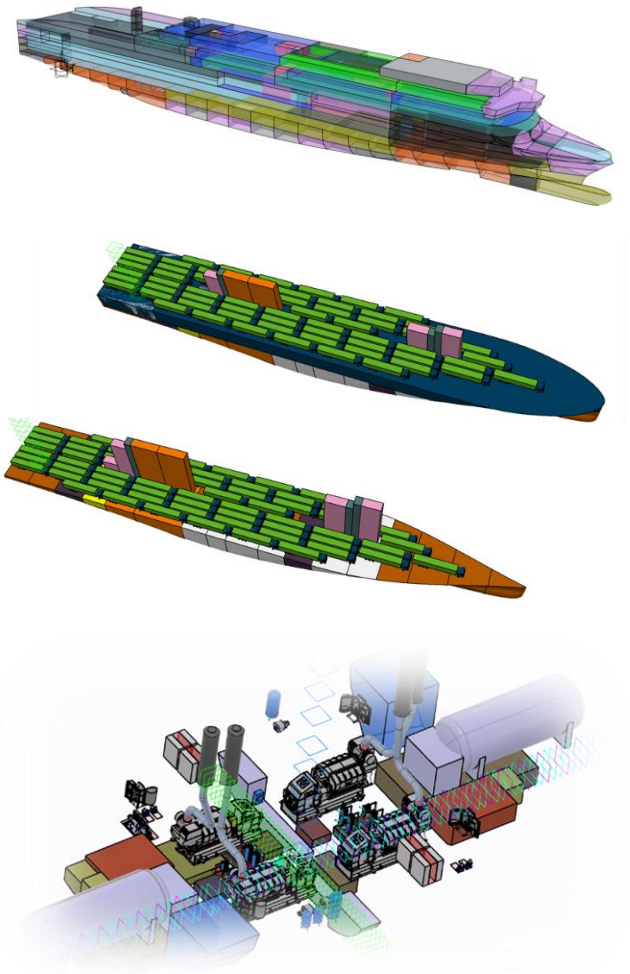

Figure 5. Examples from visualisations of the DeltaWay process where the layout is generated supported by automated functions, with ready space categories.

In the DeltaWay method, the arrangements of the vessel flows, such as cargo, passenger and proviant development, can utilize the 3D environment together with certain library templates, which allows quick verifications and modifications of the layout. Furthermore, stability calculations start based on the developed layout so that the first verification of rules is available very early in the project. 3D structural layout is effectively created on top of ship general arrangement model at early concept design phase. Such a way of early 3D-modelling approach on structural concept allows solid basis for accurate weight calculations and space utilization. It is also possible to use the created model for early phase structural response assessments using finite element method. Combining comprehensive experience on structural concept design and utilizing novel 3D-methods during the early phase of the project allow a remarkably more effective usage of steel, taking into account the strength and vibration behavior of the vessel.

During INTENS-project, Deltamarin has studied further new optimization methods that could expand the current design space. The results of this work are separately described in Chapter 3 of this publication, “Taking ship energy efficiency to a new level with cloud-based optimization”. In this case, we utilize the DeltaKey energy model for describing the case to be optimized, but the method itself is not limited to this one. The important aspect is that we are able to integrate the new optimization procedures in the existing digital design framework.

1.4 Summary

Deltamarin’s digital design “layers”, DeltaKey, DeltaSeas and Deltaway, all include individually a set of practical design tools and methods for producing a highly flexible digital representation of a ship. The aim is to optimize the ship performance in the future operational conditions, no matter whether there would be various alternative scenarios describing the future. The weight and even technical order of performing the first simulations varies, depending on the type of ship we are designing and the type of data available. This flexible development platform includes the relevant technical information that is required first for estimating the price of a ship at shipyards, and later for building the ship. After ship is built, the digital ship sets the baseline for the expected level of operational efficiency and sustainability and it is, therefore, a valuable benchmark to work against during the entire ship life cycle. Thus, for a ship designer, being involved during the ship entire lifetime is not only a possibility but also a necessity for designing future-proof ship.

2. Increasing ship energy efficiency using onboard data: opportunities and challenges

Mikael Manngård [a) 1], Joachim Hammarström [a) 1], Wictor Lund [a) 1], Jerker Björkqvist [a) 1], Wilhelm Gustafsson [b) 2]
[a)] Åbo Akademi University
[b)] Meyer Turku

2.1 Introduction

Energy efficiency is becoming more important for marine industries due to increasingly strict international maritime regulations. All ships over 400 GT built after 1 January 2013 have to follow the new Energy Efficiency Design Index (EEDI) enforced by the International Maritime Organization (IMO) to lower harmful emissions by increasing the energy efficiency [1]. To achieve the set long-term energy-efficiency goals, it is not likely that a single new technological advance will suffice, but all parts of the ship would need to be optimized for energy efficiency. Although there are existing conventional technologies related to hull improvements, propeller and rudder designs that together could achieve the set energy efficiency goals [2], not all technologies are applicable to all ships, especially to the existing ones. A list of some conventional technologies and their expected average energy efficiency gains are listed in Table 1. Although it appears that the largest potential gain is in improved ship designs, advanced control-system designs that focus on optimized waste-heat recovery have the potential to provide large improvement in energy efficiency. Simply put, even if a ship is properly designed, if it is not operated in an energy efficient way, heat will still be wasted. Thus, in this paper, we will focus on how to use onboard data and model-based technologies for improved ship control, monitoring and optimized waste-heat recovery.

In recent years, we have seen an exponential growth in the number of sensors connected to the internet of things (IoT). The spread of the IoT to new areas will provide new data sets which can give value to new markets, including the marine

[1] Contact: firstname.lastname@abo.fi
[2] Contact: firstname.lastname@meyerturku.fi

Table 1. List of technologies and average potential gain in energy efficiency [2].

Type	Technology	Expected gain
Control systems	Waste-heat recovery	10 %
Engines	Engine de-rating	3 %
Engines	Common-rail upgrade	0.30 %
Hull	Bow optimization	10 %
Hull	Hull coating	5 %
Propeller and rudders	Ducted propeller	10 %
Propeller and rudders	Contra-rotating propellers	13 %
Propeller and rudders	Wheels	10 %
Propeller and rudders	Rudder bulb	4 %
Propeller and rudders	Post swirl fins	4 %
Propeller and rudders	Twisted rudders	3 %

industries [3]. In contrast to general big data sets, industrial data typically possess spatiotemporal properties [4], i.e. both structure, dictated by physics, and time dependencies. For example, overall energy in a ship may the summation of independent energy consumers such as propulsion, hotel load, air conditioning, etc. In industrial systems, physical laws dictate how signals are related to each other and should thus be utilized when analysing data. Furthermore, time attributes in industrial big data cannot be neglected. Since any change in a physical system is always governed by dynamics, the methods used for analysis cannot rely on the assumptions that sampled data are independent and identically distributed, which is standard for statistical inference and machine learning (ML) methods. The spatiotemporal properties of industrial data may turn out to be challenging for out-of-the-box big data and machine learning algorithms, which have been developed, for a large part, in the context of explaining the complex human and societal behaviours and decision-making. Human behaviour does not necessarily possess strong spatiotemporal properties, often unpredictable, irrational and not consistent. In contrast, an industrial process or machine is designed to perform a single task with high precision, reliability and predictability. Hence, it is not a given that the same big-data and ML algorithms, which have already made a lasting impact in areas such as image recognition and recommendation systems, will have the same impact on the process and marine industries.

Control theory provides the necessary means to deal with control of dynamical systems in engineering processes and machines. Although optimal and robust control methods are readily available in the control literature [5], model-based predictive control methods are expected to form a basis of future control systems [6], and soft sensor technologies used to estimating unknown inputs and state of systems are already implemented in a wide range of industrial processes [7, 8, 9], it does not mean that there is not room for data-based ML algorithms. Control methods rely extensively on system models, either obtained experimentally or based on physics. However, not all signals affecting an industrial process are easily

modelled using physics or by expert knowledge. In a cruise ship, a few such examples are fluctuations in energy prices, ambient temperatures and hotel loading in cruise ships. Thus, although energy efficient operations of a ship are at its core an optimal control and decision problem, for a framework of optimized operations to have a lasting impact on the energy efficiency, a collection of technologies from a range of fields are likely needed. Various types of models are to be used: physics-based models will dictate the spatial behaviour of data to ensure that mass and energy balances are satisfied, statistical models will be used to describe signals with uncertainty, data-based models will be used to describe signals that are not easily modelled by first principles, and integer programming methods are needed for optimizing discrete logic and decision making.

2.2 Framework

We present a framework for energy efficient heat management in ships through optimized scheduling, improved monitoring, integrated operations, and model-based predictive control. The focus is on maximizing the energy efficiency by utilizing the available waste heat while ensuring that the ship can be operated safely. The use of faulty components or inferior spare parts can result in problems such as higher lube oil or fuel oil consumption, leading to an increase in total operating costs and lower energy efficiency [10]. By making the full use of available sensor data and system models, soft sensor technologies can be used to reconstruct unmeasured states of the system and estimate the condition of components. This will not only increase the awareness of how the plant is performing but also aid in designing predictive and prescriptive maintenance strategies that will result in improved energy efficiency. Furthermore, improved monitoring will not only aid the on-board crew in making better decisions but can also be fed forward to the regulatory control systems. Information of the condition of components could even be used as constraints in the control to extend the remaining lifetime of components by limiting performance temporarily.

2.2.1 Data-based process monitoring

Issues of how to improve product quality in the steel industry was surveyed in [11], and many of the same concepts apply to the marine industries as well. The challenges are the same between different industrial processes: how to build a reliable model of the right complexity from limited data, when to use first-principle models compared to data-based models, how to relate different types of models, and how to realize and maintain a model-based control system. We claim that a data-based process monitoring system which aids in improving the energy efficiency of a ship would at least need to have the following properties: (i) being able to estimate the current operating conditions at all locations of interest in the ship based on the collected sensor data, (ii) predicting the future available energy and demand at various locations in the ship based on current operating conditions,

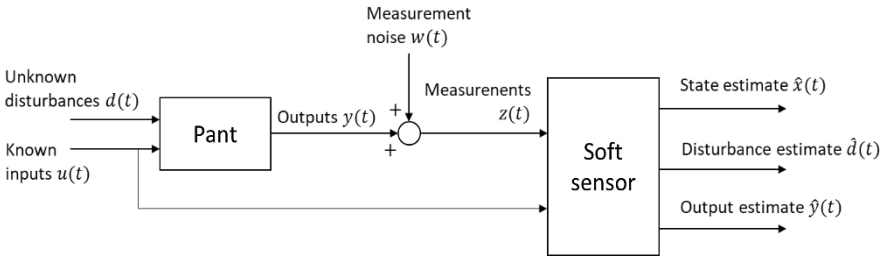

Figure 1. Block-diagram of a typical soft sensor used for estimating internal states of a process, reconstructing unknown disturbances and removing noise from measurements.

(iii) the ability to detect and isolate sensor faults and external disturbances acting on the system, and (iv) detecting faults or malfunctions in the process.

Most of the above-mentioned criteria can be managed using soft sensor technologies, which make use of available measurement data, statistical properties associated with the uncertainty of the measurements, and mathematical models of the process [12]. Soft sensors have been used, for example, for aiding condition monitoring strategies of marine propulsion system components by estimating external torque excitations acting on the propeller [13], for process monitoring in process industries [14, 15], and for sensor fault diagnostics in aircrafts [16, 17], to mention a few. The typical structure of a soft sensor is illustrated in Figure 1.

2.2.2 Integrated operations and control

A ship is a complex system involving energy systems, processes, automation systems, people and raw materials (e.g. fuels). Operating a ship involves numerous tasks, which might broadly be classified into planning, scheduling, real-time optimization and control. Communication of information between tasks typically follows a hierarchical structure as in Figure 2. [18]. Scheduling is typically performed by real-time or batch optimization from which a supervisory system computes the

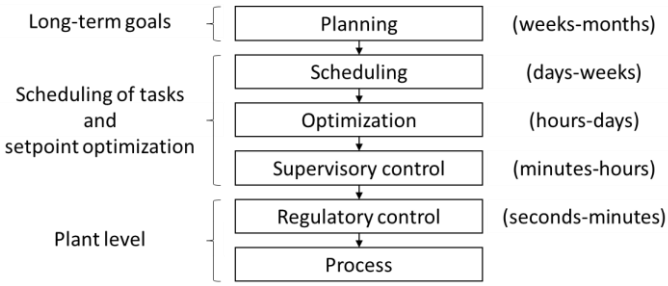

Figure 2. Typical hierarchy of process operations and control [18].

desired set points or set point trajectories which the regulatory control system takes in to perform control actions at a process level. However, in an integrated operations and control scheme for optimized energy efficiency, the classical one-directional hierarchical decision making would likely be replaced with a structure where data is more free-flowing [18].

The challenges of integrating the decision making with the control is many-fold. First, the timescales of which actions are required to be taken at the different levels vary, as shown in Figure 2. Planning, scheduling and optimization are typically done in an open-loop fashion and performed on a daily to weekly basis and might require actions taking place on an hourly basis [18]. Examples of such tasks on a ship are route planning, on-board maintenance of components that do not require a service stop, and fresh-water evaporation. Note that all these tasks affect the energy systems and require actions of the control systems (supervisory and regulatory). Control generally operates on a much smaller timescale than scheduling tasks. The difference in timescales is the main reason why it makes sense to structure these tasks in a hierarchical one-directional structure as shown in Figure 2. However, in cases when the process is not reacting to control actions correctly, e.g. a component's condition has deteriorated to a point that affects the performance of the system, such as fouling in an heat exchanger, sticking in a valve or damage to a mechanical component, information should be fed back 'up-streams' in the hierarchical table and be taken into account in the scheduling. Likewise, if a mechanical component has been damaged, it might even be possible to prolong its remaining lifetime by limiting the power transmitted through it and extending its lifetime.

The difference in timescales on which process operations take place adds constraints to the process models used. First principle models used for regulatory control would typically describe the dynamics of a system and act on a timescale of seconds to minutes. However, on the timescales relevant to discrete decision making, the effect of dynamics disappears and dynamics can be neglected. This presents a model mismatch between control and process operations. Designing a computationally efficient framework, which handles this mismatch within the timescales, might turn out to be challenging. Furthermore, there is always a trade-off between model accuracy and complexity, which needs to be accounted for.

A realization of an integrated scheduling and supervisory control approach would need to perform real-time optimization on a receding horizon with either economical or efficiency goals as objectives. This strategy has been suggested for distributed power systems connected to a grid [18, 19, 20]. Optimal model-based control on a receding horizon is referred to as model predictive control (MPC) in control literature, or Economic MPC (E-MPC) when economic (or efficiency) goals are optimized [21]. Extending the E-MPC framework to handle the discrete decision variables, required for scheduling and logic operations, would result in a fully integrated operations and control scheme. However, the challenges of realizing such framework are both computational and to some extent control-theoretical [18], and would likely require technological progress in real-time optimization, mixed-integer programming and parallel computing to be feasibly addressed in practice.

2.3 Summary

This paper outlines the opportunities and challenges of a data-based integrated operation and control strategy for improving the energy efficiency of ships. Integration of operations and control can be done using model-predictive control frameworks for optimizing economic or efficiency goals. However, for such technologies to be realizable in practice, new advances in real-time optimization, integer programming and control theory are most likely needed.

Condition monitoring using soft sensor technologies can decrease the downtime of processes, which can lead to increased efficiency. Soft-sensor technologies for condition monitoring is also expected to provide important information for scheduling and supervisory control. When dealing with data-based techniques, the quality and availability of data is key. Soft sensor technologies can be used for improving the data quality via sensor fusion, fault detection and fault isolations. When accounting for spatiotemporal properties of data in physical systems, the choice of model-type is fundamental. There is always a trade-off between model accuracy and computational complexity, and there is also a choice between data-based and first principles modelling techniques to be made.

References

[1] Hammarström, J. (2020). Validation of a Digital Twin for a Ship Engine Cooling System. ÅAU, M.Sc Thesis.

[2] Rob Winkel, Arno van den Bos, and Ulf Weddige, Energy Efficiency Technologies for Ships (Utrecht, The Netherlands: ECOFYS, 2015). Retrieved from http://publications.europa.eu/resource/cellar/302ae48e-f984-45c3-a1c0-7c82efb92661.0001.01/DOC_1.

[3] Manngård, M., Lund, W., & Björkqvist, J. Using Digital Twin Technology to Ensure Data Quality in Transport Systems. Proceedings of 8th Transport Research Arena TRA 2020, April 27-30, 2020, Helsinki, Finland.

[4] Yan, J., Meng, Y., Lu, L., & Li, L. (2017). Industrial big data in an industry 4.0 environment: Challenges, schemes, and applications for predictive maintenance. IEEE Access, 5, 23484-23491.

[5] Doyle, J. (1996, December). Robust and optimal control. In Proceedings of 35th IEEE Conference on Decision and Control (Vol. 2, pp. 1595-1598). IEEE.

[6] Morari, M., & Lee, J. H. (1999). Model predictive control: past, present and future. Computers & Chemical Engineering, 23(4-5), 667-682.

[7] Auger, F., Hilairet, M., Guerrero, J. M., Monmasson, E., Orlowska-Kowalska, T., & Katsura, S. (2013). Industrial applications of the Kalman filter: A review. IEEE Transactions on Industrial Electronics, 60(12), 5458-5471.

[8] Gillijns, S., & De Moor, B. (2007). Unbiased minimum-variance input and state estimation for linear discrete-time systems. Automatica, 43(1), 111-116.

[9] Manngård, M., Lund, W., Keski-Rahkonen, J., Nänimäinen, J., Saarela, V. P., Björkqvist, J., & Toivonen, H. T. (2019). Estimation of propeller torque in azimuth thrusters. IFAC-PapersOnLine, 52(21), 140-145.

[10] Wärtsilä (2019). Smart maintenance. Retrieved from https://www.wartsila .com/ marine/smartmarine/smart-maintenance.

[11] Kano, M., & Nakagawa, Y. (2008). Data-based process monitoring, process control, and quality improvement: Recent developments and applications in steel industry. Computers & Chemical Engineering, 32(1-2), 12-24.

[12] Åström, K. J. (2012). Introduction to stochastic control theory. Courier Corporation.

[13] Manngård, M., Lund, W., Keski-Rahkonen, J., Nänimäinen, J., Saarela, V. P., Björkqvist, J., & Toivonen, H. T. (2019). Estimation of propeller torque in azimuth thrusters. IFAC-PapersOnLine, 52(21), 140-145.

[14] Kadlec, P., Gabrys, B., & Strandt, S. (2009). Data-driven soft sensors in the process industry. Computers & chemical engineering, 33(4), 795-814.

[15] Kabugo, J. C., Jämsä-Jounela, S. L., Schiemann, R., & Binder, C. (2019, September). Process Monitoring Platform based on Industry 4.0 tools: a waste-to-energy plant case study. In 2019 4th Conference on Control and Fault Tolerant Systems (SysTol) (pp. 264-269). IEEE.

[16] Liu, X., Xue, N., & Yuan, Y. (2017). Aircraft engine sensor fault diagnostics using an on-line OBEM update method. PloS one, 12(2), e0171037.

[17] Wang, D., & Lum, K. Y. (2007). Adaptive unknown input observer approach for aircraft actuator fault detection and isolation. International Journal of Adaptive Control and Signal Processing, 21(1), 31-48.

[18] Daoutidis, P., Lee, J. H., Harjunkoski, I., Skogestad, S., Baldea, M., & Georgakis, C. (2018). Integrating operations and control: A perspective and roadmap for future research. Computers & Chemical Engineering, 115, 179-184.

[19] Trifkovic, M., Marvin, W. A., Daoutidis, P., & Sheikhzadeh, M. (2014). Dynamic real- time optimization and control of a hybrid energy system. AIChE Journal, 60(7), 2546-2556.

[20] Zachar, M., & Daoutidis, P. (2016). Microgrid/macrogrid energy exchange: A novel market structure and stochastic scheduling. IEEE Transactions on Smart Grid, 8(1), 178-189.

[21] Hovgaard, T. G., Edlund, K., & Jørgensen, J. B. (2010, December). The potential of economic MPC for power management. In 49th IEEE Conference on Decision and Control (CDC) (pp. 7533-7538). IEEE.

3. Taking ship energy efficiency to a new level with cloud-based optimization

Timo Korvola [a) 2], Mia Elg [b)], Ossi Mettälä [c)], Jari Lappalainen [d)],
Bogdan Molchanov [b)], Lien Tran [b)]
[a)] VTT Technical Research Centre of Finland Ltd
[b)] Deltamarin Ltd
[c)] Napa Ltd
[d)] Semantum Ltd

3.1 Introduction

Mathematical modelling and simulation-aided engineering are becoming a common practice in the marine industry. While mathematical modelling and dynamic simulation provide a systematic approach to evaluating novel process and control concepts with respect to energy efficiency and operability, simulation-based optimisation would bring immense extra added value.

This work started by developing a framework for simulation-based optimisation in the cloud [1]. We originally defined our main hypothesis as follows: *Today's cloud computing infrastructure enables an easy and flexible framework for taking out-of-a-box marine simulators and solving related optimization problems*. For testing this hypothesis, we developed a framework that was already reported in [2].

To evaluate the suitability of the method for actual ship design process, a generic energy simulation model of a cruise ship was utilized. The case ship and the model structure are described in Section 3.3. The optimisation study is focused on finding the best solution for enhancing the energy efficiency of the ship and lowering the carbon footprint by introducing a waste heat recovery solution, a battery or both.

We discuss our experiences gained in the model conversion and working with the framework and present the main findings of the case study. Finally, we take a brief look at the next steps.

3.2 Optimization framework

One basic idea in this work is to enable optimisation for simulation models that were not originally intended for this purpose. This rules out gradient-based algorithms, as simulators do not usually provide gradients. The model would have to be translated into a representation that provides them, which we want to avoid. We focus on black-box optimisation algorithms that only require the ability to set parameters, run simulations and obtain results. Specifically, we choose evolutionary algorithms as the primary approach because they parallelise well. Parallel computing is lucrative

[2] Contact: firstname.lastname@vtt.fi

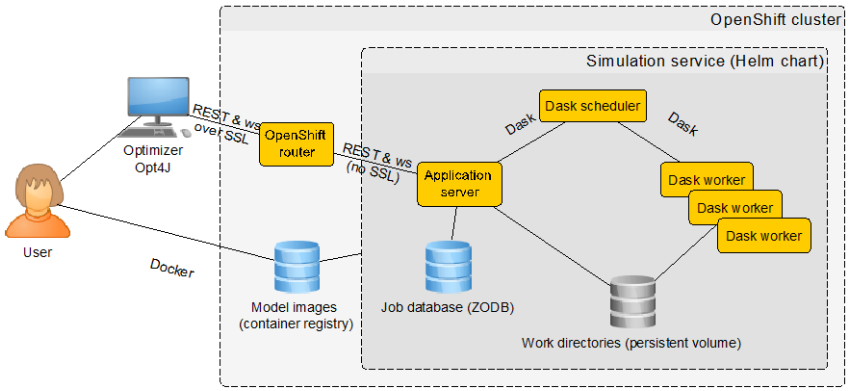

Figure 1. Schematic view of the updated optimization framework.

in the cloud because pricing tends to be per number of resources and time; if your algorithm parallelises well, you can rent more CPUs to run it for a shorter time, obtaining results faster for the same cost.

The general architecture of the framework remains essentially as described in [1]. The main change is that we have moved from Microsoft Azure to Rahti, a container cloud provided by CSC. This changed our container orchestration system from Kubernetes to OpenShift. OpenShift is a variant of Kubernetes, thus only minor changes were required in the framework. The current architecture is illustrated in Figure 1. Generally, it has been pleasant to use the CSC service, with far fewer technical problems than we had on Azure [2].

3.3 Case description

3.3.1 Case ship

The case ship is a generic cruise ship which is expected to run on MDO fuel. The cruise ship represents a typical example of a 4000 passenger cruise ship with diesel electrical propulsion plant. The total installed engine power is 75.6 MW, consisting of six medium-speed Wärtsilä 12V46F engines.

The main characteristics of the ship main machinery and heat recovery are illustrated in Figure 2. Each engine is equipped with an exhaust gas boiler (EGB). It was assumed in the study that these boilers could produce superheated steam and additional heat can be produced in an oil-fired boiler. In addition, high temperature (HT) cooling water heat is collected from the engines, during HT charge air cooling and jacket water cooling processes, and fed into a separate waste heat recovery circuit. From this circuit, the waste heat is distributed to all consumers that can utilize the hot water as their heating source. It was also assumed that this HT-heat could be utilized for air conditioning heating and for producing fresh water onboard using

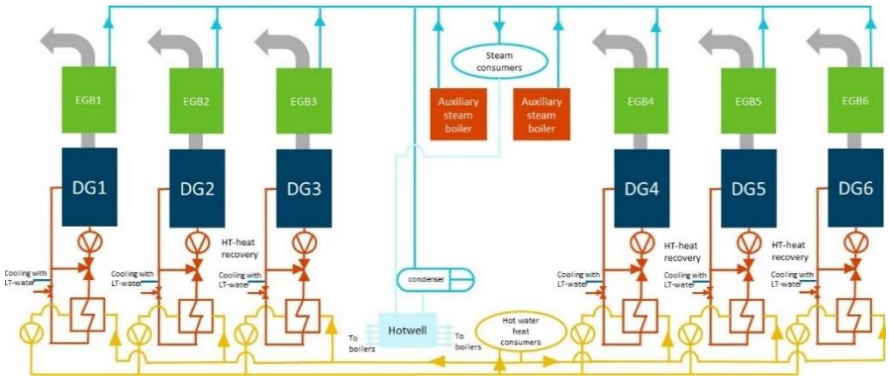

Figure 2. Schematics of ship heating and waste heat recovery main principle.

evaporators. Low temperature (LT) cooling water heat, collected from the engines during lubrication oil cooling and LT charge air cooling processes, was not utilized in the case study.

The operation profile included one year of typical operation patterns regarding vessel propulsion and hotel power. The vessel heat consumption was evaluated for the entire year in average conditions with average air temperature being 25 °C.

3.3.2 Simulation model

The modelling was done in the Matlab/Simulink environment with Deltamarin's energy flow simulation tool, which is briefly discussed in Deltamarin's digital design tool presentation in this publication, Chapter 1. In the model, the operation profile sets the power demand for the ship. The engine fuel consumption as well as heat production was evaluated with the aid of the Wärtsilä engine's project guide. The partial-load behaviour was evaluated by interpolation between the values provided in the engine project guide.

For the study, we included a possibility to install battery capacity for the ship. The variable parameter was the battery size. The state of charge range was set to 25–95 %. The eventual degradation of the battery over time was not considered. The C-rating was set to 3. The battery operation logic was set for "peak shaving" with a simple load levelling logic. The principle of the model logic is based on an assumption that the battery management system (BMS) knows engine loads and specific fuel oil consumption (SFOC) from the previous time step. At the same time, BMS predicts the SFOC of the engines without batteries in the current time step by reviewing the incoming power demands. These two readings are compared. If the SFOC in new time step is better than in the previous one, the engines can change loading. In case the performance is worse in the new time step, the battery will even out the difference and keep engines running at the same load as in the previous time step as long as there is enough energy in batter for charging or discharging.

In addition, the case ship had an option to include waste heat recovery in the ship. The chosen method in the study was a backpressure steam turbine. Their number and size could be varied in the model. The allowed maximum power for a single turbine was set to 1MW and the minimum power production was limited to 33% of the maximum.

3.3.3 Optimisation problem

In ship design projects, the typical target is to maximize the ship transport efficiency by minimizing the related costs, both capital and operational expenditures (CAPEX and OPEX). As a ship is a highly complex multi-domain energy system and the input data for any design task may include a large degree of variation, it is often hard to define a single exact target for optimization. Multi-objective optimization can be used to provide the designer a set of optimal solutions to choose from, rather than a single answer.

In the study, we present a retrofit project, where various energy or emission saving technologies are considered for an existing ship. As explained in the previous section, the chosen technologies were to install battery and steam turbines onboard. The battery size was allowed to vary between 0 and 10 MWh. The steam turbine size was allowed to vary between 0.1 and 1 MW, and the number of turbines between 0 and 4. The CAPEX was estimated to be 1000 €/kWh for the battery and 1000 €/kW for the turbine.

One objective was to reduce ship fuel consumption, thus lowering carbon dioxide emissions. However, the investment (CAPEX) should also be kept small. The third objective was to reduce the average number of main engine running hours, leading to lower maintenance costs.

3.3.4 Model conversion for the framework

The simulation model first need to be converted from Simulink into a form that allows parallel execution in the cloud, without requiring Matlab installations there. The ideal form is a shared library that can be called repeatedly to execute simulations. The model is then simulated with different input parameters, received from the optimiser, and returns output values to the optimiser. Fortunately, there is a standard packaging and interface for such executable simulation models, namely the functional mock-up interface (FMI, https://fmi-standard.org/). Model packages conforming to this standard are called functional mock-up units (FMU). We used Simulink Coder to translate the Simulink model into C code and an open source tool called Simulix to package the generated C code as an FMU. The compiled C code runs much faster than the original Simulink model, but not all features of Simulink are supported by the code generation.

3.4 Results

3.4.1 Energy system optimisation

Figures 3–5 illustrate the optimization objectives plotted pairwise against each other. The red highlighted dots represent the so-called archive of the genetic algorithm, which approximates the Pareto optimal surface. Figure 3 illustrates the relationship between ship fuel consumption and the investment costs. Figure 4 illustrates the average number of engines running. Thus, the smaller the number, the lower amount of engine hours was needed. Figure 5 plots the ship fuel consumption against engine hours. Unsurprisingly, these objectives are co-aligned; the trade-offs are against CAPEX. The full results can be examined with Figure 6, where the main decision variables, optimization objectives and some other quantities of interest are plotted together. Table 1 presents the variables that are illustrated in Figures 3 – 6.

Table 1. List of optimization objectives, decision variables and other plotted quantities.

Label	Clarification	Unit	description
fuel	fuel consumption	kg/s	average over the entire operation profile
capex	capital expenditure	1000 €	
n_me	main engines in operation	-	average number of main engines in operation
batt_cap	battery capacity	kWh	total battery capacity installed
bpst_n	turbine amount	-	the number of steam turbines installed
bpst_P	turbine power	kW	maximum power of each back pressure steam turbine
bpst_P_tot	total turbine max power	kW	total power of steam turbines installed
P_pbst_act	turbine actual power	kW	average power actually produced by the turbines
hue	Heat Utilization Efficiency	%	efficiency of utilization of the exergy in ship waste heat flows considering also ship heat consumers. The efficiency is compared to a theoretical situation without any waste heat recovery.
P_me_tot	average engine power	kW	time average of total main engine power

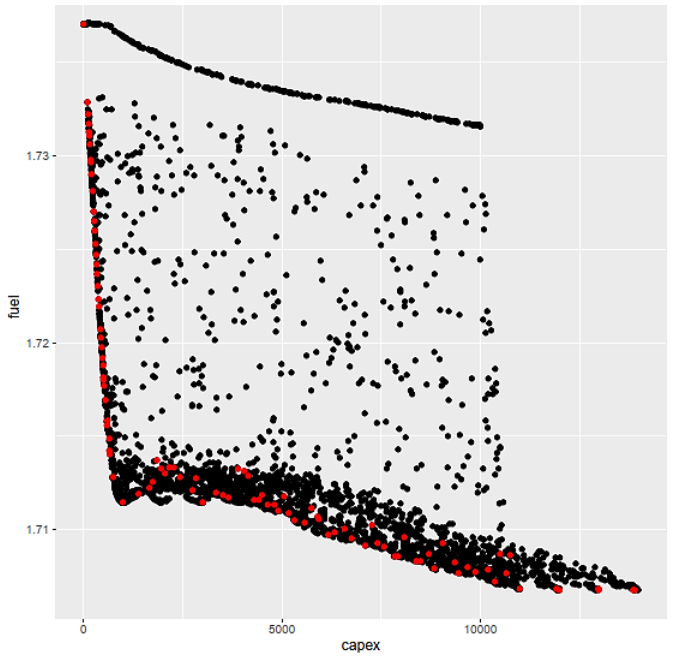

Figure 3. Ship fuel consumption and CAPEX.

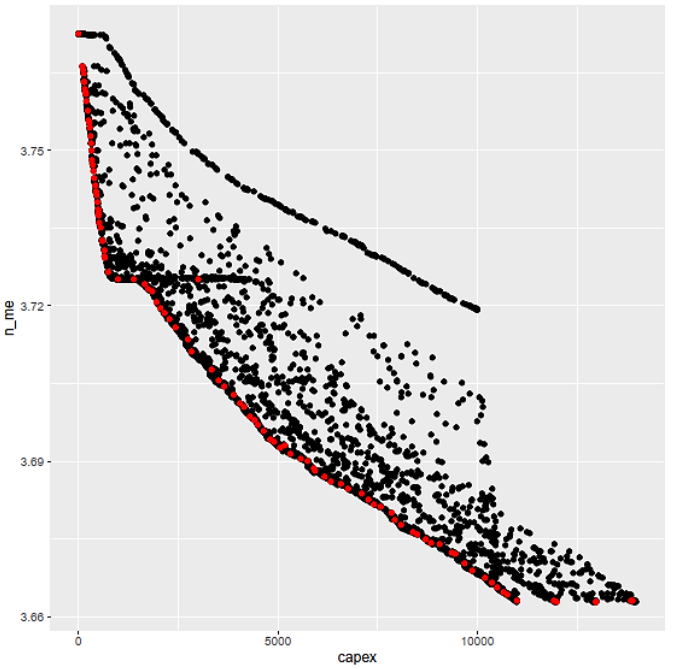

Figure 4. Ship engines in operation and CAPEX.

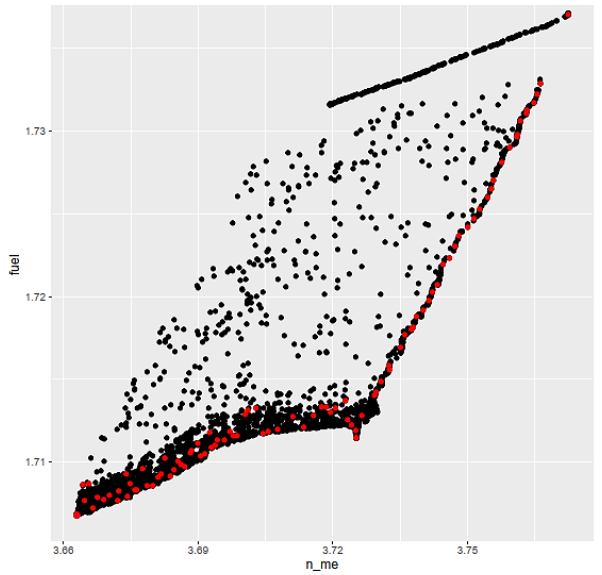

Figure 5. Ship fuel consumption and engines in operation.

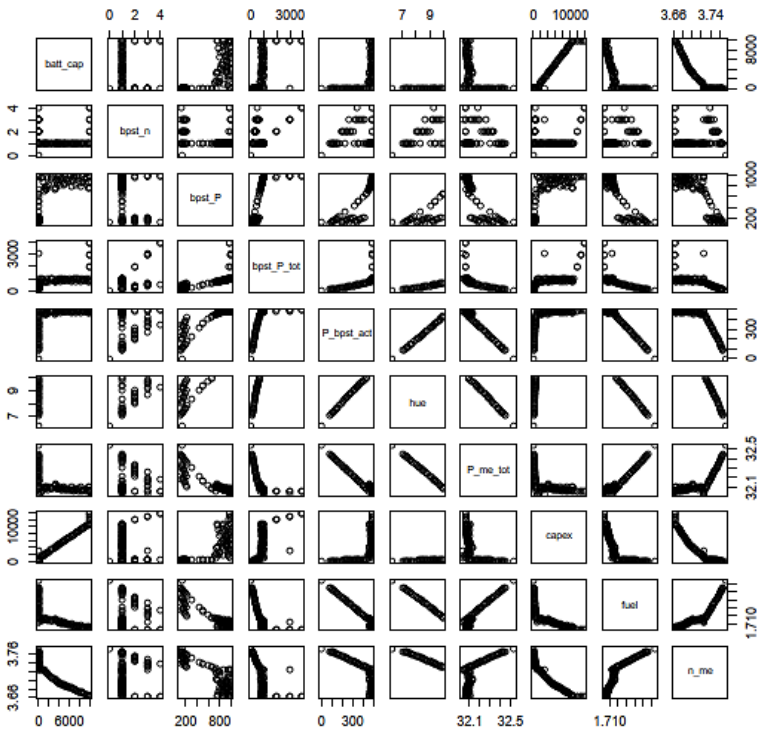

Figure 6. Main result matrix of the optimization.

3.4.2 Discussion on the case results

As Figure 3 illustrates, the maximum fuel saving range within the results varies from 0 to 1.7% of the ship total fuel consumption. However, we can clearly see that the most relevant reduction in the fuel consumption can be achieved with rather moderate investment, i.e. less than 1 M€. Figure 6 helps indicate which configurations would provide this. Approximately, 1 MW steam turbine installed power with only one turbine seems to lead to best results. Battery capacity does not bring much improvement for the fuel consumption in the results.

Increasing battery capacity continues to contribute to reduced main engine running hours, while the steam turbine configurations with over 1 MW installed power yield little benefit. Such configurations appear in the archive usually after the maximum battery capacity is met, as it would otherwise be more profitable to invest in the battery.

The results could in this case give us guidance to favour primarily steam turbine capacity over battery capacity, if the purpose of the retrofit project would mainly to lower the fuel consumption and, thus, carbon emissions of the ship.

3.4.3 Discussion on the case approach

The chosen method reveals patterns that are not trivial and, therefore, it is very promising way to support ship design. Since an energy model can be compiled for a ship at any design stage and is a part of the ship design process, it is important to be able to utilize the existing model in the optimization work. In the case example, the energy model includes a system level description and analysis of the ship entire energy system, which enables the direct profitability analysis of the proposed concepts. After successful optimization round, the most promising results can be added to the design and the ship design process may continue without interruptions. The optimization process could be performed at any relevant stage of the design process.

Once the optimization process is an integral part of the design process, it is also natural to evaluate the result with the existing conventions and methods which are already applied in the energy simulation work or other design disciplines. For instance, the heat utilization efficiency analysis, which was also a part of the results in Figure 6 shows that the hue-index values between 7 to 10. The analysis is to certain extent case-specific, but earlier work on this field would show that much higher efficiencies are possible to be gained. Therefore, this optimization task has clearly not included the most promising waste heat recovery equipment. The results of this analysis would suggest improving and re-defining the optimization case regarding the waste heat utilization methods.

In this research, one of the main goals is to lower the threshold of using optimisation in the practice of simulation aided marine engineering. As the ship energy system model already existed, surely it could be easily adapted for optimisation. In practice, it turned out to be not quite so simple. First, there was the

need to translate the model into a form that could be executed outside of Matlab. Simulink Coder can do that but produces C code with an exotic interface. Simulix adapts this exotic interface to FMI. Unfortunately, not all Simulink or Matlab features are supported by these tools. In particular, runtime error checking is lost in translation: the model mostly relied on the Matlab “assert” function, which Simulink Coder essentially ignores, i.e., translates to nothing. Mathworks has recently introduced a new product, Simulink Compiler, that should be able to generate standalone FMUs from Simulink models, but we have not had a chance to try it.

The translation tools create the FMU interface from the parameters and the top-level ports defined in the Simulink model. The existing energy system model had none of these. Instead, it read its input from a custom format Excel file into global variables and used the Simulink logging facility to write outputs into a file. Adapting this, particularly the input, took some effort. We assume that this kind of case-specific work for interfacing of inputs and outputs for the translated simulator is a common effort with future cases as well.

Simulation-based optimisation requires the simulation model to be rather robust. The optimisation problem specifies the feasible value ranges for all the parameters, and the optimisation algorithm executes simulations exploring the whole range of feasible value combinations. If the model has only been used previously with manually picked “reasonable” parameter combinations, simulations may fail surprisingly frequently, when the parameters are picked by a machine with no sense of what is “reasonable”. In this case, the problem was exacerbated by the loss of runtime error checking; instead of halting with an error message, the simulations would typically hang, and for all we know some might have finished with incorrect results. Clearly, there are many aspects in the model configuration phase that could be taken into account for supporting the model’s later black-box use inside an optimizing loop.

3.5 Conclusions

We successfully converted a dynamic energy system simulation model into FMU, containerised it and used it in our cloud-based optimisation framework (reported in the references). The results showed that an optimization process that utilizes the existing models from a normal ship design process could bring much added value with minimal additional effort in the actual ship design task. Optimization would expand the current design space, provide increased learning for designers and, most of all, support decision making during the project, resulting in a ship that is more efficient in her transport task and more environmentally friendly. This generates added value for all parties in the process, both customer and designer.

To minimise the additional effort for the optimisation process, such use should be anticipated during modelling. The model should have a reasonably clear interface that allows programmatic setting of model parameters, execution of simulations and retrieval of results. Runtime error checking is also important.

The next phase in this research is to study how machine learning approaches could be incorporated in the optimisation framework and what benefits it could bring.

Acknowledgement

We gratefully acknowledge CSC for providing their cloud computing services.

References

[1] J. Lappalainen, T. Korvola, and J. K. Nurminen, “Cloud-based framework for optimising complex systems including dynamic simulation,” in *Integrated Energy Solutions to Smart And Green Shipping: 2019 Edition*, no. 354, G. Zou, Ed. Finland: VTT Technical Research Centre of Finland, 2019, pp. 36–40.

[2] [J. Lappalainen, T. Korvola, J. K. Nurminen, V. Lepistö, and T. Mäki-Jouppila, “Cloud-based framework for simulation-based optimization of ship energy systems,” in *Proceedings of the 2nd International Conference on Modelling and Optimisation of Ship Energy Systems*, 2019, pp. 65–71.

4. Catalytic methods for methane and NOx emission removal in lean conditions

Teuvo Maunula[1], Kauko Kallinen
Dinex Finland Oy

4.1 Introduction

Smart and green is an important megatrend of global shipping, as world trade is projected to grow significantly in the coming decades. The energy efficiency is a main driving force and the need to reduce emissions has been well understood in the marine industry. On the other hand, digitalization and automation have already been shaping the future of marine shipping. After-treatment systems (ATS) are dependent on the fuel quality (Figure 1). Main efforts are focused on the emission reduction of SO_x and NO_x in marine applications but oxidation catalysts for CO and hydrocarbons (HCs) are applied also with low-sulfur fuels. NO_x emissions have been reduced with ammonia (urea) on sulfur-tolerant selective catalytic reduction (SCR) catalysts.

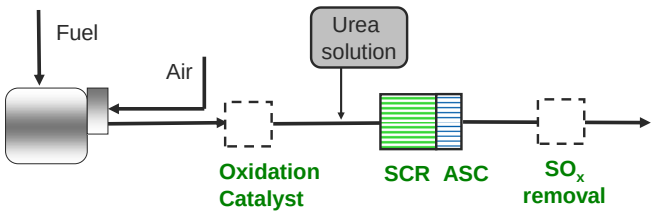

Figure 1. Decreasing emissions in marine applications.

[1] contact: tma@dinex.fi

Natural gas with very low sulfur amount (low SO_x, mainly SO_2) is a good alternative fuel for marine applications, opposite to conventional heavy-oil liquid fuels. Although it produces less carbon dioxide (CO_2) emissions compared to diesel HCs, methane itself is a strong greenhouse gas (GHG effect 25-fold compared to CO_2) and need to be limited. The particulate matter emissions are very low with natural gas. However, methane is the most difficult hydrocarbon to oxidize and expensive noble metals (palladium, platinum) are needed for methane oxidation catalysts (MOC). Pd-rich catalysts are best for methane oxidation, but they are quite sensitive to the deactivation. Thermal degradation is due to the loss of active sites by the crystallite growth of noble metal particles. Chemical poisoning covers the active sites and especially sulfur (S) is detrimental to the Pd-based oxidation catalysts. [1, 2]

Sulfur can be regenerated from the catalyst surface at elevated temperatures. However, the marine engines are working in lean conditions and very high temperatures is then required to decompose sulfates. On the other hand, sulfates can be decomposed at lower temperatures in stoichiometric or rich conditions. The catalyst performance has been restored by the regenerations in enriched gas mixtures in earlier studies [3, 4].

In the INTENS project, we investigated SO_x adsorbents or traps, which have a task to protect MOC against sulfur poisoning. Adsorption capacity and sulfur removal from MOC during the regeneration are the challenges in this method.

4.2 Experimental

Sulfur poisoning of Pd-rich MOCs was simulated in synthetic gas bench (SGB) using lean exhaust gas conditions (λ=1.8, 100 ppm SO_2). Sulfur was adsorbed on catalysts and SO_x traps at 400°C and 550°C. The lower temperature simulates the higher adsorption of SO_2 and the higher temperature the use conditions at pre-turbo position. Desulfation regeneration was examined at 550°C by a regeneration mixture, where λ was rich (0.99). Sulfur is accumulated on the surface as sulfates either on the active sites or porous support. Sulfate adsorption is dependent on SO_2 oxidation rate to SO_3 (SO_4) and the bond strength between SO_4 and metal cations on catalysts. When MOCs are usually alumina-based catalysts, the strength of Al-SO_4 (aluminium sulfate) bond is a base line for SO_x adsorbent comparisons. SO_2 oxidation on noble metals is faster than on base metal catalysts. Therefore, adsorbent catalysts or materials were examined with and without noble metals.

SCR and ammonia slip catalyst functionality was investigated by SGB and engine experiments. Due to medium temperature operation window, high sulfur in fuels and catalyst costs, the SCR has been based on vanadium/TiO_2-WO_x catalysts. SCR functionality was investigated in steady state condition with fixed or varying NH_3/NO_x ratio. Catalysts were investigated as fresh or hydrothermally aged. The feed gases in SGB simulations are summarized in Table 1.

Table 1. Feed gases in experimental simulations.

Compound	Lean NG MOC test	MOC Sulfation	MOC Regeneration	SCR
NO, ppm	500	500	500	1000
NO_2, ppm	-	-	-	-
Methane, ppm	1500	1500	3000	-
Ethane, ppm	300	300	500	-
Propane, ppm	100	100	100	-
Acetaldehyde ppm	150	150	150	-
CO, ppm	1200	1200	4000	-
Oxygen, %	10	10	0.91	10
CO_2, %	7.5	7.5	7.5	-
Water, %	8	8	8	10
NH_3, ppm	-	-	-	1000
SO_2, ppm	-	100	-	-
Nitrogen	Bal.	Bal.	Bal.	Bal.
λ	1.78	1.78	0.99	lean
Space velocity, h^{-1}	50.000 varying	50.000 varying	50.000	50.000

4.3 Results

4.3.1 Sulfur durability and regeneration of methane oxidation catalysts

When MOC is in exhaust gas, lean SO_x trap (LST) has a task to protect MOC and collect SO_x during lean driving periods. During regeneration periods SO_x is removed from LST and should further pass through MOC downstream. The effect of LST should be compared as an additional unit or it replaces MOC volume. Even if LST requires volume in design and causes pressure drop, it is much cheaper with SO_x adsorbents than PGM-rich MOC of the same volume. The cost equivalency (investment, use) for volumetric ratio of MOC/LST is a base for design (Figure 2).

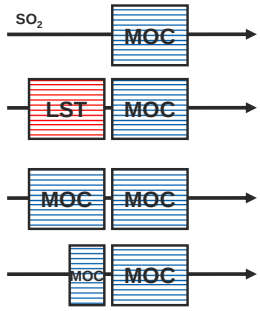

Figure 2. Lean SO_x trap with MOC.

The screening results showed that SO_x could be adsorbed at different materials. SO_2 adsorption at 550°C showed that fewer samples adsorbed clearly more; the lower the SO_2 curve during the adsorption phase the more SO_2 was adsorbed (Figure 3**).** Not all the available sulfur was trapped but a part was always passing through LST. There are differences also in the regeneration for different samples when looking at the SO_2 curves at the regeneration area. SO_2 adsorption increased for similar samples with a low amount of platinum for all the examined compositions. During the first minutes of the regeneration phase, high SO_2 peaks were observed for most samples. However, a sample (KD) did not show any release of SO_2 during regeneration. That is a composition being able to keeps SO_x even at 550°C with λ=0.99.

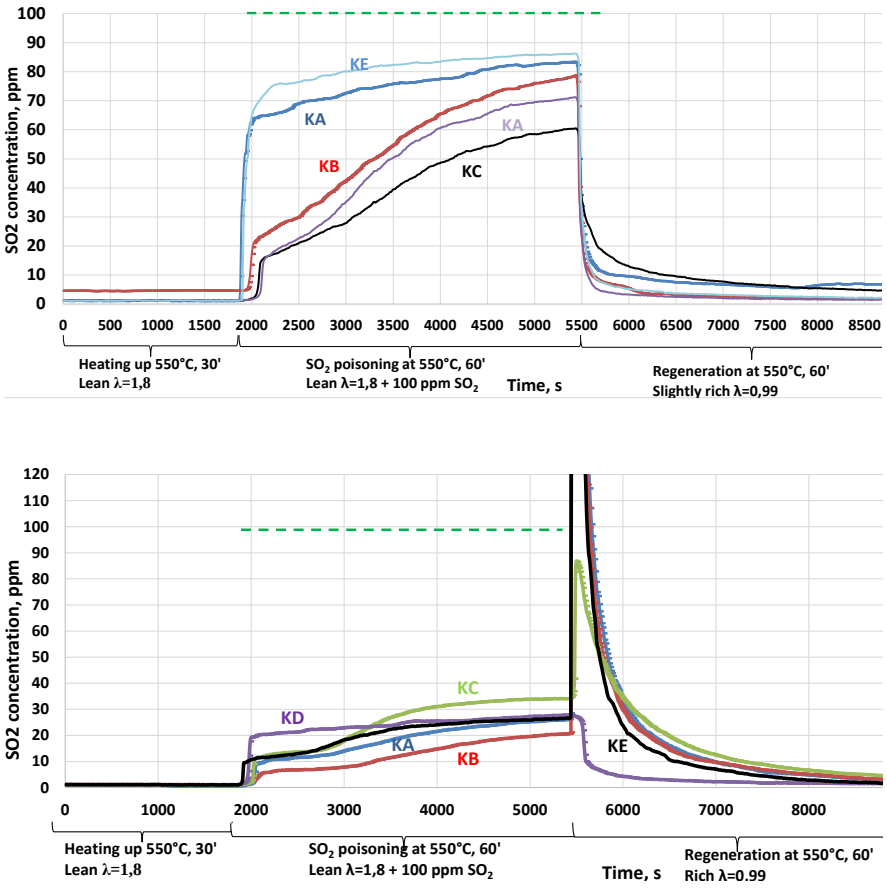

Figure 3. SO_2 adsorption and desorption on Pt-free (up) and Pt-containing (down) LSTs.

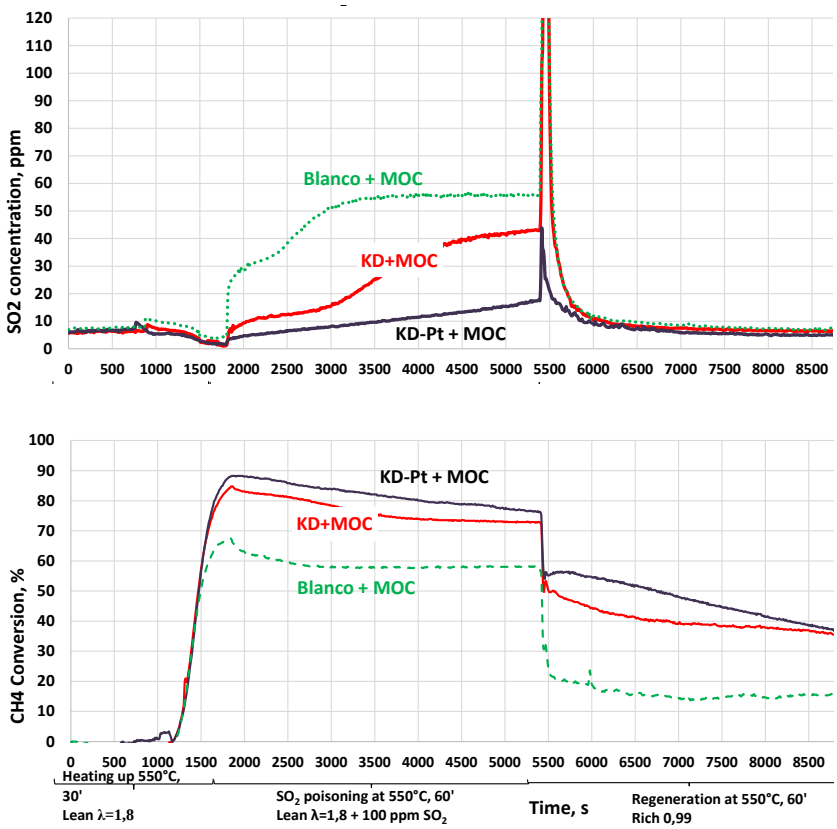

Figure 4. SO_2 adsorption and release, and methane conversion during sulfation and regeneration on LST + MOC at 550°C.

Experiments with the combinations of LST + MOC showed that the presence of sulfur adsorbent and Pt on LST enhanced SO_x adsorption and kept methane conversion on a higher level (Figure 4). It was detected a saturation by longer experiments (4 hours, corresponding about 400 h in use conditions) and then SO_2 started to by-pass LST+MOC.

4.3.2 NO_x removal with vanadium SCR catalysts

Vanadium-SCR catalysts (V_2O_5/TiO_2-WO_3) are the main stream for marine applications due to temperatures, sulfur content and costs. New types of metal vanadate were also investigated for marine applications. Traditionally Dinex has prepared metal-substrated V-SCR catalysts but similar catalyst compositions were also added on ceramic substrates in this project. The activity and hydrothermal (HT) durability was dependent on vanadium concentration (range of 1 - 4 wt-%) in porous support. Higher V_2O_5 loadings (>3 wt-%) result in improved low temperature activity

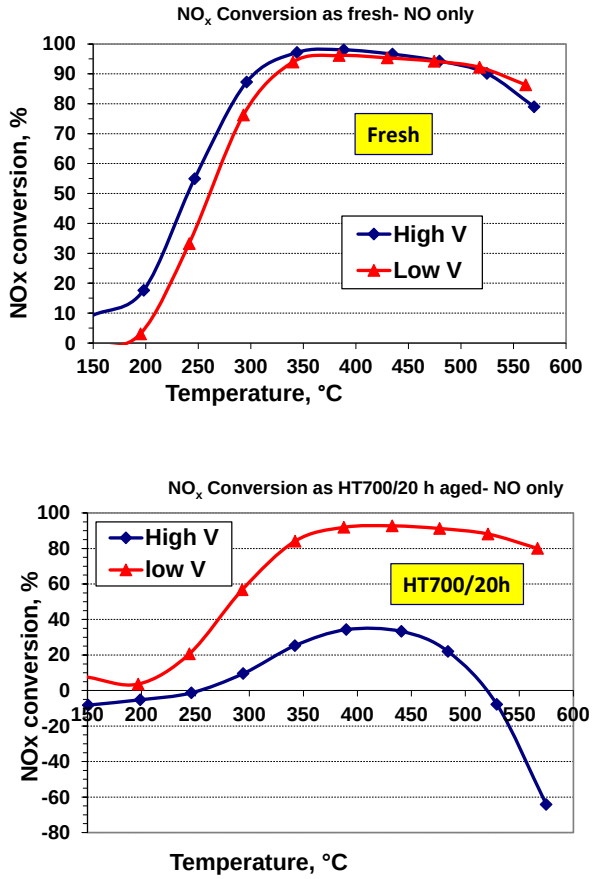

Figure 5. NO_x conversion on fresh and aged V-SCR catalyst in NO only feed gas (1000 ppm NO, 1000 ppm NH_3, 10% O_2, 10% water in N_2, ceramic 400 cpsi, SV 50.000 h^{-1}).

and lower HT durability (Figure 5). These higher V loading are applied to applications where temperatures never exceed about 550°C but V-SCR catalysts for an operation at 500 - 600°C is based on lower V loading (1.5 - 2.0 wt-%)

Ammonia slip catalyst has also additional role to remove CO and reactive HCs in marine applications, when diesel oxidation catalyst (DOC) is not present when sulfur is high (Figure 6). Even if HC raw emissions are usually low in marine engines, CO from urea can be high and aldehydes are harmful compound to be removed in diesel and NG engines. A small ASC (high SV) with a very low Pt loading has a negligible effect on sulfate formation (→ particulates) but the oxidation of CO, aldehydes and unsaturated HCs (like C_3H_6) was enhanced in comparison to V-SCR catalyst only. However, saturated HCs (CH_4, C_2H_6, C_3H_8) require a large MOC type catalyst to be oxidized efficiently.

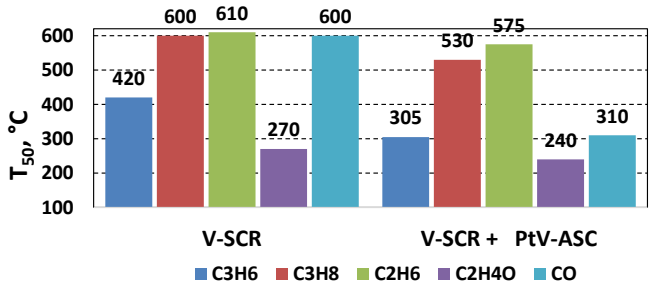

Figure 6. HC and CO light-off (T_{50}: 50% conversion) on V-SCR and V-SCR+ASC (5 g/cft Pt) in simulated lean exhaust gas (SCR+ASC: 50.000+ 100.000 h^{-1}).

4.4 Conclusions

The results gave an indication of the possible utilization of SO_x traps to improve MOC efficiency and durability. In next steps, the design and method of LST+MOC will be optimized to match best for the real applications. In future, diesel, natural gas and hybrids are alternatives requiring each tailored ATS strategy/designs for NO_x, SO_x, HCs and particulate matter (PM → DPFs) by emission legislations.

References

[1] R. Abbasi, G. Huang, G. M. Istratescu, L. Wu and R. E. Hayes, Methane Oxidation Over Pt, Pt:Pd and Pd based Catalysts: Effects of pre-treatment. *The Canadian Journal of Chemical Engineering, 9999 (2015) 1-9.*

[2] T. Maunula, K. Kallinen, N. Kinnunen, M. Keenan and T. Wolff, Methane abatement and catalyst durability in heterogeneous lean-rich and dual-fuel conditions. *Topics in Catalysis 62 (2019) 315-323.*

[3] M. Honkanen, J. Wang, M. Kärkkäinen, M. Huuhtanen, H.Jiang, K. Kallinen, R. L. Keiski, J. Akola and M. Vippola, Regeneration of sulfur-poisoned Pd-catalyst for natural gas oxidation. *Journal of Catalysis 358 (2018) 253-265.*

[4] N.M. Kinnunen, J.T. Hirvi, K. Kallinen, T. Maunula, M. Keenan and M. Suvanto, Case study of a modern lean-burn methane combustion catalyst for automotive applications: what are the deactivation and regeneration mechanisms? *Appl. Catal. B Environ. 207 (2017) 114-119.*

5. Regeneration of methane oxidation catalyst

Kati Lehtoranta [a) 1], Hannu Vesala [a) 1], Päivi Koponen [a) 1], Kauko Kallinen [b)], Teuvo Maunula [b) 2], Heikki Korpi [c) 3], Juha Kortelainen [c) 3]
[a)] VTT Technical Research Centre of Finland Ltd
[b)] Dinex Finland Oy,
[c)] Wärtsilä Finland Oy

5.1 Introduction

Liquefied natural gas (LNG) utilization as marine fuel is increasing. With LNG, both SO_x and NO_x regulations of the IMO (International Maritime Organization) can be achieved without any need for after-treatment, since natural gas (NG) is nearly sulphur free, resulting in no SO_x emissions while low NO_x levels can be achieved due to low combustion temperature of natural gas (in lean burn conditions). In addition, particle emissions form natural gas combustion are low and, in practice, no black carbon is formed from NG combustion [1]. Moreover, CO_2 emission is lower with NG use compared to diesel fuels because NG is mainly composed of methane with a higher H/C ratio compared to diesel. The hydrocarbon emissions, on the other hand, are higher with NG compared to diesel fuels [2-5]. Because natural gas is mainly methane, most of the hydrocarbon emissions is also methane. Since methane is a strong greenhouse gas, its emissions should be minimized.

One option to reduce methane emissions is the use of oxidation catalyst. In order to oxidize methane, a highly efficient catalyst is needed. Challenge in the development of methane oxidation catalyst is the catalyst deactivation since as little as 1 ppm SO_2 present in the exhaust has already been found to inhibit the oxidation of methane [6, 7].

In this study the performance and regeneration of one methane oxidation catalyst (MOC) is studied.

[1] Contact: firstname.lastname@vtt.fi
[2] Contact: tma@dinex.fi
[3] Contact: firstname.lastname@wartsila.com

5.2 Experiment setup

The research facility included a passenger car gasoline engine that was modified to run with natural gas. The engine with the test facility was presented in detail in Murtonen et al.[8]. The engine was operated with a lean air-to-fuel mixture. With this facility the exhaust gas flow and temperature (measured upstream of the catalysts) were adjusted independently, and therefore, it was possible to keep the exhaust gas composition and flow constant while changing only the temperature.

The NG was from Nord Stream and was high in CH_4 content (>95%). The sulphur content of the gas was below 1.5 ppm. The lubricating oil sulphur content was 2100 mg/kg, density was 0.85 kg/dm^3 and viscosity at 100 ºC was 13.4 mm^2/s.

Methane oxidation catalyst (MOC) utilized platinum-palladium as active metals. In addition to MOC only, similar studies were done with a SO_x trap installed in front of the MOC. The SO_x trap utilized platinum as catalyst.

Additional SO_2 was fed into the exhaust (see Figure 1) in part of the ageing tests contributing to a 1 ppm increase in the exhaust gas while any sulphur from the natural gas and lubricating oil, led to a SO_2 level of approximately 0.5 ppm in the exhaust gas. This means SO_2 level of 0.5 ppm without any additional SO_2 and SO_2 level of 1.5 ppm with the added SO_2 in the exhaust, respectively. Altogether, three similar experimental campaigns were conducted. Two tests were done with MOC only, one test with additional SO_2 and the other one without SO_2 addition. The third test was conducted with SO_x trap installed before the MOC (including the additional SO_2 in the exhaust gas).

The experiments were conducted over a 180 hours' ageing at the selected driving mode with exhaust temperature adjusted to 550º C and exhaust flow to 60 kg/h. The engine was running without stops and once a day regeneration was done by turning the engine to stoichiometric condition for 5 minutes.

Emission measurements were done at the upstream and downstream of the catalyst system (see Figure 1). This included a Horiba PG-250 analyser used to measure NO_x, CO, CO_2, and O_2. Online SO_2 emissions were determined by a Rowaco 2030 1 Hz FTIR Spectrometer. MicroGC was used to measure the hydrocarbons and hydrogen (H_2). Moreover, multiple gaseous components were measured continuously by two Gasmet FTIR spectrometers simultaneously at the upstream and downstream of the catalyst system.

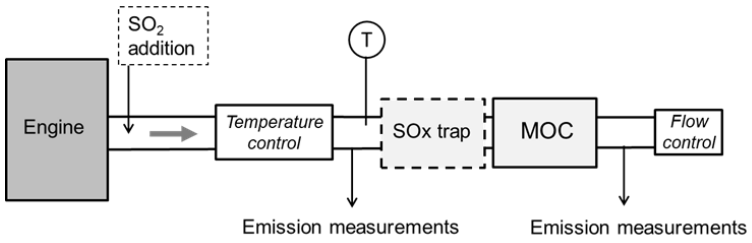

Figure 1. The experiment setup.

5.3 Results and discussion

To oxide methane, in addition to the effective catalyst, high temperature is required. This was found to be true in the present study as well. After pre-conditioning the catalyst for 48 hours in the engine exhaust, the initial performance was defined by measurements at the upstream and downstream of the catalyst. Figure 2 presents the initial methane conversion as a function of exhaust temperature and at three different exhaust flows. At exhaust temperature of 400 ºC, the methane conversion was found to be negligible (only 2%). However, when increasing the temperature, the methane conversion increases sharply, being above 20% at exhaust temperature of 460 ºC, above 60% at exhaust temperature of 500 ºC and at the highest temperature of 550 ºC the methane conversion is approx. 70%. Furthermore, the lower exhaust flow (40 kg/h) studied at 550°C increased the methane conversion to near 80% which is reasonable since the lower exhaust flows mean more time for the catalytic reactions to occur.

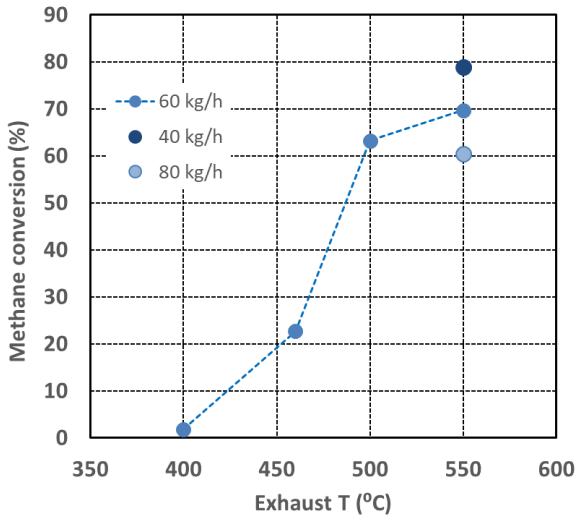

Figure 2. Initial methane conversion for 'trap+MOC' case (the line is to guide eye only).

The methane conversion of the MOC was found to decrease rather quickly over time. Regeneration, done once a day, after each 20 h of driving, was however found to be able to recover the methane efficiency of the catalyst. During the 5 minutes' regeneration, a release of SO_2 was detected at the downstream of the catalyst.

The exhaust SO_2 level had a clear influence on the methane efficiency, since when MOC was aged with 1 ppm extra SO_2 added to the exhaust, the methane conversion after each 20 h of driving was lower compared to the case where MOC was aged without any extra SO_2 in the exhaust (see Figure 3). The SO_x trap was found to shield the MOC since when the same ageing was conducted with trap

installed at the upstream of the MOC, the methane efficiency was similar to the case with no SO_2 added to the exhaust.

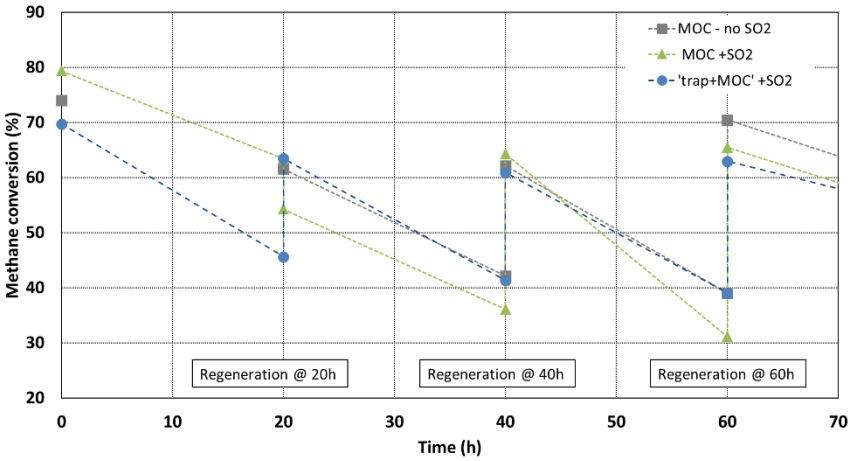

Figure 3. Methane conversion during ageing. Regenerations done after each 20h.

These results give indication of the possible utilization of MOC in LNG ships to control methane slip emissions. However, the regeneration process in real sized marine engine is an issue that needs to be investigated. Further catalyst development, regarding the efficiency and sizing, might also be needed to have the catalyst size suitable to be installed in high-temperature conditions in the exhaust line.

References

[1] Lehtoranta, K.; Aakko-Saksa, P.; Murtonen, T.; Vesala, H.; Ntziachristos, L.; Rönkkö, T.; Karjalainen, P.; Kuittinen, N.; Timonen, H. Particulate Mass and Nonvolatile Particle Number Emissions from Marine Engines Using Low-Sulfur Fuels, Natural Gas, or Scrubbers. *Environ. Sci. Technol.* 2019, *53* (6), 3315–3322. https://doi.org/10.1021/acs.est.8b05555.

[2] Anderson, M.; Salo, K.; Fridell, E. Particle- and Gaseous Emissions from an LNG Powered Ship. *Environ. Sci. Technol.* 2015, *49* (20), 12568–12575. https://doi.org/10.1021/acs.est.5b02678.

[3] Lehtoranta, K.; Murtonen, T.; Vesala, H.; Koponen, P.; Alanen, J.; Simonen, P.; Rönkkö, T.; Timonen, H.; Saarikoski, S.; Maunula, T.; et al. Natural Gas Engine Emission Reduction by Catalysts. *Emiss. Control Sci. Technol.* 2017, *3* (2), 142–152. https://doi.org/10.1007/s40825-016-0057-8.

[4] Hesterberg, T. W.; Lapin, C. A.; Bunn, W. B. A Comparison of Emissions from Vehicles Fueled with Diesel or Compressed Natural Gas. *Environ. Sci.*

Technol. 2008, *42* (17), 6437–6445. https://doi.org/10.1021/es071718i.

[5] Liu, J.; Yang, F.; Wang, H.; Ouyang, M.; Hao, S. Effects of Pilot Fuel Quantity on the Emissions Characteristics of a CNG/diesel Dual Fuel Engine with Optimized Pilot Injection Timing. *Appl. Energy* 2013, *110*, 201–206. https://doi.org/10.1016/j.apenergy.2013.03.024.

[6] Ottinger, N.; Veele, R.; Xi, Y.; Liu, Z. G. Desulfation of Pd-Based Oxidation Catalysts for Lean-Burn Natural Gas and Dual-Fuel Applications. *SAE Int. J. Engines* 2015, *8* (4), 1472–1477. https://doi.org/10.4271/20l5-0l-0991.

[7] Lampert, J. K.; Kazi, M. S.; Farrauto, R. J. Palladium Catalyst Performance for Methane Emissions Abatement from Lean Burn Natural Gas Vehicles. *Appl. Catal. B Environ.* 1997, *14* (3–4), 211–223. https://doi.org/10.1016/S0926-3373(97)00024-6.

[8] Murtonen, T.; Lehtoranta, K.; Korhonen, S.; Vesala, H.; Koponen, P. Imitating Emission Matrix of Large Natural Catalyst Studies in Engine Laboratory. In *28th CIMAC World Congress*; 2016; Vol. Paper #107.

6. Catalytic oxidation of methane: Modeling and simulations

Kirsi Spoof-Tuomi[1]
University of Vaasa

6.1 Introduction

Natural gas is of great interest nowadays in the effort to move towards less polluting marine fuels. Gas engines operating in lean conditions have proven to be successful in maintaining high efficiency while reducing NO_x, SO_x, CO_2, and PM emissions. However, these benefits are, in part, offset by unacceptable levels of methane emissions in the exhaust gas of lean-burn gas engines. In our previous study [1], we concluded that only 2.5% methane slip from LNG combustion already negated the benefit of reduced CO_2 emissions, leading to global warming potential equal to diesel fuel. This underlines the importance of controlling methane emissions from gas engines.

A methane oxidation catalyst (MOC) is increasingly being considered as a critical component in the exhaust after-treatment architecture of lean-burn gas engines. The oxygen present in exhaust gases from lean-burn engines enables the oxidation of CO and hydrocarbons (HC) over an oxidation catalyst. However, the conversion of methane remains more challenging compared to other HCs because high catalyst temperatures are necessary for the oxidation of this highly stable compound [2]. In addition, under lean-burn conditions, the oxidation reaction occurs in the presence of large quantities of water, which has a deactivating effect on catalysts. Furthermore, methane oxidation catalysts are sensitive to sulfur poisoning, even at very low sulfur levels. Sulfur present in lean-burn conditions, dominated by large excess of air, will be oxidized to SO_2, and further to SO_3, leading to the formation of sulfates and sulfites on both the noble metal active phase and the support [3]. Gremminger et al. [3] found that even less than 0.3 ppm of sulfur species led to the accumulation of sulfur on MOC and caused rapid deactivation of the catalyst.

[1] Contact: firstname.lastname@uva.fi

The ability to regain CH_4 conversion activity of deactivated catalyst via a regeneration mechanism is a critical issue for lean-burn gas engine applications. There are two ways for regenerating sulfur poisoned PGM-based catalysts. The first method is thermal regeneration. The problem with this approach is that temperatures required for regeneration are high. Studies have shown that complete regeneration is not possible even at a temperature of 650°C [2,4]. Another approach for catalyst regeneration is to change the chemistry of the exhaust gas. [4] For example, lowering the oxygen concentration in the catalyst feed gas can aid regeneration [5].

This study aims to investigate the potential of using a simulation-based approach for predicting MOC behavior over time, i.e., deactivation and the effect of regeneration. The simulation model was created by GT-SUITE software developed by Gamma Technologies, LLC. Global kinetics was used to represent the oxidation reactions over a bimetallic Pt-Pd catalyst. The SO_2 effects were further added to the model. Finally, the complete model was used to simulate catalyst regeneration by changing the temperature and exhaust gas composition.

6.2 Materials and methods

The catalyst modeled in this study was a bimetallic Pt-Pd catalyst with the Pt/Pd weight ratio of 1:4. The noble metal loading in the catalyst was 200 g/ft^3 (7.06 g/l). Gamma alumina (γ-Al_2O_3) served as the support material.

6.2.1 Kinetic modeling

According to the software provider, typically two HC's in the system is sufficient and practical for modeling purposes. In general, one fast oxidizing and one slow oxidizing, or large HC, need to be modeled [6]. In our model, C_2H_6 represented the fast oxidizing HC and CH_4 the slow HC. Among alkanes, methane is the kinetically least reactive molecule [7].

The set of oxidizing reactions considered in this work was:

$$CO + 0.5O_2 \rightarrow CO_2$$
$$H_2 + 0.5O_2 \rightarrow H_2O$$
$$C_2H_6 + 3O_2 \rightarrow 2CO_2 + 2H_2O$$
$$CH_4 + 2O_2 \rightarrow CO_2 + 2H_2O$$
$$NO + 0.5O_2 \rightarrow NO_2$$

6.2.2 Model calibration

MOC calibration means finding a set of reaction rates that best fits the measured data so that the model adequately predicts the conversion of reactants over the range of expected exhaust gas temperatures, flow rates, and species concentrations [6]. Typically, there are two rate constants for each reaction that

needs to be calibrated; the frequency factor or pre-exponent multiplier, A, and the activation energy, E_a, in units of J/mol:

$$k = A \cdot exp\left(\frac{-E_a}{RT}\right),$$

where k is the rate constant, R is the universal gas constant in units of J/mol/K, and T is the temperature in units of K. The term E_a/R is also known as the activation temperature in units of K.

According to Arrhenius reaction kinetics:

$$Rate = k[A]^a[B]^b$$

Extending this to surface reactions involving coverages, the full rate becomes:

$$Rate = k \cdot [concentration_{term}]^{order}(reactant\ coverages)(inhibition\ functions)$$
$$= A \cdot exp\left(\frac{-E_a}{RT}\right)[C_i]^j(\theta_i)(G_i)$$

6.2.3 Experimental data

The experimental data were obtained from the catalyst developer. It included HC and CO light-off performance tests on both fresh and sulfur-poisoned catalysts. The sulfur-poisoned catalyst was first aged hydrothermally at 700°C for 20 h (10% H_2O in air) and then treated for 20 h at 400°C with a sulfur-containing gas having a concentration of 25 ppm SO_2. The exact inlet gas compositions are tabulated in Table 1.

Table 1. Simulated exhaust gas and SO_2 poisoning mixtures.

	Simulated exhaust gas	**SO_2 poisoning mixture**
CH_4	1500 ppm	–
C_2H_6	300 ppm	
C_3H_8	100 ppm	–
C_2H_4O	150 ppm	
NO	500 ppm	–
CO	1200 ppm	0.05%
H_2O	8%	10%
CO_2	7.5%	10%
O_2	10%	6.5%
SO_2		25 ppm
N_2	Bal.	Bal.
GHSV	50 000 h^{-1}	

6.2.4 Sulfur deactivation

To further develop the model, the SO_2 effects were added to the model. The sulfur poisoning model used in this study is based on the work of Gayatri [8]. In this 4-site reaction mechanism, each site represents a different surface species:

- S1: Loosely bound SO_2 on PGM-site. This desorbs at low temperatures.
- S2: Surface sulfite. Present at typical MOC operating temperatures. Affect the active sites on PGM.
- S3: Surface sulfate. Present at typical MOC operating temperatures. Affect the active sites on PGM.
- S4: (Bulk) Sulfate on Alumina. SO_2 adsorbed on S4 site involves the bulk alumina and should not affect PGM active sites.

The reaction steps and rate expressions for SO_2 adsorption on and desorption from the catalyst are as follows:

$SO_2 + S1 \leftrightarrow SO_2–S1$ $\quad r1 = A_1\exp(-E_1/RT)[SO_2]\theta_{S1}$

$\quad r2 = A_2\exp(-E_2(1-\alpha_1\theta_{SO2-S1})/RT)\theta_{SO2-S1}$

$SO_2 + S2 \leftrightarrow SO_2–S2$ $\quad r3 = A_3\exp(-E_3/RT)[SO_2]\theta_{S2}^3$

$\quad r4 = A_4\exp(-E_4(1-\alpha_2\theta_{SO2-S2})/RT)\theta_{SO2-S2}^3$

$SO_2 + S3 \leftrightarrow SO_2–S3$ $\quad r5 = A_5\exp(-E_5/RT)[SO_2]\theta_{S3}^3$

$\quad r6 = A_6\exp(-E_6/RT)\theta_{SO2-S3}$

$SO_2–S3 + S4 \leftrightarrow SO_2–S4 + S3$ $\quad r7 = A_7\exp(-E_7/RT)\theta_{SO2-S3}^3\theta_{S4}$

$\quad r8 = A_8\exp(-E_8/RT)\theta_{S3}^3\theta_{SO2-S4}$

6.3 Results and discussion

The kinetic parameters for CH_4, C_2H_6 and CO were first calibrated to best fit the experimental data without sulfur effect. Thus, light-off experiments with the fresh catalyst were used as a basis for calibration. Inhibition functions were adopted from the DOC_Sampara and Bisset model in the GT-Suite library. Table 2 summarizes the temperatures for 50% and 90% conversions, frequency factors, and activation energies for CH_4, C_2H_6 and CO after calibration. A more detailed description of conversion curves for CH_4 is presented in Figure 1.

Table 2. $T_{50\%}$ and $T_{90\%}$, frequency factors and activation energies for CH_4, C_2H_6 and CO.

	$T_{50\%}$ (°C)		**$T_{90\%}$ (°C)**		**A**	**E_a (J/mol)**
	measured	simulated	measured	simulated		
CH_4	366	369	425	425	2.614E+06	88898
C_2H_6	348	348	389	393	3.692E+05	69525
CO	165	165	189	185	9.828E+04	24960

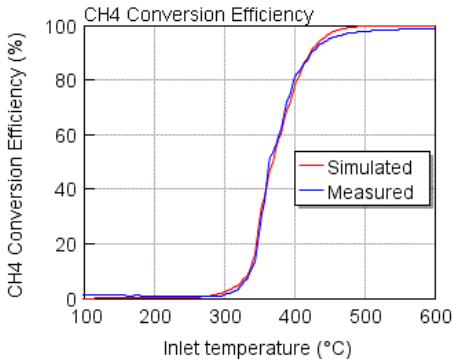

Figure 1. Measured and predicted conversion curves for CH_4 after calibration.

Following this, the SO_2 reactions were calibrated and added to the model. The completed model was then run at three different temperatures, 400°C, 450°C and 500°C, which are typical in lean operating natural gas engines [9]. Overall, the simulation indicated a fast deactivation of the catalyst in the presence of SO_2. At 400°C, a dramatic drop of the CH_4 conversion could be observed, resulting in less than 10% methane conversion after 20 h exposure time on SO_2 containing (25 ppm) stream. Similarly, at 450°C and 500°C the CH_4 conversion decreased rapidly during the first 4 h, eventually leading to CH_4 conversion of 30% and 70% after 20 h time on SO_2 containing stream (Figure 2). After 20 hours exposure on SO_2 containing stream, CO $T_{90\%}$ increased from 189°C to 224°C, and C_2H_6 $T_{90\%}$ from 389°C to 492°C, respectively.

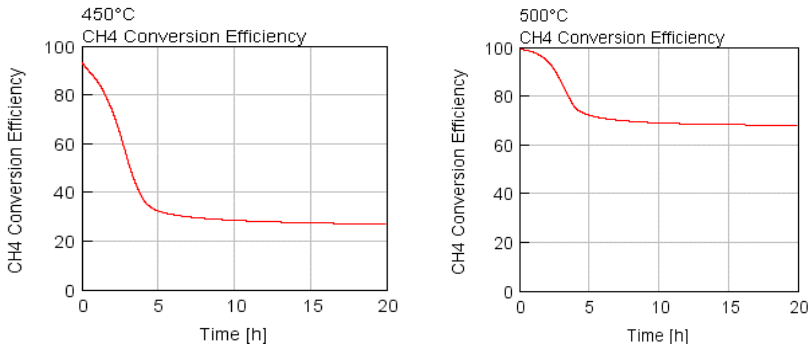

Figure 2. CH_4 conversion as function of time on SO_2 containing stream at two different temperatures.

Finally, the model was run to predict the effect of the regeneration process. In the simulations, both the air-fuel ratio and the temperature were varied. The choice of this approach was based on Gremminger et al. [3]. They found that regeneration by reductive treatment combined with temperatures above 500°C was the most efficient for catalyst regeneration.

Results from the simulation are depicted in Figure 3. The first 5 hours demonstrates the deactivation of a fresh catalyst at 450°C with

- 25 ppm SO_2
- 1500 ppm CH_4
- 300 ppm C_2H_6
- 100 ppm C_3H_8
- 500 ppm NO
- 1200 ppm CO
- 10% O_2
- 8% H_2O
- 7.5% CO_2

in N_2. The model predicted a CH_4 conversion decrease from over 90% in fresh state to 35% in SO_2-poisoned state. After 5 hours, the regeneration period takes place. To regenerate the SO_2-poisoned catalyst, a 30 min reductive treatment is applied at 550°C. The regeneration mixture consisted of

- 9800 ppm CH_4
- 200 ppm C_2H_6
- 2.02% O_2 (λ=1)

in N_2. The model now predicted a CH_4 conversion increase from 35% in SO_2-poisoned state (at 450°C) to 95% in regenerated state (at 550°C). The result is in line with the experimental data, which showed a 95% conversion at 550°C after 30 min regeneration by reductive treatment. The decrease in CH_4 conversion during the process is due to lack of excess O_2 in the reaction gas feed [10]. Figure 3 also illustrates the release of SO_2 from the catalyst during the regeneration procedure.

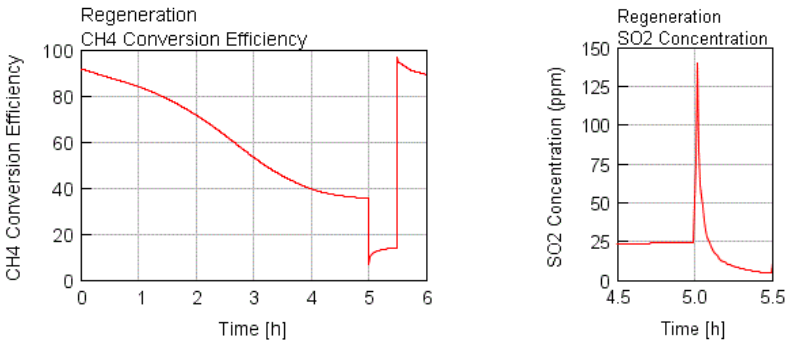

Figure 3. CH_4 conversion (left) and SO_2 release (right) during regeneration.

To elaborate the model further, more detailed modelling of the reactions that may occur during regeneration could be incorporated. For example, in wet conditions, steam reforming and possibly water–gas shift reactions may take place during reductive treatment, providing hydrogen gas for low-temperature sulfate decomposition [10].

The accuracy level of the model created in this study is limited due to the limited experimental data available. To achieve reasonable confidence in a predictive after-treatment model, the test protocol should be designed in such a way that it enables accurate calibration. The user should be able to verify the thermal properties with confidence before moving on to calibrating kinetics. Therefore, a stand-alone experiment to characterize the thermal behavior of the reactor should be performed before attempting to calibrate reaction kinetics. To be able to simulate changes occurring under transient conditions, the set of experiments should cover a wide range of inlet conditions in terms of space velocity and gas temperature [6]. Furthermore, varying the concentrations of gas-phase components (CH_4, NO, SO_2, O_2, and H_2O) in the inlet stream would benefit, e.g., tuning the inhibition terms [11].

6.4 Conclusions

The objective of this study was to explore the feasibility of using a simulation-based approach to predict MOC behavior over time, i.e., deactivation and the effect of regeneration. The catalyst simulation model was created with GT-SUITE software. The model was calibrated against experimental data collected from light-off performance tests on fresh, aged, and regenerated catalysts.

The main conclusions were:

1. For the fresh catalyst, the model agreement with the experimental observations was good.
2. Catalyst deactivation due to sulfur poisoning was successfully modeled by linking the CH_4 oxidation reaction dependent on the empty PGM-site coverages.
3. The catalyst model, and its underlying kinetic parameter set, predicted catalyst regeneration by varying the temperature and exhaust composition reasonably. The accuracy of the model under transient conditions could be improved by fine-tuning it further against varying inlet concentrations and flow rates.
4. To ensure the reliability of a predictive after-treatment model, a very careful test protocol design is required.

Acknowledgments

The author would like to express her gratitude to Dinex Finland Oy for providing the experimental data for model calibration.

References

[1] Spoof-Tuomi, K.; Niemi, S. Environmental and Economic Evaluation of Fuel Choices for Short Sea Shipping. *Clean Technol.* 2020, *2*, 34-52, doi: 10.3390/cleantechnol2010004.

[2] Gélin, P., Urfels, L., Primet, M., Tena, E. Complete oxidation of methane at low temperature over Pt and Pd catalysts for the abatement of lean-burn natural gas fuelled vehicles emissions: influence of water and sulphur containing compounds. *Catal. Today* 2003, 83, 45–57, doi:10.1016/S0920-5861(03)00215-3.

[3] Gremminger, A., Lott, P., Merts, M., Casapu,M., Grunwaldt, J-D., Deutschmann, O. Sulfur poisoning and regeneration of bimetallic Pd-Pt methane oxidation catalysts. *Appl. Catal. B* 2017**,** 218, 833–843, doi: 10.1016/j.apcatb.2017.06.048.

[4] Leprince, T., Aleixo, J.,Williams, S., Naseri, M. Regeneration of palladium based catalyst for methane abatement. *CIMAC Congress* 2004, Kyoto. Paper no. 210. Available at: https://www.dcl-inc.com/pdf/papers-publications/13.pdf.

[5] Kinnunen, N.M., Hirvi, J.T., Kallinen, K., Maunula, T., Keenan, M., Suvanto, M. Case study of a modern lean-burn methane combustion catalyst for automotive applications: What are the deactivation and regeneration mechanisms? *Appl. Catal. B* 2017, 207, 114–119, doi: 10.1016/j.apcatb.2017.02.018.

[6] Gamma Technologies LLC. GT-Suite, Exhaust Aftertreatment Application Manual, 2020.

[7] Gremminger, A.T., Pereira de Carvalho, H.W., Popescu, R., Grunwaldt, J-D., Deutschmann, O. Influence of gas composition on activity and durability of bimetallic Pd-Pt/Al2O3 catalysts for total oxidation of methane. *Catal. Today* 2015*,* 258, 470–480, doi: 10.1016/j.cattod.2015.01.034.

[8] Gayatri, Mohit. A Global Kinetic Model for a Diesel Oxidation Catalyst Incorporating Mechanisms for Sulfur Poisoning and Surface Oxidation. CLEERS Workshop September 17th–19th 2019. Available at: https://cleers.org/wp-content/uploads/formidable/3/2019CLEERS_Gayatri.pdf.

[9] Auvinen, P., Kinnunen, N.M., Hirvi, J.T., Maunula, T., Kallinen, K., Keenan, M., Baert, R., van den Tillaart, E., Suvanto, M. Development of a rapid ageing technique for modern methane combustion catalysts in the laboratory: Why does SO2 concentration play an essential role? *Appl. Catal. B* 2019, 258,117976, doi: 10.1016/j.apcatb.2019.117976.

[10] Kinnunen, N.M., Nissinen, V.H., Hirvi, J.T., Kallinen, K., Maunula, T., Keenan, M., Suvanto, M. Decomposition of Al2O3-Supported PdSO4 and Al2(SO4)3 in the Regeneration of Methane Combustion Catalyst: A Model Catalyst Study. *Catalysts* 2019, *9*(5), 427, doi: 10.3390/catal9050427.

[11] Sadokhina, N., Ghasempour, F., Auvray, X. et al. An Experimental and Kinetic Modelling Study for Methane Oxidation over Pd-based Catalyst: Inhibition by Water. *Catal Lett* 2017, 147, 2360–2371, doi: 10.1007/s10562-017-2133-2.

7. Assessing future marine technologies for reducing emissions

Janne Huotari[1]
Aalto University

The maritime sector is projected to undergo a drastic energy transition that will start affecting the industry soon. The main goal of this transition is to reduce the carbon emissions of shipping by 70% by 2050. According to predictions, this carbon emissions reduction can be achieved with a combination of emission reduction technologies and adopting alternative fuels, with each of these measures contributing an approximately equal amount to the end carbon emissions reduction. Technologies like fuel cells and batteries have the potential to reduce carbon emissions significantly, but technological maturity and adoption rates need to improve significantly to make them economically competitive. LNG is expected to be the most prominent fuel to replace current fuel oils and MGO in the short term. In the long term, the used fuel mix will need to gradually shift towards CO_2-free alternatives like ammonia or synthetic methane produced from renewable hydrogen. Biofuels may also be a long-term solution, but more research is needed on their environmental and socioeconomic effects.

7.1 Introduction

The International Maritime Organization (IMO) has made a preliminary plan to reduce maritime greenhouse gas (GHG) emissions by 50% by 2050, in accordance with the Paris Agreement. As a result, the design and operation of maritime vessels will undergo drastic changes in near future. Currently, shipping related emissions are regulated by MARPOL Annex VI (IMO, 2020), which limits the amount of CO_2, NO_x, SO_x, and particulate matter (PM) a ship may emit. Shipping was responsible for about 2.2% of total anthropogenic GHG emissions in 2014 (IMO, 2015). However, this figure may rise drastically in the future, as maritime trade is projected to increase by 39% by 2050 (DNV GL, 2019) and business-as-usual scenario

[1] Contact: firstname.lastname@aalto.fi

predictions paint a grim picture of potential GHG emissions in the future (IMO, 2015).

CO_2 emission reductions are realized for newbuilds through a specified energy efficiency design index (EEDI). This index allows less and less CO_2 emissions progressively towards the future. In early 2020, the global sulphur limit of marine fuels was reduced from 3.5% to 0.5%. In addition, fuel sulphur content has been limited to 0.1% in specified emission control areas (ECA) from 2015 onwards. Ships can still operate with fuels containing more sulphur than these limits allow, but in this case, they must be fitted with exhaust gas treatment systems that reduce SO_x emissions.

NO_x emissions are regulated for ships that operate in specified NO_x control ECAs. These regulations will apply also to ships that operate in regions where future NO_x control ECAs are established. Newbuilds must comply with tier III NO_x regulations, which limit NO_x emissions to 9*n g/kWh, where n is the revolutions per minute (RPM) region the ships engine is operated as. For example, a 720 RPM motor is limited to 2.4 g/kWh NO_x emissions.

According to the current understanding, EEDI will not be enough to reduce shipping related GHG emissions by 50% by 2050. Carbon emissions of shipping will need to reduce by 70% by 2050 to reach this goal. Additional measures in the form of more stringent regulations or carbon pricing can be expected for the shipping sector soon. DNV-GL predicts that in a possible pathway to this goal, energy usage per tonne-mile will decrease by 35% - 40% by 2050 as a result from hull and machinery improvements, intelligent solutions and speed reductions. Rest of the carbon emissions will need to be reduced by having carbon neutral fuels account for 30%-40% of the total fuel mix of marine vessels by 2050. (DNV GL, 2019) (Anderson & Bows, 2012)

7.2 Technology options

Various technological improvements and new technologies can help decrease the energy usage of shipping per ton-mile by 35% - 40%. The adoption of many of these technologies is still in its infancy in the maritime sector, and thus they hold great potential in reducing overall GHG emissions. Some technologies may already be economically efficient, but significant barriers prevent widespread adoption. According to (Rehmatulla;Parker;Smith;& Stulgis, 2017), lack of sea-trials and split incentives was cited as the most important barriers in the way of adopting energy efficient technologies.

Lack of sea-trials for emerging technologies remains a large problem for the industry as few want to risk being early adopters. Investors might not be comfortable in making their decisions based on simulations alone, as they might be blind to several hidden costs associated with a technology. Better access to high quality ship energy consumption data is cited as a solution to this problem, accompanied by research utilizing this data of course.

Split incentive barriers arise from the length of contracts between charterers and ship owners, which applies to most merchandise vessels. The length of most chartering contracts falls well below the payback time of energy efficiency increasing measures. On the other hand, only 40% of savings accrued by using less fuel reflect back to the ship owners. These issues deter both parties from investing in these technologies. Third party financing solutions may be a solution to this issue.

7.2.1 Fuel cells

Interest towards fuel cells in maritime applications stems from their higher efficiency than ICEs. Low temperature fuel cells, such as proton exchange membrane (PEM) cells can reach efficiencies of 50%-60%, and high temperature cells, like the solid-oxide fuel cell (SOFC), can have an electrical efficiency as high as 80% if heat recovery systems are used. According to (Tronstad;Åstrand;Haugom;& Langfeldt, 2017), PEM fuel cells are the most feasible fuel cell solutions for smaller vessels, whereas high temperature PEM fuel cells and SOFCs are most feasible for larger vessels. Significant research is underway to scale up fuel cell technology, increase their efficiency and lower costs. Especially PEM cells have reached technological maturity due to their application to the automotive sector. DNV-GL predicts that fuel cells will be cost competitive for heavy vehicles in 2030 (DNV GL, 2019).

Fuel cells operate by converting the potential chemical energy of hydrogen-based fuels into electricity. The by-product of this conversion is water, which makes the technology locally emission-free. Low temperature cells are more stringent to what fuel they accept, with the PEM cell allowing only hydrogen to be used as fuel. High temperature cells are more flexible in this regard, and fuels such as ammonia, LNG or methanol may be considered.

The CAPEX of installing fuel cells has been estimated to be between 2000 – 6000 per kW. PEM fuel cells occupy the smaller cost range of this prediction, with high temperature PEM cells in the middle and SOFCs at the higher end. The OPEX for marine applications is expected to be 2-8 times as high as for a comparable internal combustion engine running on fossil fuel. Further adoption of the technology is expected to drive CAPEX down. For example, the cost of automotive PEM fuel cells is expected to drop to 280 USD per installed kW if manufacturing reaches 20,000 units per year. International rules regarding fuel cell installations on vessels is currently under development by the IMO. Fuel storage and supply rules currently cover LNG, with methanol underway. (DNV GL, 2019)

7.2.2 Batteries

Lithium-ion batteries have been recently installed on board smaller scale ferries and passenger vessels either as the primary energy source, or then as a hybrid solution. Massive research and economy of scale development is currently driven by the automotive sector. Various lithium-ion battery chemistries are available, with multiple sources pointing at NMC as the most feasible solution for ships. This is

mainly due to its high overall energy density. Maritime battery CAPEX is somewhat hard to estimate. Some studies predict that mass production of battery cells for the automotive sector will drop the price of batteries to 100-200 USD/kWh. This might offer some insight into how the cost of maritime batteries will develop as well. However, maritime battery systems are more tailor-made and thus more expensive than these mass-produced alternatives. Current estimates of maritime battery costs are about 1500 USD/kWh including the cost of the needed power electronics. (European Maritime Safety Agency, 2020)

While batteries may be sufficient as the sole energy provider in very small vessels, their price, mass and volume make them infeasible for the majority of ocean-going vessels. However, they may have a place in increasing the efficiency of the main power train of all vessels, or then as a power source during port operations. Possible future innovations such as solid-state batteries may improve battery energy density significantly, making them feasible for larger vessels and longer trips.

7.2.3 Wind propulsion

Wind propulsion technologies include applications that use wind energy to reduce the overall propulsion demand of a ship. These include Flettner rotors, kites and sails. While wind propulsion technology is not likely to act as the sole power producer of ships, it may be effective in contributing towards the goal of reducing energy usage per tonne-mile by 35% - 40%, which was discussed earlier.

According to (Rehmatulla;Parker;Smith;& Stulgis, 2017), Flettner rotor providers cite a payback time of five years or lower for their technology. However, the adoption of Flettner rotors in shipping remains in its infancy. Structural integrity of the rotor and cargo handling issues were seen as the most prominent barriers to adopting this specific technology. Classification societies play an important role in solving these problems. Furthermore, investors are worried about hidden costs that are not accounted for in the technology providers' models. For example, the recuperation of capital spent on Flettner rotors may necessitate altering the ships route to favour better wind conditions. This may in turn reflect negatively on profits due to longer shipping durations.

7.2.4 Other technologies

Waste heat recovery systems utilize the energy stored as heat in exhaust gas or high-temperature engine cooling cycles. The excess heat is typically used to generate high pressure steam in a boiler, which in turn can be used to generate electricity. Typical payback times of such systems are between 2 to 5 years, reflecting potential fuel savings between 4% - 16%. The payback time and fuel savings depend on the extent of the system installed. (Baldi & Cecilia, 2015)

Intelligent solutions such as optimized energy system unit commitment, route optimization, speed optimization and capacity utilization form their own group of

technological advancements. The benefits of such systems are of course highly case dependent, but their impact on CO_2 reduction potential is estimated in (Bouman;Lindstad;Rialland;& Strømman, 2017) to be between up to 25%. Such methods are attractive since they promise to utilize the available fleet more effectively without expensive modifications. However, more research is needed around these topics to realize their full potential.

Air lubrication of the ship hull has generated interest recently and some installations already exist. Typical reported fuel saving estimations range between 5% - 10% for these installations. The economic efficiency of these installations is hard to determine, since the type of technology employed differs significantly and no study specifically on this topic seems to be available. The benefit of applying such technology is that it can be relatively easily retrofitted to existing hulls. (Silverstream technologies, 2020), (Wärtsilä, 2020)

7.3 Fuel options

One of the most important properties of ship fuels is their volumetric energy density. A higher volumetric energy density allows a ship to operate longer without bunkering and thus generate more profits. Figure 1 demonstrates this energy density for a variety of selected fuels. Based on the figure, it is evident that batteries and hydrogen are infeasible as the primary energy sources for the majority of shipping. Most of the potential alternative fuels occupy the middle region of the graph, just below 20 MJ/l.

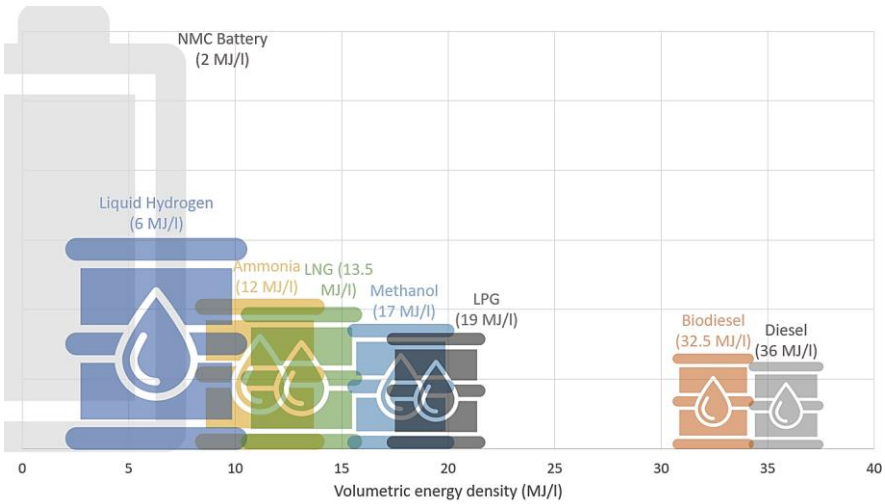

Figure 1. Fuel volumetric energy density comparison. The sizes of the fuel tanks illustrate the increasing storage space needed to store the same amount of energy.

7.3.1 LPG

Liquefied petroleum gas (LPG) is an oil refinery product, composed mostly of a mix of butane and propane that could potentially play a part in replacing HFO/MGO soon in the used fuel mix. It needs to be stored aboard either refrigerated, or then pressurized. Pressurized storage seems to be the more feasible option. LPG has a high volumetric energy density of 19 MJ/l, no SOx emissions and relatively low NO_x emissions. LPG is also expected to have significantly lower PM emissions compared to HFO. CO_2 emissions from LPG are approximately 16% lower compared to HFO. (DNV GL, 2019)

Only a 2-stroke full power ICE burning LPG is on the market. A de-rated 4-stroke variant is offered by Wärtsilä. Furthermore, Wärtsilä also offers a system where LPG is reformed to methanol, which can then be used as fuel in dual-fuel engines. The 2-stroke engine needs ECR/SCR systems to comply with tier III NO_x regulations. It is unclear whether a 4-stroke ICE would need these systems. (DNV GL, 2019)

The availability of LPG could in theory currently cover the marine sector. However, this would leave no LPG to be used elsewhere if production capacity is not increased. The CAPEX cost of an LPG tank is estimated to be roughly half of that of LNG tanks. LPG can somewhat compete with HFO in terms of pricing, just like LNG. It is currently more expensive than LNG, but cheaper than low sulphur fuel oils. International legislation regarding LPG as a marine fuel will take some time to be completed. (DNV GL, 2019)

7.3.2 Biofuels

Biofuels are fuels derived from biomass or biomass residue. The most promising derivatives of these for shipping include hydrotreated vegetable oil (HVO), fatty acid methyl ester (FAME) and liquefied biogas (LBG). Biofuels are an interesting candidate for replacing fuel oils, MGO and LNG in the future, because they can be used with the current infrastructure and technology with little or no modifications, and they promise significant CO_2 reductions. Biofuels of course produce similar emissions as fossil fuels when burned in an ICE, but the premise is that the GHG emissions are captured by the growing biomass used for biofuel production. This premise is however slightly controversial. Estimations of CO_2 reduction range between 19% - 88%. Some land-use and socio-economic problems are also associated with mass production of biofuels. In addition to CO_2 reductions, using biofuels emits very low SO_x and PM emissions. HVO and FAME need NO_x abatement technology, whereas LBG has similar NO_x emissions as LNG and meets Tier III NO_x regulations as is. (DNV GL, 2019)

Current usage of biofuels in shipping is very limited. The main barriers in way of its adoption include pricing and production at sufficient volumes. The pricing of biofuels is hard to estimate as the market for it is in its infancy, and regional prices vary by a large margin. International legislation regarding biofuel production and usage is underway. (DNV GL, 2019)

7.3.3 LNG

Liquefied natural gas is a fossil fuel that can be stored cryogenically onboard with medium volumetric energy density and used as fuel in modern dual-fuel ICEs. LNG can also be used as fuel in high temperature fuel cells. It is a promising alternative that could replace HFO and MGO soon, because it is cost competitive with HFO, abundantly available and reduces CO_2 emissions by up to 24% compared to HFO, depending on the type of engine technology used. Infrastructure for LNG bunkering is still quite limited but being developed around the world. LNG has very low SO_x emissions and similar NO_x and PM emissions as HFO with ECR/SCR. On the other hand, using LNG introduces the problem of methane slip, which is an issue since methane is about 34 times as potent GHG as CO_2. LNG storage tanks require about 3 times as much space as HFO, which makes it a suitable fuel for deep-sea ships. (DNV GL, 2019)

LNG emissions depend a bit on the used engine technology. Some studies have suggested that high pressure engines reduce GHG emissions by 20-24% compared to HFO, taking methane slip into account. However, these types of engines need NO_x abatement technology to comply with tier III NO_x regulations. Low pressure engines have naturally lower NO_x emissions, but the GHG reduction potential is only 0-18% since they are more susceptible to methane slip. (DNV GL, 2019)

The capital costs of LNG engine and fuel systems need to be reduced to make them economically competitive with builds that are more traditional. The CAPEX of an LNG powered ship is estimated to be 10-30% higher than a similar ship powered by HFO. Despite this, LNG is cited as the most promising alternative fuel, due to the cost competitiveness and availability of the fuel itself. LNG is the only alternative fuel that can meet the projected fuel demand for the next 10 year. There are currently 165 LNG powered vessels in operation, 154 confirmed orders and 500 LNG carriers using LNG as fuel. International legislation regarding LNG is ready. (DNV GL, 2019)

7.3.4 Methanol

Methanol is a fuel that can be used either in ICEs or in fuel cells. It is liquid in ambient temperature and thus easily stored aboard, although its volumetric energy density demands a fuel tank approximately 2.5 times the size of a comparable oil-based fuel. It has no SO_x emissions, but ECR/SCR systems need to be used with methanol to comply with NO_x tier III regulations. Most methanol today is produced from natural gas and the total CO_2 emissions of its life cycle are higher than HFOs comparative CO_2 emissions. However, methanol can also be produced from biomass reducing its life cycle GHG emissions drastically. Furthermore, methanol can also be produced from hydrogen and CO_2, making it a potential green fuel in the future. (DNV GL, 2020)

The CAPEX of methanol storage tanks is about 1/3 the cost of LNG tanks. Retrofitting traditional ICEs to use methanol as fuel is estimated to cost between

250-350 EUR per kilowatt for larger engines. The fuel is also widely available, although bunkering infrastructure is very limited. The price of methanol itself is close to MGO or slightly higher which acts as a significant barrier for its uptake. Methanol is unlikely to see widespread adoption due to its high price and poor current environmental performance. International legislation regarding using methanol as fuel should be covered soon. (DNV GL, 2019)

7.3.5 Hydrogen

Hydrogen has huge potential in the future, but low adoption rate currently. Storage options vary from storing it in medium to high pressure, with the possibility of also storing it as a liquid cryogenically. The latter option is preferable since it has the best volumetric energy density; the property in which hydrogen lacks most. Liquid hydrogen has a volumetric energy density of only 6 MJ/l, when the storage facility is accounted for. This results in a fuel tank 6 times the size of a fuel oil alternative, which makes hydrogen infeasible to use in deep-sea shipping. Furthermore, the cost of hydrogen a hydrogen storage tank is estimated to be a bit over twice the cost of an LNG storage tank. Hydrogen is most associated as the fuel used in fuel cells. However, it can also be used in ICEs with efficiencies of about 40-50%. Emissions from using hydrogen depend entirely on the emissions of the production method used, as hydrogen is emissions free locally. (DNV GL, 2019)

Currently, 95% of hydrogen is produced by steam reforming natural gas, a process with significant GHG emissions. In fact, total GHG emissions of using hydrogen produced with this method are higher than using traditional HFO. Despite this, hydrogen is a very expensive fuel and will not be cost competitive with the alternatives in a while. There is no infrastructure for distributing or bunkering hydrogen, and it will take some time before international legislation is ready for using hydrogen as a marine fuel. (DNV GL, 2019)

Hydrogen could potentially be produced nearly emission free with electrolysis powered by renewable or nuclear energy. Hydrogen produced with this technology forms the basis for all future power-to-fuel alternatives, such as ammonia and synthetic methane. These fuels are projected to be vital for achieving IMOs emission goals. In addition, hydrogen may serve as the primary energy source of short-sea vessels in the future.

7.3.6 Ammonia

Ammonia as a fuel is similar to hydrogen, with the decisive difference of it having a higher volumetric energy density of 12 MJ/l: slightly lower than LNG. Furthermore, ammonia liquefies in much higher temperatures compared to hydrogen or methane, which makes its storage easier. It can potentially be used as a fuel in high temperature fuel cells emission free. However, this technology is not mature. ICEs that use ammonia as fuel are currently under development but will most likely need NOx abatement technology to comply with tier III NOx regulations. Ammonia is toxic

which might reflect as higher costs due to the needed safety equipment and stricter regulations. Currently, ammonia is seen as the most promising carbon-neutral option in the long term, because of the lower cost of its storage, energy converter and the fuel itself compared to hydrogen or synthetic methane. (DNV GL, 2019)

7.4 Discussion & conclusion

Reaching the goal of 50% reduced emissions in shipping by 2050 will be difficult and current regulations and policies do not incentivize investors enough to reach this goal. Since shipping is very closely tied to globalization and world trade, policies that influence the competitiveness of this sector have wide reaching effects, which makes developing and enforcing new policies a huge effort. Nevertheless, some further policies can be expected in the shipping sector soon, such as carbon pricing. Ships built today will need to be competitive for up to 40 years, and thus, a ship's environmental impact is one of the most important considerations for new-builds today.

The short-sea shipping sector is more flexible in which technologies and fuels it may adopt. Emerging technologies like batteries and fuel cells may become cost effective in this sector soon. The deep-sea segment, on the other hand, is restricted to fuels that boast a high volumetric energy density. Furthermore, new technologies take time to develop to such a scale that would be required for large ocean-going vessels. On the other hand, wind propulsion technology like Flettner rotors may be very well close to wide scale adoption in this sector. This is dependent on increased sea trials for the technology, as well as third party financial instruments for investing in such technology. Technologies like fuel cells, batteries and wind propulsion need to be employed along hull improvements, waste heat recovery systems and intelligent solutions to work towards the target of 40% reduced energy used per tonne-mile.

LNG is regarded as the most promising fuel out of the current alternatives. It reduces CO_2 emissions significantly compared to HFO/MGO, dual-fuel engine technology is mature, bunkering infrastructure for LNG is being developed constantly and it is the only alternative fuel that can meet the projected fuel demand for the next 10 years. In addition, it is cost competitive with current fuels.

However, to reach target emission levels, switching to LNG is not enough. Towards 2050, adoption of carbon-free fuels needs to occur. It is still unclear which green fuel will eventually prevail. Ammonia looks like the most cost competitive option currently. On the other hand, if short-term predictions regarding LNG hold true, the shipping sector may be more inclined to shift towards synthetic methane since it can be used as is with LNG infrastructure and technology.

Ships come with a wide range of different sizes, purposes and operational profiles. As such, it is impossible to pinpoint a single technology or fuel as the best overall. The choice of which technology or fuel to invest in is highly dependent on the specific use case and assumptions about the regulatory framework of the future.

Because of this, the selection process of such technologies should be done individually for each ship.

References

[1] IMO, "Prevention of Air Pollution From Ships," 2020. [Online]. Available: http://www.imo.org/en/OurWork/Environment/PollutionPrevention/AirPollution/Pages/Air-Pollution.aspx. [Accessed 24 August 2020].

[2] IMO, "Third IMO GHG Study 2014," International Maritime Organization, London, 2015.

[3] DNV GL, "Maritime forecast to 2050 - Energy transition outlook 2019," 2019.

[4] K. Anderson and A. Bows, "Executing a Scharnow turn: reconciling shipping emissions with international commitments on climate change," *Carbon management,* vol. 3, no. 6, pp. 615-628, 2012.

[5] N. Rehmatulla, S. Parker, T. Smith and V. Stulgis, "Wind technologies: Opportunities and barriers to a low carbon shipping industry," *Marine Policy,* vol. 75, pp. 217-226, 2017.

[6] T. Tronstad, H. Åstrand, G. Haugom and L. Langfeldt, "Study on the use of fuel cells in shipping," European Maritime Safety Agency, 2017.

[7] DNV GL, "Assesment of selected alternative fuels and technologies," 2019.

[8] European Maritime Safety Agency, "Study on electrical energy storage for ships," 2020.

[9] F. Baldi and G. Cecilia, "A feasibility analysis of waste heat recovery systems for marine applications," *Energy,* vol. 80, pp. 654-665, 2015.

[10] E. Bouman, E. Lindstad, A. Rialland and A. Strømman, "State-of-the-art technologies, measures, and potential for reducing {GHG} emissions from shipping--a review," *Transportation Research Part D: Transport and Environment,* vol. 52, pp. 408-421, 2017.

[11] Silverstream technologies, "Case Studies," 2020. [Online]. Available: https://www.silverstream-tech.com/the-technology/case-studies/d. [Accessed 24 August 2020].

[12] Wärtsilä, "Wärtsilä and Silverstream to collaborate on accelerating deployment of air lubrication technology," 2020. [Online]. Available: https://www.wartsila.com/media/news/02-12-2019-wartsila-and-silverstream-to-collaborate-on-accelerating-deployment-of-air-lubrication-technology-2587106. [Accessed 24 August 2020].

[13] DNV GL, "Alternative Fuels Insight," 2020. [Online]. Available: https://www.dnvgl.com/services/alternative-fuels-insight-128171. [Accessed 24 August 2020].

8. Numerical simulation of dual-fuel spray ignition under RCCI conditions

Bulut Tekgül [a) 1], Heikki Kahila [b) 2], Ossi Kaario [a) 1], Jari Hyvönen [b) 2], Eric Lendormy [b) 2], Ville Vuorinen [a) 1]
[a)] Aalto University
[b)] Wärtsilä Finland Oy

8.1 Introduction

In this study, we present our recent groundwork analysis of large-eddy simulation (LES) modeling of RCCI combustion. Mixing and ignition of a high-reactivity diesel spray and a low-reactivity, lean methane-air mixture is investigated using numerical methods. With increasing concern over environmental preservation, one solution for reducing harmful emissions is utilizing low temperature combustion (LTC) at leaner mixture conditions [1]. Reactivity Controlled Compression Ignition (RCCI) offers a viable solution for emission reduction while still providing very high engine efficiency [2]. It targets at controlled heat-release rate and ignition timing through controlling in-cylinder reactivity stratification. In this study, the effect of injection timing in combustion characteristics is investigated by advancing the start of injection (SOI) away from the top dead center with a constant injection duration. A compression-heating model is utilized to account for the ambient temperature and pressure increase due to compression effects. A diesel surrogate (*n*-dodecane) is injected into a homogeneous air-methane mixture with varying injection timing to investigate the effect of injection timing and overall mixture reactivity on dual-fuel ignition process, as shown in Figure 1.

[1] Contact: firstname.lastname@aalto.fi
[2] Contact: firstname.lastname@wartsila.com

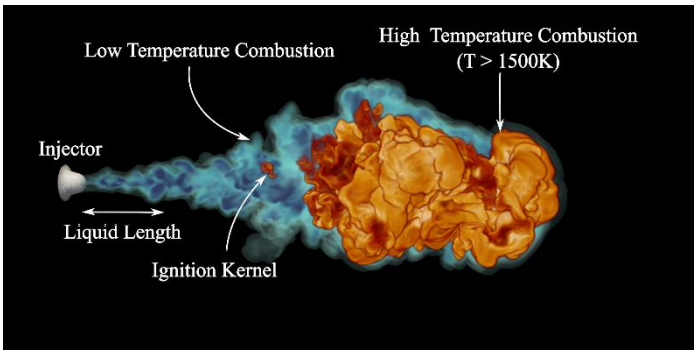

Figure 1. An illustration of the dual-fuel ignition process.

8.2 Case Definition

8.2.1 Numerical Methods

For the gas phase, compressible Navier-Stokes equations are solved via Large-Eddy Simulation (LES) using the OpenFOAM-6 CFD solver [3]. The pressure implicit splitting of operators (PISO) method is used for pressure-velocity coupling.

The injected high-reactivity liquid diesel spray is modeled using Lagrangian Particle Tracking (LPT) method. A no-breakup model is used with a constant droplet diameter, with the assumption that the injected particles have already undergone the droplet breakup process.

For combustion modeling, our in-house solvers, implemented on OpenFOAM, are used to speed up the chemistry reaction-rate calculation process. A finite-rate chemistry method is adopted and a chemical mechanism from Yao et al. [4] (54 species, 269 reactions) is utilized. The open-source pyJac library [5] is used for replacing the finite-difference chemistry ODE Jacobian with an analytical one. In addition, the ODE solver that handles the stiff chemistry problem is enhanced by utilizing LAPACK libraries for matrix operations. Finally, a run-time dynamic load balancing routine is implemented to increase the parallel-computing efficiency of the chemical reaction rates. The main framework of our numerical models is described in detail in our previous studies [6, 7].

8.2.2 Compression Effects

To be able to model the combustion process under RCCI conditions more accurately, the rise in pressure and subsequent temperature due to engine compression should be taken into account. A compression heating source term is added to the CFD governing equations to achieve this, following the works [8] and [9]. The derivation of the source term is described in Equations 1 and 2.

$$P_m(t) = P_{0,m}[1 + g^2\pi^2 \frac{t - {t_0}^2}{{t_c}^2}]^{-n} \quad (1)$$

$$\dot{m} = \frac{\rho}{P}\frac{dP_m}{dt} \quad (2)$$

8.2.3 Investigated Conditions

A single injection diesel configuration (T_{inj} = 0.5 ms) is adopted by varying the start of injection (SOI) in the range of 7.2 to 36 CAD (crank angle degree) before top dead center (BTDC), details of which are given in Table 1. A simple 3D geometry is simulated under this source term and its thermophysical properties are compared with a 0D homogeneous reactor under same compression conditions in Figure 2.

Table 1. Investigated SOI timings and subsequent ambient conditions.

	SOI-7.2	SOI-14.4	SOI-21.6	SOI-28.8	SOI-36
Initial conditions					
t_{SOI} [CAD BTDC]	7.2	14.4	21.6	28.8	36
T_{SOI} [K]	886	842	784	723	663
p_{SOI} [bar]	53.6	43.6	32.7	23.7	17.0

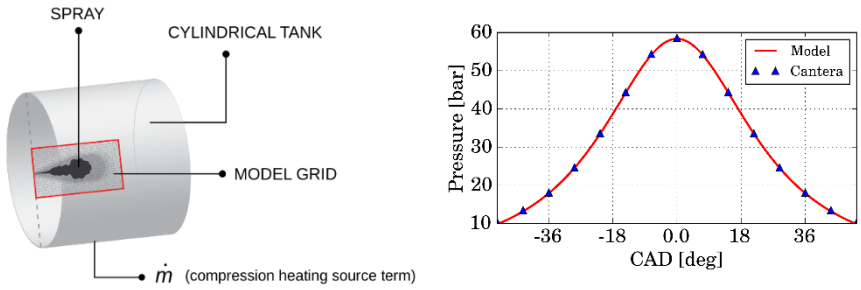

(a) (b)

Figure 2. (a) A schematic of the numerical setup used in the simulations (b) Motored pressure with compression heating model (red) and a 0D homogeneous reactor (blue) under same compression conditions.

8.3 Results and Discussion

As seen in Figure 3, advancing the SOI from 7.2 up to 21.6 CAD BTDC advances both first (τ_1) and second stage (τ_2) ignition. However, with further advanced SOI,

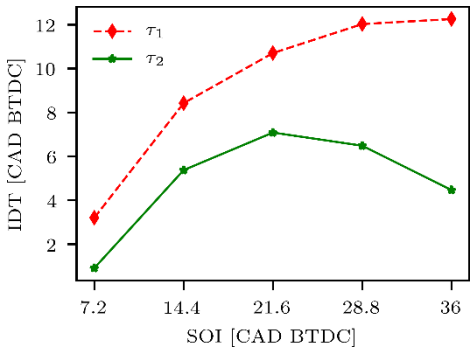

Figure 3. First and second stage ignition (τ_1, τ_2) times obtained from the 5 simulations with varying SOI with respect to TDC.

the τ_2 starts to retard towards TDC, caused by lower reactivity of the spray charge due to over-dilution and subsequent shift in ignition timing characteristics. This observation supports the findings of Li et al. [10], where they observed the ignition to first advance and then retard with advancing the SOI with respect to TDC. In addition, it can be observed that while τ_1 does not exhibit the same non-linear behavior with respect to TDC, its rate of change decreases when SOI is further advanced.

The cut-planes of various fields obtained from cases SOI-7.2, 21.6 and 36 are presented in Figure 4 at their corresponding τ_1+0.2 ms time instances. The change

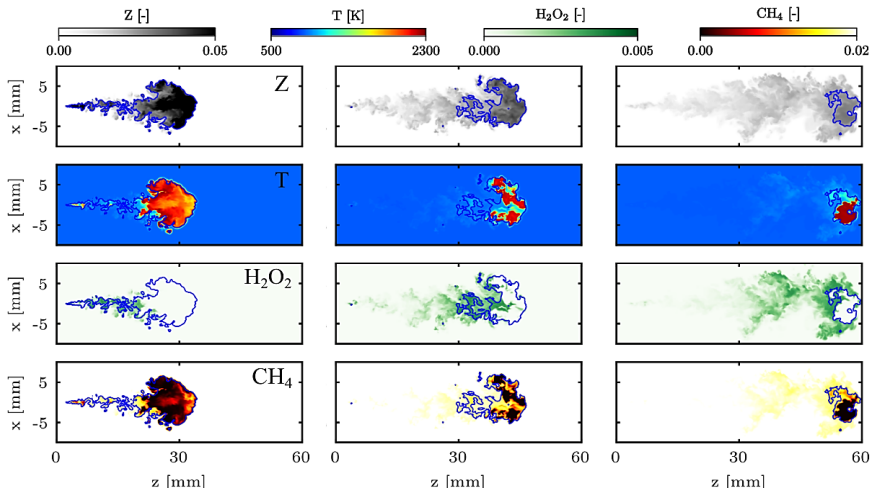

Figure 4. Mixture fraction, temperature, H_2O_2 and CH_4 cutplanes for cases SOI- 7.2 (left), 21.6 (middle) and 36 (right), at their corresponding τ_2+0.2 ms time instances (blue isoline represents stoichiometric mixture fraction).

in mixture characteristics and ignition strength is clearly observed: for SOI closer to TDC at 7.2 CAD (left), the overall mixture is above stoichiometry due to small mixing time. Due to the rich conditions, the high-temperature ignition kernel is large in volume and forms a robust energy source for the subsequent propagation into the ambient charge. The specie H_2O_2, associated with low-temperature chemistry (LTC), is fully consumed within the rich spray charge, indicating that the shift from LTC and high-temperature chemistry (HTC) regime is already underway within this region. Finally, the ambient CH_4 within the spray charge is almost fully consumed, further showing that the ignition is strong and already locally consuming the ambient fuel.

The main findings of the study are:

- When SOI is advanced, ignition time also advances. When a critical SOI point is reached, ignition retards towards TDC due to spray dilution.
- For early SOI ignition, kernels are small in size, leading to possible issues of premixed flame initiation.
- By advancing SOI, the propagation mode of combustion can be influenced from spontaneous to deflagrative, due to larger reactivity stratification in the system.

Acknowledgements

The authors acknowledge Wärtsilä Co. for financial and academic support. The computational resources for this study were provided by CSC - Finnish IT Center for Science.

References

[1] Reitz, R. D. (2013). Directions in internal combustion engine research. Combustion and Flame, Vol. 160, pp. 1–8. https://doi.org/10.1016 /j.combustflame.2012.11.002

[2] Reitz, R. D., & Duraisamy, G. (2015). Review of high efficiency and clean reactivity controlled compression ignition (RCCI) combustion in internal combustion engines. Progress in Energy and Combustion Science, 46, 12–71. https://doi.org/10.1016/j.pecs.2014.05.003

[3] H. G. Weller, G. Tabor, H. Jasak, C. Fureby, A tensorial approach to computational continuum mechanics using object-oriented techniques, Computers in Physics 12 (6) (1998) 620. doi:10.1063/1.168744.

[4] Yao, T., Pei, Y., Zhong, B. J., Som, S., Lu, T., & Luo, K. H. (2017). A compact skeletal mechanism for n-dodecane with optimized semi-global low-temperature chemistry for diesel engine simulations. Fuel, 191, 339–349. https://doi.org/10.1016/j.fuel.2016.11.083

[5] Niemeyer, K. E., Curtis, N. J., & Sung, C. J. (2017). pyJac: Analytical Jacobian generator for chemical kinetics. Computer Physics Communications, 215, 188–203. https://doi.org/10.1016/j.cpc.2017.02.004

[6] Kahila, H., Kaario, O., Ahmad, Z., Ghaderi Masouleh, M., Tekgül, B., Larmi, M., & Vuorinen, V. (2019). A large-eddy simulation study on the influence of diesel pilot spray quantity on methane-air flame initiation. Combustion and Flame, 206, 506–521. https://doi.org/10.1016/j.combustflame.2019.05.025

[7] Tekgül, B., Kahila, H., Kaario, O., & Vuorinen, V. (2020). Large-eddy simulation of dual-fuel spray ignition at different ambient temperatures. Combustion and Flame, 215, 51–65. https://doi.org/10.1016/j.combustflame.2020.01.017

[8] Bhagatwala, A., Sankaran, R., Kokjohn, S., & Chen, J. H. (2015). Numerical investigation of spontaneous flame propagation under RCCI conditions. Combustion and Flame, 162(9), 3412–3426. https://doi.org/10.1016/j.combustflame.2015.06.005

[9] Luong, M. B., Sankaran, R., Yu, G. H., Chung, S. H., & Yoo, C. S. (2017). On the effect of injection timing on the ignition of lean PRF/air/EGR mixtures under direct dual fuel stratification conditions. Combustion and Flame, 183, 309–321. https://doi.org/10.1016/j.combustflame.2017.05.023

[10] Li, Y., Jia, M., Liu, Y., & Xie, M. (2013). Numerical study on the combustion and emission characteristics of a methanol/diesel reactivity controlled compression ignition (RCCI) engine. Applied Energy, 106, 184–197. https://doi.org/10.1016/j.apenergy.2013.01.058

9. Effective exhaust gas heat recovery

Valtteri Haavisto[1], Kerttu Kupiainen[1]
Vahterus Oy

9.1 Introduction

Vahterus is always developing new solutions to improving the current heat transfer. Marine industry is forced to reduce the emissions and increase the overall energy efficiency of ships. As the main source of energy waste in the ships is still exhaust gas, it is important to improve conventional ways to recover heat from the exhaust gases.

Vahterus have tested a new exhaust gas heat-recovery system together with the LUT University. The target for the development and test work was to develop new heat recovery solutions for exhaust gases utilizing plate heat exchanger technology and to utilize the exhaust gas in Organic Rankine Cycle (ORC).

9.2 Exhaust gas heat recovery with plates

Exhaust gas heat recovery is made by cooling down the exhaust gas during a heat exchanging process in a heat exchanger where, at the cold side, either evaporating or liquid fluid is heated up. Traditionally, the heat exchanger with finned tubes is used for the purpose. Traditional tube type heat exchanger can be used with different enhancement devices, but it typically has larger hydraulic diameters and surface-area-to-volume ratio than a plate heat exchanger does.

In addition, plate heat exchanger has following advantages in comparison to traditional tube type heat exchanger [1]:

- Plate surface corrugation has a significantly better heat transfer coefficient than the tube type because of the highly vortex flow, disruption and reattachment of boundary layers and increased effective heat transfer area.

[1] Contact: firstname.lastname@vahterus.com

- Plate type heat exchanger usually is a much smaller, reducing the overall space requirement, weight and vibration problems.

Because of the aforementioned characteristics, it was decided to further optimize the plate geometry for the exhaust gas heat recovery use.

9.3 Exhaust gas powered ORC-system

The Vahterus new heat exchanger type was tested in the LUT test lab. The heat exchanger was installed to an existing ORC system, as shown in Figure 1. Exhaust gas heat was used to evaporate working fluid, octamethyltrisiloxane, also known as MDM. During the process, the MDM in the heat exchanger is first heated up to evaporation temperature, evaporated and in the final part superheated. Heat source was a diesel generator (AGCO SG275).

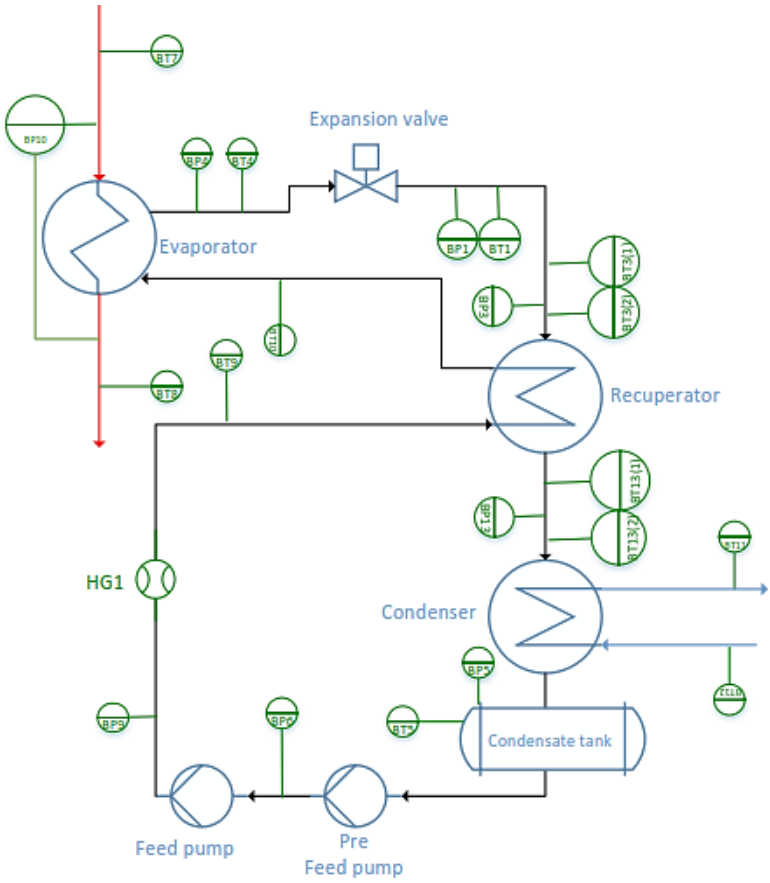

Figure 1. Schematic process diagram of the test loop.

The target of the test was to understand how well the designed plate geometry would work and what the heat recovery potential of the cross flow plate heat exchanger is. The tested plate type is SH type Vahterus plate, having longer thermal length for cold side and very short thermal length for exhaust gas side. This is to keep the exhaust gas side pressure drop low and to ease mechanical cleaning. The new modified plate shape also fit well into exhaust gas funnel.

Figure 2. Picture of the tested plate type

The test indicated that the plate type performed well in an ORC system powered by exhaust gas. Although the flow arrangement was crossflow, good temperature crossing of the fluids was noticed.

An example of one test instance shows:

- Exhaust gas inlet temperature 420°C and outlet 225°C.
- MDM inlet temperature 160°C, evaporating at 220°C and gas outlet temperature 250°C.

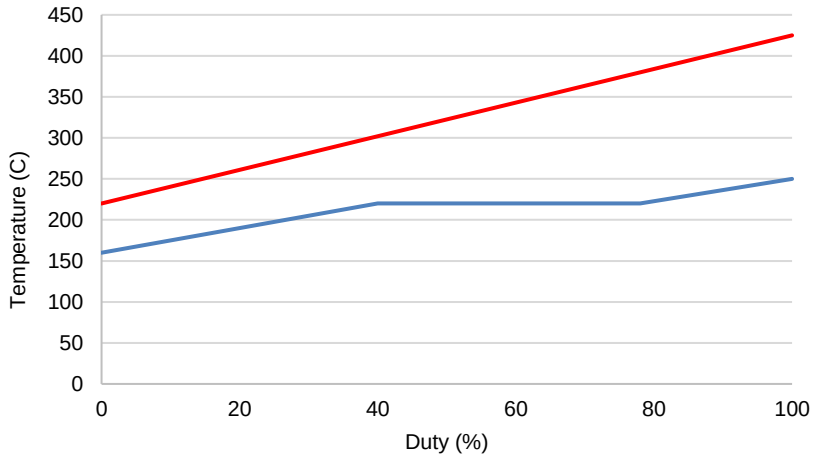

Figure 3. Sample of single point temperature profile.

The tested heat exchanger was undersized for the duty to make the heat transfer calculation more accurate. Specifically, very small temperature differences in the heat exchanger makes the calculation of heat transfer coefficient unreliable, thus it is recommended to use a heat exchanger with very little surface areas in the test conditions. The real scale heat exchanger is later designed to meet the required temperature differences.

9.4 Next steps

The test work together with LUT and Vahterus made it clear that exhaust gas can be directly used in an ORC process without intermediate loop. Together with the finding from Vahterus' own long-term diesel exhaust-gas heat recovery test, it is proven that plate heat exchangers are suitable for the duty.

The introduction of gaseous fuels to diesels engines is enabling lower exhaust gas exit temperatures without corrosion risks. This will challenge the tradition in exhaust gas heat recovery.

In summary, the 100-year-old plate heat exchanger technology is one option both to improve the exhaust gas heat recovery rate and to reduce the heat exchanger weight and space in the system. A full-scale exhaust gas heat recovery system is currently being set up at Vahterus for further studies and test.

Reference

[1] L. Wang, B.Sunden, and R.M. Malik , "Plate heat exchangers: Design, applications and performance. Southampton, UK. WIT Press, 2007.

10. Waste heat recovery - Dynamic modelling and simulation

Radheesh Dhanasegaran[1], Antti Uusitalo[1], Teemu Turunen-Saaresti[1]
LUT University

10.1 Introduction

For the recovery of low-grade waste heat in energy-to-power conversion processes, Organic Rankine Cycle (ORC) technology has demonstrated its capability in the last two decades. Deploying such technology for Waste Heat Recovery (WHR) in marine environment would allow to reach notable fuel savings and to reduce emissions. However, using ORC technology in marine environment also demands for continuous performance assessment of the ORC systems and requires improved control strategies due to the highly transient operational characteristics of marine applications. For this purpose, dynamic simulation and digital twins have been recognized as powerful tools for predicting the system operation under different conditions.

For building an accurate dynamic model for an ORC system, mathematical representation of the cycle components is needed in order to be able to describe and predict the behaviour of the cycle at both design and off-design conditions, as well as under highly transient operating conditions. A dynamic model has been developed using MATLAB-SIMULINK environment for a small-scale and high temperature ORC facility at the LUT University. The modelling of transient response taking into account the thermal inertia of the heat exchangers has been recently developed and tested with simulations for the individual heat exchangers of the system.

[1] Contact: firstname.lastname@lut.fi

10.2 Simulation Process

10.2.1 Dynamic Modeling

Understanding the transient behaviour of power cycles is important as they are operated under different operating conditions, including the start-up, shutdown, design point operation and other off-design conditions. In principle, this dynamic behaviour can be described by a set of transient governing differential equations and inherent physical characteristics [1]. Apart from the modelling of turbomachinery components, the simulation of the heat exchangers is equally important in predicting the system operation characteristics as well as to reduce possible failures and the maintenance costs of ORC systems [2]. In the literature, there are only very few dynamic models developed and validated for a small-scale and high temperature ORC system, which highlights the need and the novelty of the current work.

10.2.2 Modelling Process

The Matlab-Simulink environment has been utilized to create the dynamic model, whereas CoolProp, an open-source thermodynamic transport database, is used for defining the thermophysical properties of the working fluid at different process nodes. The modelling process can be divided into two steps: (a) Modelling of Turbogenerator blocks and (b) Modelling of Heat exchanger blocks. The schematic representation of the ORC Plant in question is shown in Figure 1. For predicting the transient behaviour due to the effects of thermal inertia, a thermal network modelling approach has been adopted for the modelling of heat exchanger components shown in Figure 2.

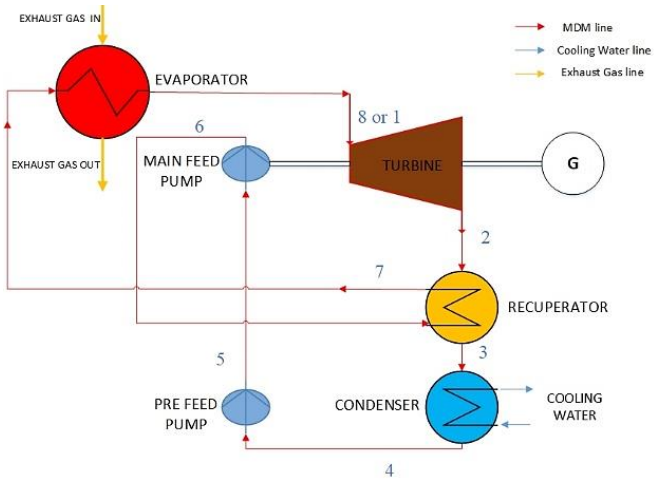

Figure 1. Schematic of the ORC Plant at the LUT University.

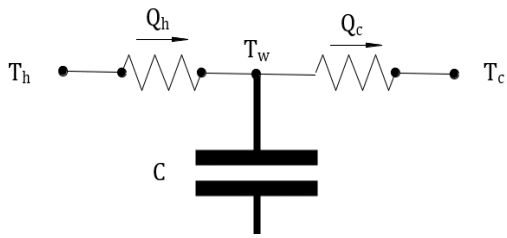

Figure 2. Thermal Network Modelling Approach for Heat Exchangers.

10.2.2.1 Turbogenerator block

The turbogenerator block consists of the turbine and the main feed pump. The dynamics of the turbogenerator are related to the changes in the turbogenerator rotational speed, which varies between 12 000 rpm and 30 000 rpm during the normal operation, the changes in working fluid thermodynamic properties at the inlet and outlet and the changes in performance of the turbine and feed pump. The turbine efficiency is determined based on the rotational speed and the mass flow rate. The polynomials derived from the experimental data are used for describing the turbine isentropic efficiency and the pressure rise under different rotational speeds and conditions. The turbine calculation process is explained in the flowchart shown in Figure 3.

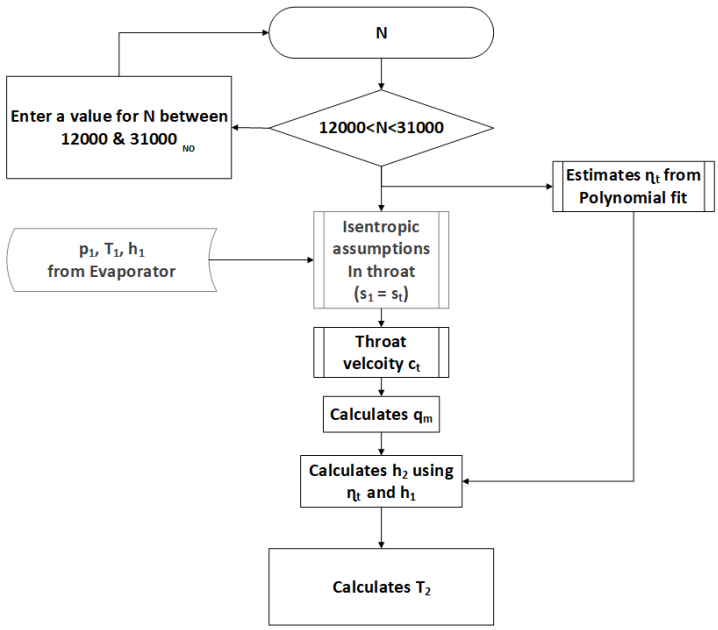

Figure 3. Turbine Calculation Process Flowchart.

10.2.2.2 Heat Exchanger blocks

In the heat exchanger calculation process, two known inlet and two unknown outlet temperatures are solved using a bi-section algorithm. The heat rate equations to be solved for the heat exchangers, namely the recuperator condenser and evaporator, are shown in Equation (1), (5) and (9). The outlet temperature calculation process is explained in the flow chart shown in Figure 4.

$$\phi_{1,\mathrm{R}\_hot} = \phi_{2,\mathrm{R}\_cold} = \phi_{3,\mathrm{R}} \tag{1}$$

where,

$$\phi_{1,\mathrm{R}\_hot} = q_{m_h}(h_2 - h_3) \tag{2}$$

$$\phi_{2,\mathrm{R}\_cold} = q_{m_c}(h_7 - h_6) \tag{3}$$

$$\phi_{3,\mathrm{R}\_hot} = U.A.\Delta T_{LMTD} \tag{4}$$

and

$$\phi_{1,\mathrm{C}_{\mathrm{hot}}} = \phi_{2,\mathrm{C}_{\mathrm{cold}}} = \phi_{3,\mathrm{C}} \tag{5}$$

where

$$\phi_{1,\mathrm{C}\_hot} = q_{m_h}(h_3 - h_4) \tag{6}$$

$$\phi_{2,\mathrm{C}\_cold} = q_{m_h}.c_p.(T_{co} - T_{ci}) \tag{7}$$

$$\phi_{3,\mathrm{R}\_hot} = U.A.\Delta T_{LMTD} \tag{8}$$

and

$$\phi_{1,\mathrm{E}\_cold} = \phi_{2,\mathrm{E\_hot}} = \phi_{3,\mathrm{E}} \tag{9}$$

where

$$\phi_{1,\mathrm{R}\_hot} = q_{m_h}(h_8 - h_7) \tag{10}$$

$$\phi_{2,\mathrm{R}\_hot} = q_{m_c}(h_{ho} - h_{hi}) \tag{11}$$

$$\phi_{3,\mathrm{R}\_hot} = U.A.\Delta T_{LMTD} \tag{12}$$

To calculate the dynamics arising from the thermal inertia in the heat exchanger components, a thermal network modelling approach is followed, which simplifies the heat exchanger to a thermal resistance network where the heat is transferred from the hot source to a heat sink through a nodal wall in between as shown in Figure 2. The accumulated heat in this node gives rise to the thermal inertia. The corresponding equation is shown in the Equation (13).

$$T_w^{n+1} = T_w^n + \frac{\Delta t}{\rho_m V_m c_p}[h_h A(T_h - T_w) - cA(T_w - T_c)] \tag{13}$$

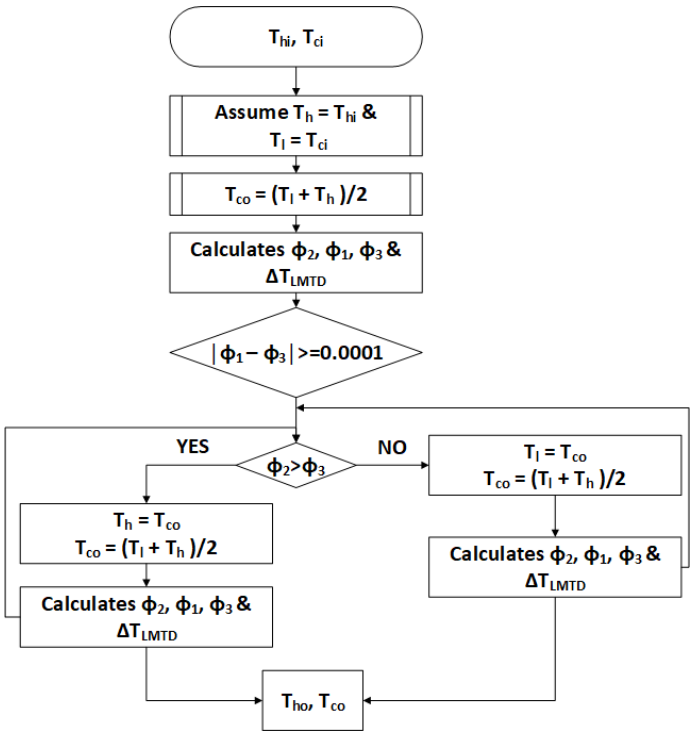

Figure 4. Heat Exchanger Outlet Temperatures Calculation Process Flowchart.

Currently, we have implemented the thermal inertial effects, arising from the material for the individual heat exchanger block components, by programming its physics in the Level-2 S-functions code to test their performance. We are in the process of testing the full-scale simulation by connecting all the individual block components together to form a closed-loop cycle, representing the entire ORC system.

10.2.3 Future work

After adding the effects of thermal inertia of the heat exchangers to the dynamic model, the following features will be considered and added to the dynamic model in the near future to improve the accuracy of the model.

1. Adding the rotational inertia of the turbogenerator to the model. The rotational inertia effect is important as the turbogenerator speed in constantly adjusted based on the operating conditions and the amount of available waste heat. The rotational inertia can be also considered important during the start-up and shut down stages of the ORC system. This feature has been already taken into account in Excel based dynamic

cycle model at LUT and the same calculation approach will be added to the present Matlab/Simulink model.

2. Adding inertial effect caused by the working fluid on heat exchanger models. In the present model, the inertial effect in the heat exchangers has been assumed to be caused by the heat exchanger material, but the inertial effects caused by the working fluid will be also investigated in the future.

References

[1] J. Galindo, V. Dolz, L R Pascual and A Brizard, Dynamic Modeling of an Organic Rankine Cycle to recover Waste, Energy Procedia, 2017

[2] M. Assadi, Y M Barzi, Dynamic Modeling of ORC Power Plants, 2018.

[3] F. Casella, T. Mathijssen, P. Colonna and J. Buijtenen Dynamic Modeling of Organic Rankine Cycle Power Systems, Journal of Engineering for Gas Turbines and Power, Vol. 135, April 2013.

[4] D. Kum, N K. Bucknor, Dynamic Modeling of The Organic Rankine Cycle For The Waste Heat Recovery Of Internal Combustion Engines, Proceedings of the JSME 2012 11th Motion and Vibration Conference, 2012.

[5] T. Prisecaru, I. Soriga, Control strategy and thermal inertia influence on evacuated tube solar water heating systems, Braz. Soc. Mech. Sci. Eng., 2017.

11. Optimization of heat integrated ship systems

Antti Ritari[1], Janne Huotari[1], Kari Tammi[1] and Armin Narimanzadeh[1]
Aalto University

11.1 Introduction

Heat integration addresses the problem of matching hot and cold streams and recovering as much heat as possible. Increased heat recovery translates into reduced heating and cooling supply from fuel consuming utility equipment, such as boilers and chillers. Significant progress in ship energy efficiency has been achieved by recovering and allocating the waste heat from internal combustion engine exhaust gas to the most valuable targets. Recently there have been increased efforts to recover low-grade heat from engine cooling circuits. Moreover, novel energy conversion technologies, such as high temperature fuel cells, will create new opportunities and challenges for heat integration in the coming years [1].

This paper develops a mathematical programming model formulation that provides a systematic approach to the design of heat-integrated ship energy systems. The developed model aims to simultaneously optimise complex energy system configuration and heat integration while minimizing total cost. This modelling approach represents a shift from individual component integration in isolation towards automated system level integration of all processes and equipment choices, considering the relevant interactions.

11.2 Heat integration

A network of heat exchangers must be synthesised to realise the efficient heat exchange between hot and cold streams. The large number of possible network configurations and non-convexity of heat exchange area function result in a difficult combinatorial design problem. However, a designer can take advantage of the insight that the maximum potential of heat integration can be identified without knowing explicitly the detailed design of the heat exchanger network [2, 3]. Pinch

[1] contact: firstname.lastname@aalto.fi

analysis is a well-known graphical and intuitive technique that enables this insight. In the context of ship design, a few recent successful applications of pinch analysis can be found in Organic Ranking Cycles (ORC) design [4, 5].

11.2.1 Pinch analysis and maximum heat recovery target

The computation of the maximum heat integration potential for a given set of thermal streams with fixed supply and target temperatures is based on three principles: (1) energy is conserved, (2) heat flows only from higher temperature stream to lower temperature stream, and (3) driving force for heat exchange in a heat exchanger is a function of the minimum temperature difference between the hot and cold streams (ΔT_{min}) [2, 3].

Based on these principles, the graphical pinch analysis identifies a pinch point, where the hot and cold composite curves have the smallest gap in the temperature (y-axis) direction (Figure 1). The pinch point is a constraint that prevents further heat exchange. There should be no heat exchange across the pinch, as this would increase the external heating (utility) requirement above the pinch and increase the cooling need below the pinch.

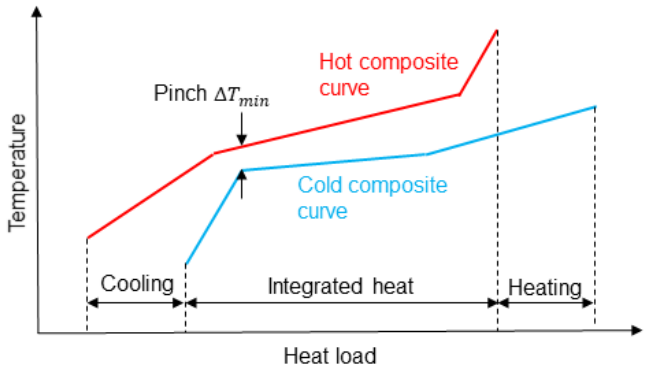

Figure 1. Pinch method: composite thermal streams adjusted for maximum heat integration.

Taking advantage of the pinch temperature information, a designer can then make changes in supply and target temperatures and mass flows of streams, which results in a more favourable pinch point that provides better heat integration opportunity. However, graphical pinch methods limit the search process to iteration by hand.

11.2.2 Mathematical programming approach to heat integration and stream selection

The three heat exchange principles can be expressed as a set of constraints in a linear mathematical programming model, which enables automated execution of the

steps in the graphical pinch method. This approach is based on the decomposition of the entire temperature interval of all streams into a number of smaller intervals [3]. A heat balance constraint is defined for each interval separately (Figure 2). This ensures the thermodynamic feasibility of heat exchange. The heat balance forces the interval input and output heat residuals ($\dot{Q}_k^R$, $\dot{Q}_{k+1}^R$) and the sum of hot and cold stream heat loads to match at each temperature interval. In addition, heat residual is nonnegative so that heat flow direction is towards the lower interval only.

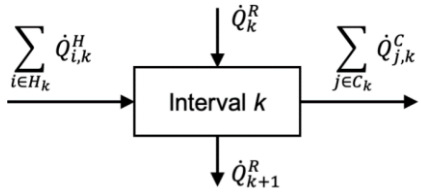

Figure 2. Temperature interval heat balance.

The solution to this optimisation problem gives the same result as the graphical pinch method: maximum heat integration, heat exchanged at different temperature intervals, and the pinch temperature. Within the scope of mathematical programming, the heat exchange constraints can be embedded within an equipment selection and dimensioning optimisation model. The supply and target temperatures of streams must be fixed, but the mass flows can vary continuously. These mass flows can then be defined as a function of the load of the equipment that they are associated with. For example, engine cooling water circuit mass flow is a function of engine power output. The advantage of this embedding approach is that the heat exchange and process modifications are automated and executed simultaneously, instead of iteratively as with the graphical pinch method.

11.2.3 Minimum cost energy system design problem

In the general energy system design, the task is to select which equipment to install, sizes of installed equipment and their operation over time. The objective is to minimise annualised capital and operation costs while meeting the demand for electric power, freshwater generation, heating and cooling.

Let U denote the set of candidate equipment available for installation. This set contains main engines, boilers, evaporators, sea water pumps, air handling units and all other equipment that performs a distinct function. Each equipment $u \in U$ is associated with three variables that represent decisions a designer needs to make. First, each candidate equipment is either selected or not, and this yes/no decision is represented by a binary variable y_u. Second, the size of equipment is a continuous variable z_u, which can receive nonnegative values only if the respective equipment is installed. The final decision concerns the load of each equipment, denoted by $x_{u,i}$.

This variable receives a different value for each operating period $i \in I$ and is not allowed to exceed the installed size.

For each equipment $u \in U$, there is a set S_u of thermal streams. If the set is empty, the equipment has no thermal streams. Parameter $\dot{q}_{u,s,k}$ gives the heat duty of stream $s \in S_u$ per unit of load of equipment u for temperature interval k. Hot streams (require cooling) receive positive parameter values and cold streams (require heating) negative values. Note that this formulation combines the separate nonnegative hot and cold streams $\dot{Q}^C$ and $\dot{Q}^H$ in Figure 2.

The general form of the optimisation problem is formulated as a mixed-integer problem as follows (decision variables are bolded for clarity):

$$\underset{Q_k, \boldsymbol{y_u}, \boldsymbol{x_u}, \boldsymbol{z_u}}{minimize} \sum_{u \in U} \left[\sum_{i \in I} \left(t_i C_u^{op} \boldsymbol{x_{u,i}} \right) + \frac{1}{\tau} \left(C_u^{inv1} \boldsymbol{y_u} + C_u^{inv2} \boldsymbol{z_u} \right) \right] \quad \text{(Annualized cost)} \quad (1)$$

subject to

$$\sum_{u \in U} \sum_{s \in S_u} \boldsymbol{x_{u,i}} \dot{q}_{u,s,k} + \dot{\boldsymbol{Q}}^{\boldsymbol{R}}_{\boldsymbol{k,i}} - \dot{\boldsymbol{Q}}^{\boldsymbol{R}}_{\boldsymbol{k+1,i}} = 0 \qquad \forall k \in K, \forall i \in I \quad \text{(Heat balance)} \quad (2)$$

$$\sum_{u \in U} \boldsymbol{x_{u,i}} \dot{W}_u - \dot{W}_D \geq 0 \qquad \forall i \in I \quad \text{(Power balance)} \quad (3)$$

$$\sum_{u \in U} \boldsymbol{x_{u,i}} \dot{m}_u^w - \dot{m}_D^w \geq 0 \qquad \forall i \in I \quad \text{(Water balance)} \quad (4)$$

$$\sum_{i \in I} \boldsymbol{x_{u,i}} - \boldsymbol{z}_u \leq 0 \qquad \forall u \in U \quad \text{(Equipment size)} \quad (5)$$

$$z_u^{min} \boldsymbol{y_u} \leq \boldsymbol{z_u} \leq z_u^{max} \boldsymbol{y_u} \qquad \forall u \in U \quad \text{(Domain bounds)} \quad (6)$$

$$y_w \in \{0,1\}, \;\; R_{\min(K)} = 0, \;\; R_{\max(K)+1} = 0, \;\; R_k \geq 0$$

The objective function (1) to be minimised is the total cost including annualised operating costs and investment cost of equipment. Parameter C_u^{op} is the operation cost proportional to load, t_i is annual operating duration in mode i, τ is investment annualising factor and C_u^{inv1} and C_u^{inv2} are the fixed and proportional investment cost parameters.

Each equipment is associated with a parameter that represents its specific electric power generation or consumption. A similar principle applies to freshwater. Constraints (3) and (4) account for power balance and freshwater balance, respectively. Constraint (6) incorporates a logic relation between the binary variable y_u and the equipment installed size variable z_u. The constraint simultaneously bounds the size between minimum and maximum allowed and ensures that if the size is nonnegative, the binary variable must have a value of one and the fixed investment cost is activated in the objective function.

11.2.4 Integration of refrigeration cycles

Refrigeration cycle devices are heat pumps that are used to provide a cold utility below seawater temperature, mainly to cool chilled water for air conditioning units. In this cycle, mechanical work is converted into a heat flow from a heat source to a heat sink at a higher temperature. From a pinch analysis point of view, a refrigeration cycle is composed of one hot stream, one cold stream and the corresponding electricity consumption of a compressor [4].

11.3 Numerical example problem

The following small example problem illustrates the application of the optimisation framework for determining equipment configuration with heat recovery in order to minimize total cost. In this case, the solution can be represented graphically in a concise manner.

The problem involves a 2500 passenger LNG cruise ship for Caribbean climate. Constant conditions are assumed: 27 °C seawater temperature, 35 °C air temperature, 80% air humidity and 15 MW electrical power demand for hotel and propulsion. Additionally, the requirement of hot water is 10 t/h, air flow in air conditioning 50 t/h, and freshwater production 40 t/h. In the scope of this study, the major choices that a designer faces are determining the sizes of the utility equipment (boiler, compression chiller) and freshwater production by reverse osmosis (RO), evaporation (EV) or a mix of both. RO has higher energy efficiency, but EV utilises heat that may be available ‘for free’.

The first column in Table 1 shows the candidate equipment available for selection. Columns four to ten represent thermal streams associated with the equipment. Heat duty is positive for hot streams and negative for cold streams. The total heat duty of a stream is given by multiplying this value by the output of the equipment that the stream belongs to. For instance, the 10 MW power output of the dual fuel engine requires 167 kW LNG heating duty. A more detailed description of the case study, including cost parameters, is given in an online Python notebook (*Supplementary material*).

Table 1. Equipment and thermal stream data.

Equipment	ID	Size	Stream	ID	Type	Supply temp [C]	Target temp [C]	Heat capacity [kJ/kg C]	Heat duty [kW]
Dual fuel engine	ENG	Elec power [MW]	LNG heating	LNG	Cold	-160	30	2.09	-16.7
			Exhaust gas	EG	Hot	360	277	1.08	136
			Charge air	CAC	Hot	215	50	1.08	294
			Cylinder wall	JWC	Hot	150	150	-	155
			Lubricating oil	LOC	Hot	80	56	1.9	59
Exhaust gas economizer	EGE	Heat [MW]	Heat discarded	DMP	Cold	267	267	-	-1000
Compression chiller	CCC	Cooling duty [MW]	Refrigerant condensation	CND	Hot	35	35	-	1500
			Refrigerant evaporation	EVP	Cold	1	1	-	-1000
Water heater exchangers	HWH	Water flow [t/h]	Heating	WH	Cold	27	70	4.09	-648
Air conditioning	AC	Air flow [t/h]	Air cooling	AHU_C	Hot	35	12	1.08	86
			Air heating	AHU_H	Cold	12	23	1.08	-42.8
Gas fired boiler	GFB	Heat duty [MW]	10 bar steam	MPS	Hot	184	184	-	1000
Sea water pumps	SWP	Water flow [t/h]	Cooling water heat input	SW	Cold	27	30	4.19	-45.2
Multi-stage evaporator	MSF	Water flow [t/h]	Preheating	SWF	Cold	27	80	4.19	-799
Reverse osmosis unit	RO	Water flow [t/h]	-	-	-	-	-	-	-

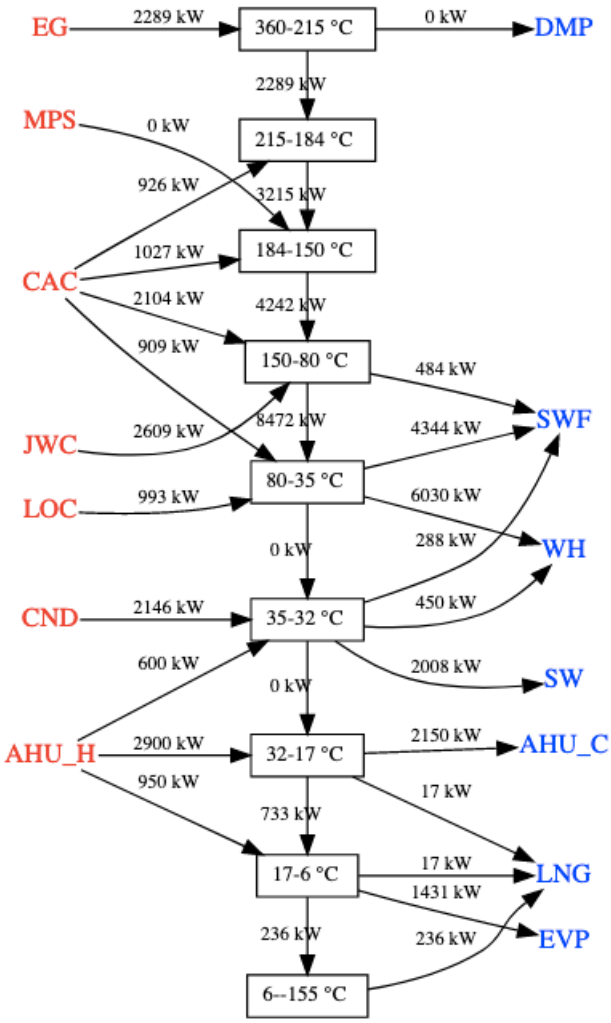

Figure 3. Heat cascade in the cost optimal configuration.

The obtained heat cascade in the cost optimal configuration is shown in Figure 3 and the optimal equipment sizes are listed in Table 2. In this case, the problem is formulated and solved for a single period only and there is no distinction between the equipment's load decision variable and capacity variable. However, this small example problem does not reflect the performance of state-of-the art solvers, as larger problems of many orders of magnitude can be solved efficiently in practice.

Table 2. Optimal equipment sizes.

Equipment	Size	Unit	Stream	Heat duty [MW]
ENG	16.8	Elec power [MW]	EG	2.3
			CAC	5.0
			JWC	2.6
			LOC	1.0
			LNG	-0.3
EGE	0.0	Heat [MW]	DMP	0.0
CCC	1.4	Cooling duty [MW]	CND	2.1
			EVP	-1.4
HWH	10.0	Water flow [t/h]	WH	-6.5
AC	50.0	Air flow [t/h]	AHU_C	4.5
			AHU_H	-2.1
GFB	0.0	Heat duty [MW]	MPS	0.0
SWP	44.6	Water flow [t/h]	SW	-2.0
MSF	11.5	Water flow [t/h]	SWF	-5.1
RO	28.5	Water flow [t/h]	-	0.0

11.4 Conclusions

The optimisation model formulation presented in this work provides a systematic approach for heat integrated ship energy system design. The heat integration problem was formulated as a linear programming problem, which can be solved very efficiently. This model was embedded in a mixed-integer programming model, which features the decisions on the selection, sizing and operation of available equipment. As a result, the searching process of process integration is automated. The optimisation framework presented covers the main aspects of complex heat integration design problems for ships. Within this framework, many important problems can be tackled, including sink and source temperature selection in thermodynamic cycles, working medium selection and steam network design [2].

A number of extensions increase the usefulness of the model. Some streams may not exchange heat with each other due to physical location, heat exchange coefficient or control issues. Such forbidden matches must be enforced by additional constraints and light reformulation of the problem. However, this comes at the cost of an increased number of decision variables.

The heat integration model gives the target for maximum heat recovery potential, but not the detailed heat exchanger network configuration. The pinch point(s) derived from the heat cascade can aid in the design of the detailed network, as these points split the network to two or more disconnected parts that do not exchange heat. Although the pinch point may change between operation periods, the small number of periods that account for the largest share of total heat load should guide the heat exchanger network design.

Supplementary materials

Python script for the optimization model formulation is available at https://users.aalto.fi/~aritari/intens.html

References

[1] F. Baldi, S. Moret, K.Tammi and F. Marechal, “The role of solid oxide fuel cells in future ship energy systems” Energy, vol 194, 2020.

[2] F. Marechal and B. Kalitventzeff, “Computer-aided Integration of Utility Systems” in Computer Aided Process and Product Engineering, L Puigagianer and G. Heyen, Eds. Weinheim: Wiley Verlag GMBH & Co, 2008.

[3] LT Biegler and I. Grossmann, “Systematic methods of chemical process design”, Prentice Hall, 1997.

[4] F. Baldi, T-V. Nguyen and F. Ahlgren, “The application of process integration to the optimisation of cruise ship energy systems: a case study“, 2016, in Proceedings of ECOS 2016.

[5] J. Vanttola and M. Kuosa, ” Pinch analysis of a case bulk carrier ship and integration of a steam Rankine cycle”, in Ship energy efficiency technologies – now and the future, Z. Guangrong, Edt. VTT Technology, 2016.

12. Ship hybridization - system configurations and their comparison

Paula Immonen[1], Pasi Peltoniemi[1], Iurii Demidov[1],
Andrey Lana[1], Olli Pyrhönen[1], Tuomo Lindh[1], Henri Montonen[1]
LUT University

12.1 Introduction

Energy efficiency is one of the key indicators of the vessel electric system because it directly affects engines' fuel consumption. Nowadays, the vessel electric system is typically based on alternating current (AC) technology. However, in hybrid vessels, power electronic converters are used to connect many of the subsystems, such as propulsion systems, and energy storage systems to the electric system. Power electronic converter could also be used in direct current (DC) based electric systems. In DC-based power distribution systems, less conversion stages are needed, making the DC-based approach attractive. In this paper, we investigated the hybridization of the electrical network of a cruise vessel, as shown in Figure 1, especially concerning different system configurations and their comparison.

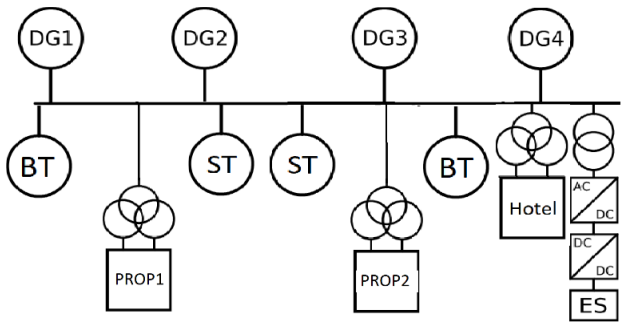

Figure 1. Investigated cruise vessel network.

[1] Contact: firstname.lastname@lut.fi

12.2 Case study

First, different configuration options are determined and rough performances, with respect to fuel consumption, operation hours, fuel price and maintenance cost, are defined for the different options. The output is system configurations: number of diesel generators, power of diesel generators and battery capacity, power and minimum required C-value, if there is battery energy storage system (BESS) in configuration. Calculation is implemented with Matlab.

Load data and power distribution

The power distribution is analysed based on diesel generators load. Power distribution and energy in different load are determined. Figure 2 presents power distribution and energy in different load.

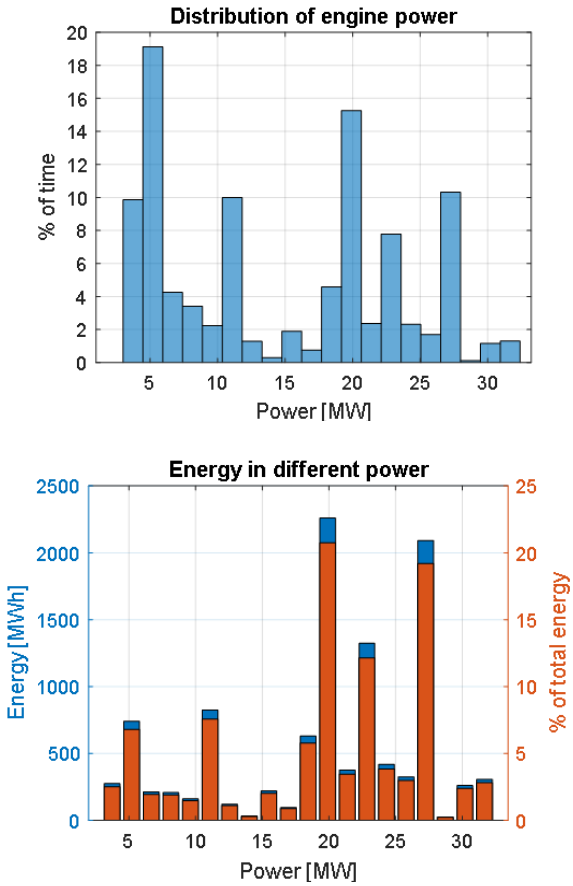

Figure 2. Power distribution and energy in different load (in power).

Engine data, specific fuel oil consumption curves

The specific fuel oil consumption (SFOC) of different engines is determined based on the available data. The fuel consumption is given from 100 % load to 50 %. The fuel consumption has been estimated when the load is below 50 %. Specific fuel consumption curves are derived for 13 different diesel engines.

Configurations

All possible diesel generator combination options are determined. For each option, the following information is provided: the number of diesel generators (N), the maximum power of the diesel generators (max_p), which equals to the total rated power of the diesel generators, and the power range (P_min, P_max).

Mode 0: diesel generators only mode

There are three different mode options when implementing the configurations. In mode 0, only diesel generators are included in configuration and all load power is distributed among diesel engines.

All configurations that meet the criteria are selected and, for each configuration, the estimates of the fuel consumption and operating hours of diesel generators during the load cycle are determined. The total power of the diesel generators P_{total} is between 46 MW and 60 MW, and the number of diesel generators at configuration is 4. Diesel generators are operated at a maximum power of 85 % of the diesel generator's rated power. Table 1 presents ten different configuration options with the lowest fuel consumption and Figure 3 presents the fuel consumption and operating hours (with mode 0) of all different configurations.

Table 1. Ten different configuration options with the lowest fuel consumption, showing the steady state fuel consumption and operation hours.

DG1 [MW]	DG2 [MW]	DG3 [MW]	DG4 [MW]	Total [MW]	Fuel cons. [ton]	Operation hours [h]
5.9	9.44	14.4	16.8	46.54	1987	1309
5.9	10.8	14.4	16.8	47.9	1992	1301
5.9	10.8	16.8	16.8	48.94	1993	1397
5.9	7.08	16.8	16.8	46.58	1993	1363
5.9	10.8	16.8	16.8	50.3	1997	1381
5.9	14.4	14.4	16.8	51.5	1999	1250
5.9	14.4	16.8	16.8	53.9	2000	1250
7.08	8.26	14.4	16.8	46.54	2000	1353
5.9	8.26	16.8	16.8	47.76	2000	1364
7.08	9.44	14.4	16.8	47.72	2003	1260

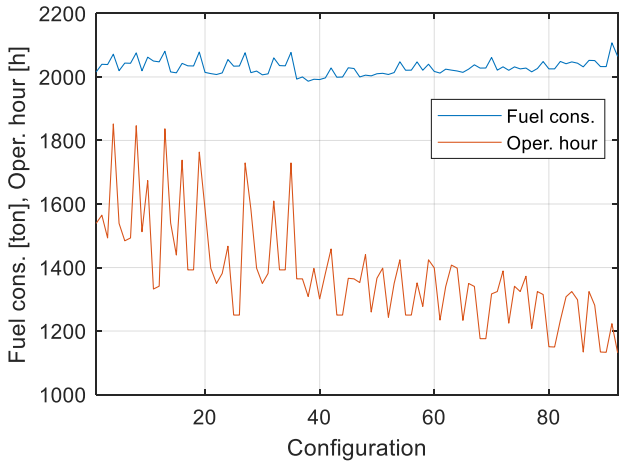

Figure 3. Fuel consumption and operation hours of all different configurations.

Fuel consumption and operation hours are estimated in steady state. The operational strategy on how the power should be distributed between the diesel generators in order to minimize the fuel consumption is derived. The chosen operational strategy is shown in Figure 4. Based on the operation achieved using the strategy, the total fuel consumption is calculated during one full load cycle. The step of engines power ΔP_{dg} is 8.5 %.

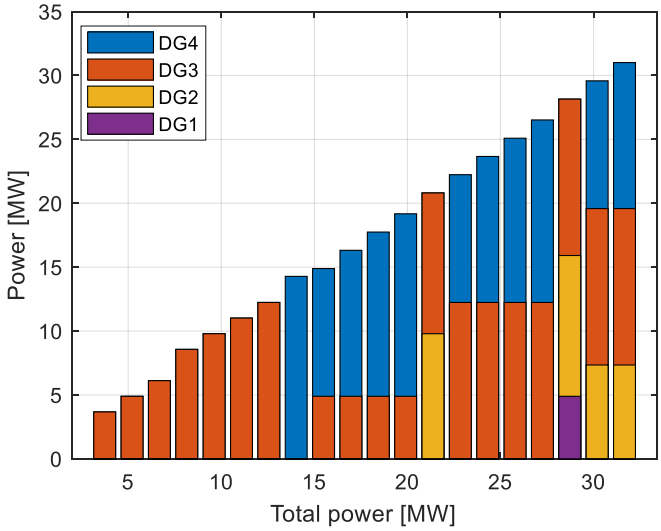

Figure 4. Power distribution between diesel generators.

Mode 1: peak shaving

Mode 1 is a peak shaving mode. If the load is greater than the total power of the diesel generators, the BESS works at the discharging mode to compensate the difference. The BESS works at the charging mode if the load is smaller than the selected minimum power of the diesel generators.

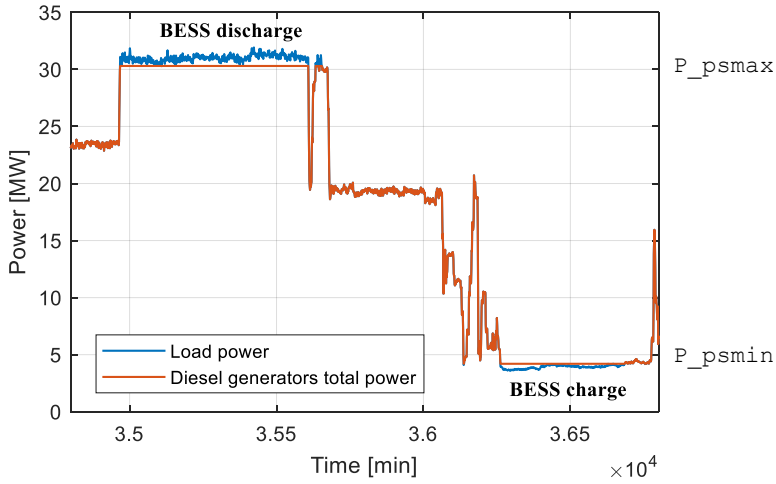

Figure 5. Peak shaving mode.

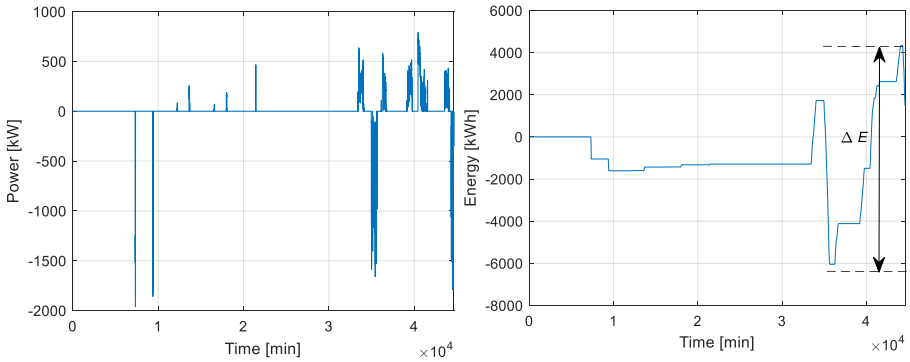

Figure 6. BESS power and BESS energy during load cycle with peak shaving mode.

The minimum BESS capacity is calculated based on the variation of energy (ΔE) during the load cycle (Figure 6). Specifically, the needed energy ΔE during the cycle is assumed to be 60% of energy storage capacity. Then the ΔE is enough also by the end of the BESS lifetime when the used state of charge (SOC) is changed from 80% to 20% (Figure 7).

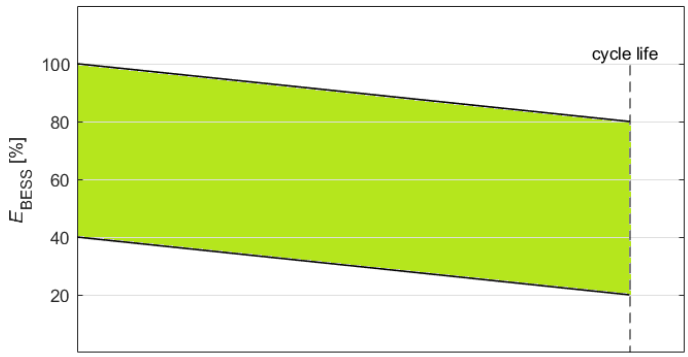

Figure 7. E_{BESS} during battery cycle life.

Other than peak shaving, the power distribution between the diesel generators follows the same principles as in Mode 0.

Mode 2: Reserve Power

Mode 2 is reserve power mode. In this mode, the BESS acts as a reserve power and the total nominal power of diesel generators can be sized then smaller. The BESS power is half of the nominal power of the largest diesel generator and the BESS capacity is enough for 15 minutes if used BESS maximum power. The power distribution between the diesel generators also follow same principles as in Mode 0.

12.3 Conclusions

The selection of diesel generator configurations of hybrid power distribution system (PDS) was studied for the case vessel. Fuel consumption and operating hours were specifically analysed. Results in Table 2 show only minor differences in operational costs between different configurations, however. Work carried out gives a basis for optimizing the battery usage for the case vessel.

Table 2. Cost of selected configurations. Fuel price is 500 $/ton; maintenance cost is 10 $/h.

	Config. 1 (Mode 0 min. Fuel cons.)	**Config. 2 (DGs only min. Oper. hours)**	**Config. 3 (Peak shaving mode min. Fuel cons.)**	**Config. 4 (Reserve power min. Fuel cons.)**
	1x5.2 MW + 1x9.44 MW + 1x14.4 MW + 1x16.8 MW (DG tot 45.84 MW)	3x14.4 MW + 1x16.8 MW (DG tot60 MW)	1x4.72 MW + 1x8.26 MW + 1x10.8 MW + 1x14.4 MW + BESS 17.3 MW, 17.3 MWh (DG tot 38.18 MW)	1x7.08 MW + 1x14.4 MW + 1x16.8 MW + BESS 8.4 MW 3.5 MWh (DG tot 38.28 MW)
Fuel consumption [ton]	1987	2065	1975	2027
CO_2 emission [ton]	6357	6608	6319	6486
Operating hours [h]	1309	1132	1465	1250
Fuel price [k$]	993 500	1 032 500	987 500	1 013 500
Maintenance cost [$]	13 090	11 320	14 650	12 500
OPEX [k$]	1 006 590	1 043 820	1 002 150	1 026 000

Reference

[1] A. Lana et al., "Methodology of Power Distribution System Design for Hybrid Short Sea Shipping," in IEEE Transactions on Industrial Electronics, doi: 10.1109/TIE.2019.2892665, URL: http://ieeexplore.ieee.org/stamp/stamp.jsp?tp=&arnumber=8617696&isnumber=4387790.

13. Data driven smart oil filter

Wictor Lund [a) 1], Jerker Björkqvist [a) 1], Jagan Gorle [b) 2]
[a)] Åbo Akademi University
[b)] Parker Hannifin Manufacturing Finland Oy

13.1 Introduction

Oil filters are membranes wrapped in a casing, through which oil is passed in order to clean it from contamination. The contamination is either contained in the source oil itself, such as fuel oils, or generated in the process that the oil is used in, such as hydraulic systems or for lubricating. Oil filters are typically passive and non-expensive components, but replacing them requires time, service and component availability and might need a stop of the equipment. Consequently, oil filters are typically replaced at regular intervals which are short enough to avoid the risk of being clogged or broken during the operation, which however may lead to unnecessary replacement of well functioning filters. On the other hand, even an almost new oil filter could get clogged, if the environment is harsh.

In the INTENS project, we aimed to develop a type of smart oil filter that can be self-aware of its own status and communicate with the environment. We address such questions as: How could sensors, IoT and data be used to predict the Remaining Useful Lifetime (RUL) of an oil filter with good precision, schedule optimal filter replacement and avoid any unscheduled stops due to filter faults? Specifically, we explored the extents of sensors, data processing and communications needed for achieving precise RUL estimation. Both theoretical work and lab experiments were necessary for developing efficient algorithms for predicting the RUL of an oil filter. These algorithms have been implemented in an edge-computing environment and validated in the lab and are to be further validated both with field data and in field tests.

[1] Contact: firstname.lastname@abo.fi
[2] Contact: firstname.lastname@parker.com

13.2 Methodology for building a Smart Oil Filter

Oil filters are used to remove contamination in fuel systems, hydraulic systems and lubrication systems. When a specified amount of contaminant is accumulated, the filter must be replaced in order to guarantee desired filtration performance and avoid filter failure. The replacement is usually pre-scheduled in practice, which however may happen at wrong time, either too early or too late. There are also sensors that can detect pressure peaks indicating faster-than-expected contaminant accumulation but still cannot tell the real condition of the filters precisely.

When an oil filter is in operation, it is of interest to know how much contaminant have been accumulated in order to know when the filter should be replaced. One way to estimate the amount of accumulated contaminant is to monitor the pressure drop over the filter manifold, i.e. the pressure difference over the filter. When the filter is free from contaminants, the differential pressure should be at its lowest. As contaminants start accumulating, the differential pressure increases over time.

The proposed smart oil filter can monitor its condition continuously, track the average change in differential pressure and thus estimate its RUL, i.e. the remaining time to the point when the critical pressure threshold is exceeded. Once the RUL of a filter is known, the replacement can then be scheduled in advance accordingly.

A quantitative model of how various parameters affect the differential pressure in steady state has been developed by Jokinen, Calonius, Gorle and Pietola, which is based on data from experiments performed at Parkers premises in Urjala, Finland [1, 2]. The measured variables include the oil flow rate, temperature, contamination level, differential pressure and the mass of the accumulated contaminants. Using the physical knowledge as a guidance, a parametric model with algebraic function is then developed to approximate the mass of the accumulated contaminants in the steady state. A valuable conclusion from the work is that, under the studied conditions, all steady state curves have the same shape, as shown in Figure 1.

While this basic idea is simple, there is unfortunately no direct relation between the amount of accumulated contaminant and the differential pressure. To address the issue in a more approachable manner, consider the oil pressure in a car whose oil and oil filter have recently been changed. The oil pressure in an engine contains

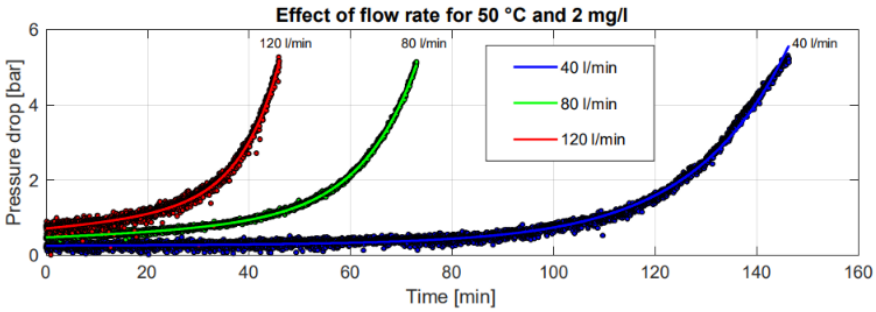

Figure 1. Typical pressure drop build-up. [3]

a larger number of components compared to the manifold differential pressure measured in a smart filter. Using the car engine as a model, we can get insight into the dynamics of oil pressure and some of the aspects that makes it difficult to estimate the current rate of contaminant accumulation. As the speed of the engine increases, the oil pressure increases to some extent because the operational speed of the pump increases. When a car is cold started in the absence of preheating, at a temperature of, for example, –10°C, the oil pressure will initially be very high because the cold oil temperature makes the viscosity of the oil very high. However, as the oil heats up while the engine is running, the viscosity of the oil decreases.

Based on this we can define some of the constraints under which the smart oil filter must be implemented. Thus, in order to estimate the RUL, we cannot solely rely on steady-state methods. To keep the manufacturing costs of the final smart oil filter product low, we only measure the differential pressure and possibly the temperature close to the smart filter computer, leaving out the flow rate and the contamination level from the experiments. The computer attached to the smart oil filter must be of microcontroller scale, in order to keep costs down and to avoid extra overhead due to larger energy consumption. The attached computer also must not require connectivity to perform the tasks needed for RUL estimation. An implication of the small scale of the smart filter computer is that the machine learning algorithms we want to perform on the edge must be constrained in terms of memory usage and computational demand.

By tracking the evolution of the differential pressure over a given oil filter throughout its lifetime, we can find the most likely differential pressure caused by the accumulated contaminant. We first need a way to identify when a plant operates at nominal oil pressure, which can be done either deterministically or probabilistically. After we have determined that the plant is operating at nominal oil pressure, we can start recording the pressure drop. Even though the plant operates at nominal oil pressure, there are still fluctuations in the differential pressure, which can be handled using, for example, a Kalman filter. The recorded data points can be used to estimate when the differential pressure will reach the critical threshold, preferably augmented with the knowledge gathered from the lab experiments. Salman Gill did a master thesis on this subject in the scope of this project [3], which contributed to this study in two ways: It produced a prototype algorithm with an accompanying software implementation for RUL estimation; and it helped conceptualize the methodological framework.

The methodology makes few assumptions about the characteristics of the filter and the usage of filter. For example, motivated by the limited lab results, we assume that filters degrade in the same way independently of their type or environment. We assume almost nothing about how the filter is used, except that there ought to be a nominal oil pressure that can be identified. However, motivated by speculation, we do assume that there are differences in how filters degrade between different plants although our methodology does not differentiate between these, apart from the maximal allowed pressure drop over the filter. For example, we believe that there may be differences in degradation behaviour among the fuel oil filter on a ship, the lubrication oil filter in a car and the hydraulic oil filter in an excavator.

Another question is what will happen in the next cycle after an oil filter is replaced. Will we see the same differential pressure development? Will we see trends? Will there be surprises? We do not have the data to make conclusions yet, but we explore how the different alternatives can be addressed. We currently assume that each filter cycle will be the same in order to improve the prediction accuracy. Similarly, we could add the assumption that in a new installation, the filter will behave the same as in other similar installations. Besides, from a collection of differential pressure evolution datasets, we can create profiles that represent the statistical behaviour of the filters. A statistical profile can give more confidence in the historical data compared to any single differential pressure evolution dataset.

More quantitatively, information about inter-cycle behaviour can be used for RUL estimation when we have no other information available. For instance, the method for estimating the RUL requires that we have a large enough number of data points about the nominal differential pressure. To get one nominal pressure data point, the method needs to decide that the plant is in a specific operating point. This may take a long time to reach or may not even happen at all under some operating conditions. The amount of time necessary to reach a decision is affected by the properties of the plant itself, the sensitivity of the method and the method's rate of convergence. When there are too few data points available to make an estimate, we can use prior data as discussed previously.

13.3 Research and implementation

The work towards a Smart Oil Filter implementation is divided into phases. The goal is to implement a device, attached to the oil filter manifold, which uses measured differential pressure over the manifold as input, and adopts a data driven approach to a real-time estimate of the filter RUL as output.

13.3.1 Phase 1 - Technology review

The first step to make an overview of which techniques can be used to predict the RUL. The following were considered:

1. **Statistics based** – Using autoregression, the next data points are assumed to be a linear combination of previous values and a stochastic term.
2. **Kalman filter** – In a Kalman filter, the internal state of the system model is updated using a combination of internal state updates and measurements. Kalman filters assumes that the model is linear. If the systems is non-linear, an extended Kalman filter can be used.
3. **Particle filters** – In a particle filter, the internal state is estimated based on all previous observations. As a result, the probability density of the current state is achieved. The main difference from Kalman filters is that the system model does not need to be linear. The challenge with this method is that it is computationally heavy.

Figure 2 gives a comparison of aforementioned techniques for estimating RUL. [3]

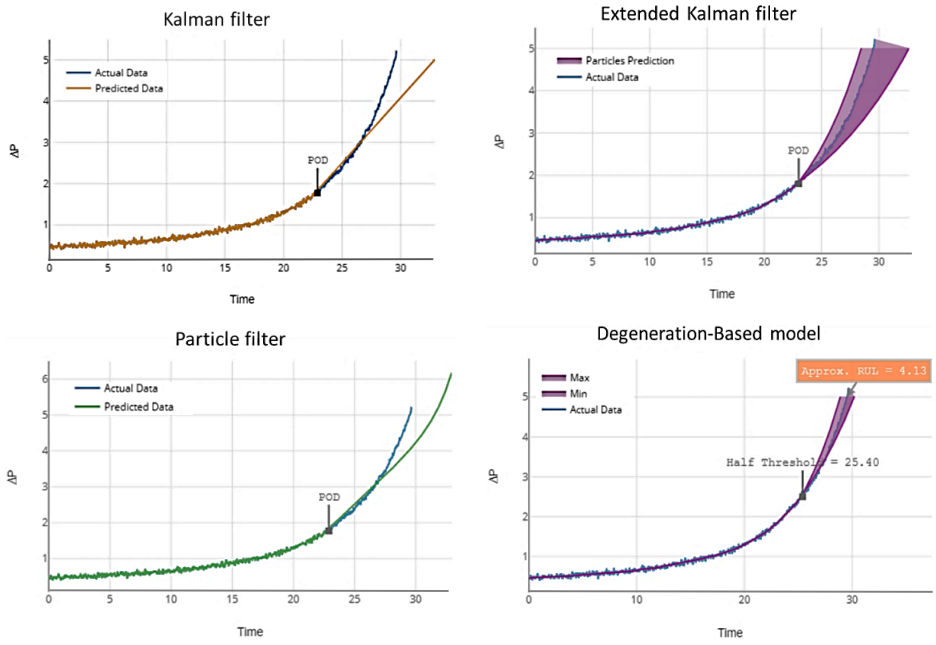

Figure 2. Comparison of techniques for estimating RUL. [3]

13.3.2 Phase 2 - Proof of concept and lab tests

First a few design decisions are made. We wanted a prototype which we could use to run experiments at the lab in Urjala. For this, we needed a platform which is easily programmable with the support for existing machine learning libraries together with robust analog I/O.

The hardware platform for the intended product should be in the microcontroller scale. However, we could not find a good candidate that would provide enough flexibility to test different kind of implementation options. We decided to use the modular Revolution Pi platform, which is an open source industrial PC based on the Raspberry Pi. For ours study, we needed one compute module and an analog I/O module, which support both voltage I/O and mA current I/O.

The Revolution Pi runs by default a customized version of Raspbian that allows the installation of a wide variety of packages out of the box. Since there are libraries for the python programming language to program the I/O ports, it was possible to make calculations using the familiar Numpy and Scipy libraries from python with data directly from the I/O ports. When we use python together with commonly available libraries, it is possible to develop parts of the software on a normal workstation computer even without the access to the embedded system, making the development process faster.

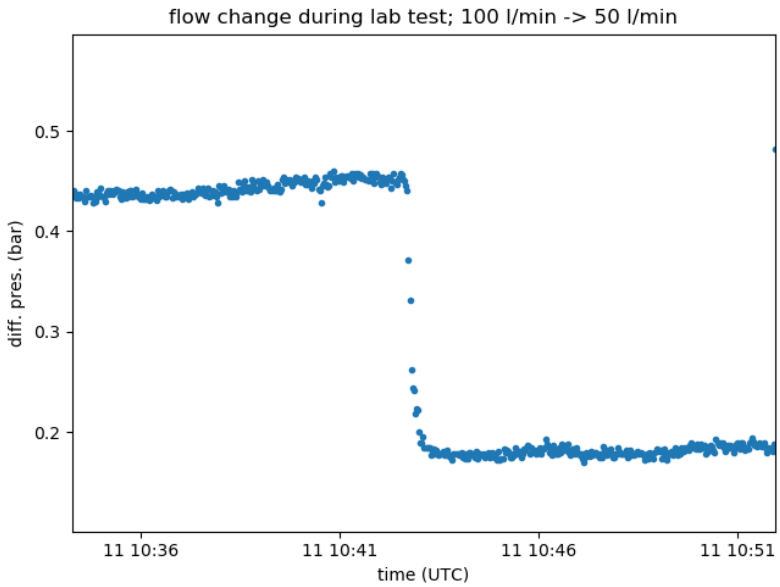

Figure 3. Pressure drop as flow rate through filter is changed.

We developed a prototype software at the premises of Åbo Akademi, even without access to a differential pressure sensor, testing the software only with lab data and synthetic data. When we got enough confidence in our prototype, we went to Urjala to test it. There we plugged in the Revolution Pi into the 4-20 mA current loop used by the pressure sensors. The results help us understand the fluctuating behaviour of the differential pressure as well as more insight into what kinds of things can go wrong. As an example, Figure 3 shows the reaction of the differential pressure to the sudden change of oil flow rate through the filter.

13.3.3 Phase 3 - Field study.

The Smart Filter algorithms have proven to work both in the simulation and in the lab, however in rather steady state situations. The next step is to investigate how the algorithms perform in the situations where there are large variations in temperatures as well as multiple start-stop cycles. The plan is to get data from plants operated in the field and to feed the differential pressure data into the algorithm.

The Phase 3 is still ongoing.

13.4 Discussions

The Smart Oil Filter methodology is taking shape. While the development of a Smart Oil Filter may seem like a bread and butter IoT development task, the constraints on the artefact we have adds considerably the development complexity.

1. We have only a small number of measurements at disposal to estimate the RUL.
2. The environment is rough and diverse.
3. The amount of space and energy at disposal is limited.
4. There is limited connectivity.

Without some of these constraints, the validation phase would be a lot simpler. If we would have a larger number of measurements, we could use more reliable estimation methodologies. If the environment for the Smart Oil Filter would be more friendly for electronics and other equipment, the field study would be easier to implement. With less environmental diversity, the field study would not even be necessary.

While there are challenges, we believe that this approach is promising. The largest weakness in the methodology we presented for estimating the RUL is that it may be difficult to identify or reach stable conditions of the plant. However, we have very little knowledge about how the field data looks like before the field test, and there may still be interesting surprises ahead.

References

[1] Jokinen, A., Calonius, O., Gorle, J. & Pietola, M. *Effects of flow and oil properties on filter service life*, Integrated Energy Solutions to Smart And Green Shipping: 2019 Edition. Helsinki, Finland: VTT Technology: 45-50

[2] Jokinen, A., Calonius, O., Gorle, J. & Pietola, M. *Data correlation model for hydraulic fluid filter condition monitoring*, 16th Scandinavian International Conference on Fluid Power (SICFP 2019). Tampere, Finland: 212-220

[3] Gill, Salman Aslam, Evaluation of Prediction Models for Smart Oil Filters, Master's Thesis 2019, Åbo Akademi University, http://urn.fi/URN:NBN:fi-fe2019050914881

14. Fault detection in marine systems using soft sensors

Mikael Manngård[1], Jerker Björkqvist[1]
Åbo Akademi University

14.1 Introduction

Knowing when sensor data can be trusted is crucial for an automated process. Model-based fault detection and isolation (FDI) has received considerable attention during the past decades [1,2] and has been applied for aircraft control [3], in automotive industries [4,5], and in chemical [6] and paper processes [7], just to mention a few. Typically, FDI-schemes rely on mathematical models to capture the dynamics of the process. The mathematical models are used to derive observers (aka soft sensors) which are used to generate signal residuals of output estimate errors. By making the observers insensitive to different types of faults that occur at various locations in the process, faults can be detected and isolated by comparing the signal residuals [8].

When a system is subject to unknown external disturbances or inputs, in order to avoid false alarms, it is important that either the unknown disturbances are estimated or the estimated signal disturbances are decoupled from the unknown inputs [9]. The problem of FDI using unknown input observers is closely related to the simultaneous input and state estimation (SISE) problem. A solution to the problem of estimation in the presence of unknown input signals was originally proposed in 1987 in [10], but was as late as in 2008 shown to provide optimal state estimates [11]. The recursive observer proposed in [11] provides unbiased and minimum-variance optimal input and state estimates for the case when we are completely ignorant of the statistical nature of the unknown input signals.

In practice, we are usually not completely ignorant about the statistical nature of input signals. It is not completely unrealistic that the variance of unknown inputs or disturbances is known prior to the estimation. Thus, in this paper, by assuming that input disturbances have known variances, following similar lines as in [12], a

[1] Contact: firstname.lastname@abo.fi

Kalman-filter type of input-and-state estimator (KF-SISE) is derived. Furthermore, we show that the output error residuals of the KF-SISE filters are completely decoupled from the unknown inputs and can hence be used to detect and isolate sensor faults.

14.2 System description

In control engineering, it is common practice to represent physical systems with state-space models, where the relation between inputs, outputs (measurements), state and noise variables are represented as a set of first order differential equations. A linear discrete linear time invariant (LTI) state-space model is of the form

$$x(k+1) = Ax(k) + Bu(k) + Fv(k),$$
$$y(k) = Cx(k) + w(k),$$

where $x(k) \in \mathbb{R}^n$ is a vector of states, $u(k) \in \mathbb{R}^n$ is a vector of input signals affecting the system and $v(k) \in \mathbb{R}^n$ is white noise which is assumed to be uncorrelated with the inputs. The vector $y(k) \in \mathbb{R}^p$ contain the available measurements, which are assumed to be a linear combination of the states and to be affected by white noise $w(k) \in \mathbb{R}^p$. For simplicity, we assume that the noise vectors $w(k), v(k)$ are uncorrelated. However, all results to follow can be extended to including correlations. Many physical systems can be modelled in the above form. For example, rotating machinery such as engine-and-generator sets [13, 14] and azimuth thruster drivelines [15] are naturally represented by a state-space model under some ideal conditions using Newton's laws of rotation.

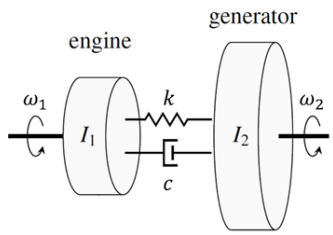

Figure 1. Two-mass model of an engine-generator set.

Example 1. *Consider the mechanical system of an engine connected to a generator through a flexible coupling. The motor is represented by a single mass with inertia I_1, and the generator by a mass with inertia I_2, as shown in Figure 1. Newton's laws of rotation describe the change in angular velocities ω_1, ω_2 and shaft angles θ_1, θ_2 through the following set of ordinary differential equations:*

$$\dot{\omega}_1 = -c/I_1\,(\omega_1 - \omega_2) - k/I_1\,(\theta_1 - \theta_2) + 1/I_1\,\tau_1,$$

$$\dot{\omega}_2 = c/I_2\,(\omega_1 - \omega_2) + k/I_2\,(\theta_1 - \theta_2) + 1/I_2\,\tau_2,$$
$$\dot{\theta}_1 = \omega_1, \qquad \dot{\theta}_2 = \omega_2$$

where c and k are the damping and stiffness coefficients of the coupling respectively. The external signals τ_1 and τ_2 represent the motor and generator torques respectively. Defining a state vector $x = [\omega_1 \quad \omega_2 \quad \theta_1 \quad \theta_2]^T$ and an input vector $u = [\tau_1 \quad \tau_2]^T$, the system is readily expressed in a state-space form and a discrete-time model is obtained by discretization e.g. using zero-order-hold or bilinear transform.

14.2.1 Sensor faults and unknown disturbances

In practice, there are often unknown external excitations affecting the states of a system and it is also common that measurements contain faults. Denoting unknown external excitations $d(k)$ and sensor faults (including noise) $f(k)$, we have the following state-space model

$$\begin{aligned} x(k+1) &= Ax(k) + Bu(k) + Fv(k) + Gd(k), \\ y(k) &= Cx(k) + f(k). \end{aligned} \tag{1}$$

The goal in this paper is two-fold: (i) reconstruct the states and input disturbances based on available measurements; (ii) use redundancy in measurements to detect and isolate sensor faults. Formally, we would like to design a linear and stable filter for estimating the states $x(k)$ and input disturbances $d(k-L)$, $L > 0$, from measurements $y(k), y(k-1), \ldots$. Note that a time-delay L in the input disturbance has been introduced. This is a necessity since there disturbance $d(k)$ does not affect the measurement $y(k)$ at time instance k. In case there is a redundancy in the available measurements, a bank of SISE-filters, where each filter uses a subset of the available measurements, can be constructed. By analysing the estimated output residuals between the filters, sensor faults can be detected and isolated.

14.3 Simultaneous input and state estimation

A standard problem in control engineering is the design of linear filters (aka observer/estimators/soft sensors) to reconstruct the state-vector $x(k)$ based on the known input signals $u(k)$ and available measurements $y(k), y(k-1), \ldots$ up to time-instance k. The problem of finding a minimum-variance optimal observer in the presence of noise was famously solved by Rudolf E. Kálmán and is nowadays simply referred to as the Kalman filter. The Kalman filter is widely considered one of the great achievements in control theory [16]. The steady-state versions of the filter come in two forms: the predictive Kalman filter

$$\hat{x}(k+1) = (A - KC)\hat{x}(k) + Bu(k) + Ky(k), \tag{2a}$$

and the filtering Kalman filter

$$\hat{x}(k) = (I - KC)A\hat{x}(k-1) + (I - KC)Bu(k-1) + Ky(k), \tag{2b}$$

where the matrices K are the Kalman-filter gains and are given as a solution to a discrete algebraic Riccati equation.

The Kalman filter does not directly provide a solution to the SISE problem, and the general SISE-problem for the case where the input excitations are completely unknown, i.e. no prior knowledge of the statistical or spectral properties of the signals is available, was solved as late as in 2007 in [10]. Statistically, a signal being completely unknown would correspond to the signal being white noise with infinite variance. However, such an assumption makes little sense physically. Thus, in this paper, we assume instead that the unknown input disturbances have finite (but possible large) variance. This allows us to formulate the SISE problem as a Kalman-filtering problem (KF-SISE).

14.3.1 KF-SISE

Consider the case in (1) where $f(k) = w(k)$ is zero-mean white noise with covariance Q and $v(k)$ has covariance R. The unknown input signal $d(k)$ is modelled as white noise with covariance Q_d or equivalently as a noise process

$$d(k) = Ee(k), \tag{3}$$

where $e(k)$ is zero-mean white noise with unit covariance and $E = Q_d^{1/2}$. Substituting (3) into (1) gives the extended state-space model

$$\begin{bmatrix} d(k) \\ x(k+1) \end{bmatrix} = \begin{bmatrix} 0 & 0 \\ 0 & A \end{bmatrix}\begin{bmatrix} d(k-1) \\ x(k) \end{bmatrix} + \begin{bmatrix} 0 \\ B \end{bmatrix}u(k) + \begin{bmatrix} E & 0 \\ GE & F \end{bmatrix}\begin{bmatrix} e(k) \\ v(k) \end{bmatrix},$$
$$y(k) = \begin{bmatrix} 0 & C \end{bmatrix}\begin{bmatrix} d(k-1) \\ x(k) \end{bmatrix}.$$

Note that standard Kalman-filtering techniques readily provide minimum-variance estimates of $d(k-1)$ and $x(k)$ of the above model. Furthermore, simple algebraic manipulation of the steady-state Kalman filter (2b) gives the following input and state observers:

$$\begin{aligned} \hat{x}(k) &= (I - K_2C)A\hat{x}(k-1) + (I - K_2C)Bu(k) + K_2y(k), \\ \hat{d}(k-1) &= -K_1CA\hat{x}(k-1) - K_1CBu(k) + K_1y(k), \end{aligned} \tag{4}$$

where the filter gains

$$\begin{aligned} K_1 &= P_2C^T(CP_3C^T + R)^{-1}, \\ K_2 &= P_3C^T(CP_3C^T + R)^{-1}, \end{aligned} \tag{5}$$

the error covariances

$$P_1 = \mathrm{cov}\left(d - \hat{d}, d - \hat{d}\right) = EE^T = Q_d,$$

$$P_2 = \mathrm{cov}\left(d - \hat{d}, x - \hat{x}\right) = EE^T G^T = Q_d G^T$$

and $P_3 = \mathrm{cov}(x - \hat{x}, x - \hat{x})$ is given by the unique positive solution to the Riccati equation

$$P_3 = AP_3A^T + GQ_dG^T + FQF^T - (AP_3C^T)(CP_3C^T + R)^{-1}(AP_3C^T)^T.$$

Estimates are unbiased, i.e. $\mathrm{E}[\hat{x}(k)] = x(k)$ and $\mathrm{E}[\hat{d}(k)] = d(k)$ as $k \to \infty$, and the error covariances are minimized. Observe that, although the disturbance error variance P_1 is large, in fact, it is the same as the assumed signal variance, and the estimates $\hat{d}(k)$ have been obtained with only a single time-lag $L = 1$ with respect to the available measurements. By introducing a larger time-lag $L > 1$, the error variance can be significantly reduced, cf. [13,15]. This is referred to as fixed-lag smoothing in the control literature [15].

Example 2. *Consider the system in Example 1. We assume that angular velocities are measured from both the engine and generator, torque is measured from the flexible coupling, and average torque loads are known and contained in* $u(k)$*. Torque excitations, e.g. from combustion, are unknown, represented by* $d(k)$*, and to be estimated. This example illustrates the effect that fixed-lag smoothing has on the error covariances of the input torque estimates.*

It is assumed that the state noise vector $v(k) = 0$ *and measurement errors are white noise* $w(k)$ *with known covariance matrix* $Q = 10^{-4}I$*. The variance of input torque excitations is assumed to be* $Q_u = 10^3 I$*. Stiffness and damping coefficients are* $c = 3.4 \times 10^3$ *Nm/(rad/s) and* $k = 905 \times 10^3$ *Nm/rad respectively, and the moment of inertias* $I_1 = 570, I_2 = 950$ *kgm². The error variances for the instantaneous torque excitations are illustrated in Figure 2 for time-lags L*$= 1, \ldots, 10$*.*

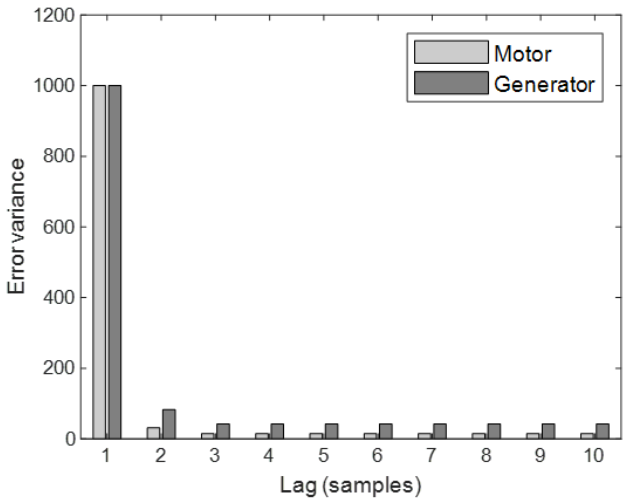

Figure 2. The impact of fixed-lag smoothing on the error variances of the input estimates.

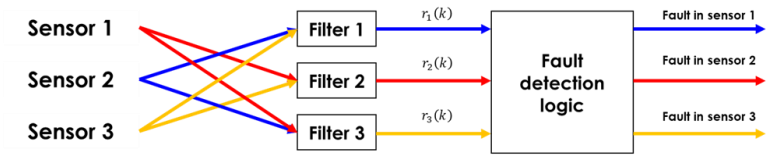

Figure 3. Fault detection and isolation scheme for a system with three sensors.

14.4 Fault detection and isolation

A simple FDI scheme that uses redundancy in measurements to detect sensor faults is to create a bank of Kalman filters where one sensor has been left out from each filter. This is illustrated in Figure 3. The resulting filter bank contains as many filters as sensors.

The state estimation residual for a KF-SISE (4) is obtained by combining (1) and (2b) and given by

$$\varepsilon(k) = x(k) - \hat{x}(k) = (I - K_2C)A\varepsilon(k) + (I - K_2C)Fv(k) - K_2f(k). \tag{6}$$

and the output-error residual is

$$r(k) = y(k) - \hat{y}(k) = y(k) - C\hat{x}(k) = C\varepsilon(k) + f(k). \tag{7}$$

Defining a new state variable $z(k) = \varepsilon(k) + K_2f(k)$, the dynamics of the residual system is described by the following state-space model

$$\begin{aligned} z(k+1) &= (I - K_2C)Az(k) + (I - K_2C)Fv(k) \\ r(k) &= Cz(k) + (I - CK_2)f(k). \end{aligned} \tag{8}$$

Any filter-gain K_2 is designed such that $|\text{eig}(A - K_2CA)| < 1$ ensures that the system (8) is stable and the residual $r(k) \to 0$ is asymptotical if there is no sensor fault present, i.e. $f(k) = 0$ and $v(k) = 0$. Conversely, if $f(k) \neq 0$, the error residual is non-zero. Note that in (8), a sensor fault $f(k)$ affects the output residual $r(k)$ directly with gain $(I - CK_2)$. If the state noise $v(k)$ is small compared to the magnitude of the sensor faults, faults can be detected by analysing the residual $r(k)$. Furthermore, by excluding a single (but different) sensor from each filter, a fault in that sensor will be visible in all filter residuals, except the filter from which that sensor has been left out. This allows us to both detect and isolate faults by comparing output-error residuals. A limitation of the proposed FDI-scheme is that only a single sensor fault can be detected at any given time.

Example 3. *Consider the same setup as in Example 2. A filter bank containing three KF-SISE filters designed as in Section 3.2 are implemented, where the velocity*

measurement from the motor has been left out from the first filter, the velocity measurement from the generator has been left out in the second, and the torque measurement from the flexible coupling has been left out in the third. In Figure 4, the magnitudes of the residuals relative to the sensor fault are illustrated. It is of interest to note that faults in torque measurements cannot be detected in this example. This is, however, an artefact of this specific problem and does not hold in general.

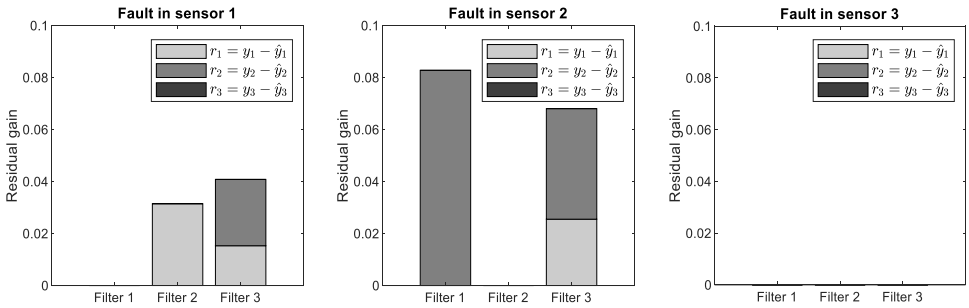

Figure 4. Residuals relative to the fault magnitude $|r_i/f_j|$.

14.5 Summary

In this paper, a soft sensor for simultaneous input and state estimation and fault detection and isolation has been derived. By assuming that the unknown input signals have known signal variance, input and state observers can be derived using standard Kalman-filtering techniques. Furthermore, the resulting output-error residuals have been decoupled from the unknown input signals, which allows us to both detect and isolate sensor faults. An example of an engine-generator set has been used to demonstrate that unknown inputs can be accurately estimated by fixed-lag smoothing, and sensor faults can be detected and isolated from the output-error residuals.

References

[1] Willsky, A. S. (1976). A survey of design methods for failure detection in dynamic systems. *Automatica*, *12*(6), 601-611.

[2] Patton, R. J., & Chen, J. (1997). Observer-based fault detection and isolation: Robustness and applications. Control Engineering Practice, 5(5), 671-682.

[3] Wang, D., & Lum, K. Y. (2007). Adaptive unknown input observer approach for aircraft actuator fault detection and isolation. International Journal of Adaptive Control and Signal Processing, 21(1), 31-48.

[4] Gertler, J. J., Costin, M., Fang, X., Hira, R., Kowalczuk, Z., & Luo, Q. (1993). Model-based on-board fault detection and diagnosis for automotive engines. Control Engineering Practice, 1(1), 3-17.

[5] Hsu, P. L., Lin, K. L., & Shen, L. C. (1995). Diagnosis of multiple sensor and actuator failures in automotive engines. IEEE transactions on vehicular technology, 44(4), 779-789.

[6] Pierri, F., Paviglianiti, G., Caccavale, F., & Mattei, M. (2008). Observer-based sensor fault detection and isolation for chemical batch reactors. Engineering Applications of Artificial Intelligence, 21(8), 1204-1216.

[7] Jämsä-Jounela, S. L., Tikkala, V. M., Zakharov, A., Garcia, O. P., Laavi, H., Myller, T., ... & Hämäläinen, V. (2013). Outline of a fault diagnosis system for a large-scale board machine. The International Journal of Advanced Manufacturing Technology, 65(9-12), 1741-1755.

[8] Clark, R. N., Frank, P. M., & Patton, R. J. (Eds.). (1989). *Fault Diagnosis in Dynamic Systems: Theory and Applications*. Prentice Hall.

[9] Edwards, C., Spurgeon, S. K., & Patton, R. J. (2000). Sliding mode observers for fault detection and isolation. *Automatica*, *36*(4), 541-553.

[10] Kitanidis, P. K. (1987). Unbiased minimum-variance linear state estimation. Automatica, 23(6), 775-778.

[11] Gillijns, S., & De Moor, B. (2007). Unbiased minimum-variance input and state estimation for linear discrete-time systems. *Automatica*, *43*(1), 111-116.

[12] Bitmead, R. R., Hovd, M., & Abooshahab, M. A. (2019). A Kalman-filtering derivation of simultaneous input and state estimation. Automatica, 108, 108478.

[13] Östman, F., & Toivonen, H. T. (2008). Model-based torsional vibration control of internal combustion engines. *IET Control Theory & Applications*, *2*(11), 1024-1032.

[14] Manngård, M., & Böling, J. M. (2017). Online frequency estimation with applications to engine and generator sets. *Mechanical Systems and Signal Processing*, *91*, 233-249.

[15] Manngård, M., Lund, W., Keski-Rahkonen, J., Nänimäinen, J., Saarela, V. P., Björkqvist, J., & Toivonen, H. T. (2019). Estimation of propeller torque in azimuth thrusters. IFAC-PapersOnLine, 52(21), 140-145.

[16] National Academy of Science (2008). Charles Stark Draper Prize for Engineering. Retrieved from https://www.nae.edu/54971/page2008.

[17] Moore, J. B. (1973). Discrete-time fixed-lag smoothing algorithms. Automatica, 9(2), 163-173.M. Young, The Technical Writer's Handbook. Mill Valley, CA: University Science, 1989.

15. Data-enriched electro-hydraulic valve-train fault diagnostics

Hannu Rummukainen[1], Antti Hynninen[1], Juha Kortelainen[1]
VTT Technical Research Centre of Finland Ltd

15.1 Introduction

Fault diagnostics aims to detect faults and their causes in the system by computational methods [1]. Faults can be detected and diagnosed either by a model-based approach, in which the expected behaviour of the system is described by a mathematical model, or by a data-based approach in which the expected behaviour of the system is described by historical data of its operation [2,3]. Hybrid approaches combining the two have also been developed [4, 5].

One of the challenges of data-based fault detection is that realistic data about faults in operation is not available; vast majority of data is typically about system operation in normal, healthy conditions. In addition, smart systems relying on artificial intelligence (AI) need vast amount of data for training. One way to address this challenge is data-enriched system fault diagnostics, where variety of data with system fault situations is generated using simulations. In data-enriched system fault diagnostics, simulated data is used as supplementary data for learning algorithms.

Internal combustion engine (ICE) can be optimized in many ways to gain better performance. Performance depends on the fuel mixture, injection amount and timing, and the engine breathing via the timing of air intake and exhaust controlled with valve-train. Faults within the valve-train result in a reduction of performance and reliability. In the conventional camshaft mechanism, the position of intake and exhaust valves is fixed to the crank rotation and cam profile. Fault detection and diagnostics system in the conventional mechanism can be based on e.g. engine vibrations [6]. In cam-less valve-train solutions, such as electro-hydraulic system [7], the valve motion is not mechanically restricted and therefore cannot be straightforwardly connected to the engine vibrations, for example. Still, the timing and lift of the valves should be fully controllable to avoid unwanted situations, such as valve collision with piston.

[1] Contact: firstname.lastname@vtt.fi

The goal of the study is to devise a system to estimate the correct valve position in electro-hydraulic valve-train system despite intermittent signal faults, or to flag the sensor as faulty whenever the valve position cannot be reliably estimated. The fault correction and detection system should operate at sub-millisecond latency, as the engine speed can be on the order of 1200 rpm (50 ms per revolution), and the system should be reliable even in a case of engine faults or abnormal operation.

15.2 Faults considered in the study

Magnetic quadrature sensors provide signal on incremental position changes of the valves in discrete steps. Speed and direction of the valve is indicated from the sensor signal. The sensors have been observed to experience intermittent signal loss, which might be due to engine vibrations, sensor assembly alignment, harsh environment or electromagnetic disturbances, for example. Investigating the reason for the signal loss is beyond the scope of this study. A data-based model of the sensor is built based on the measured data of a valve-sensor system operating in healthy or failed state.

Another fault studied here is a failure in the valve spring. Realistic experimental data in which a valve spring fails is difficult and expensive to acquire. Therefore, all the experiments were run with healthy spring. Using a first-principles simulation model describing the valve system, we simulated spring faults by decreasing the spring load from its nominal value down to 10% with 10% steps.

15.3 Experimental data

Wärtsilä has provided us with measured position data from two inlet valves of an electro-hydraulic engine. One of the inlet valve position sensors suffers from intermittent loss of quadrature signal, which means the decoded position signal may suddenly freeze. The other inlet valve position sensor functions reliably and can be used as a relatively accurate reference for the correct valve position, since the two cylinders are interlocked. There are six data sets for both valves, described in **Table**. A basic solution for the fault detection and correction of a valve sensor using the measurement data was presented earlier in this project [8], based on data set 1.

Table 1. Overview of measurement data sets.

Data set	Sample rate (kHz)	Duration (s)	Dropouts, % of duration	RPM range	Notes
1	200	15	2.0	500–750	
2	1000	5	0.4	750	
3	200	30	1.6	750	
4	200	15	0.2	180–750	Engine start-up
5	200	26	3.3	550–850	Controlled RPM variations
6	200	16	0.1	0–750	Engine shutdown

15.4 Simulation results

In addition to measurement data, Wärtsilä has provided us access to a physics-based system simulation model of the electro-hydraulic valve-train system. Using this model as the basis, spring faults were simulated with the GT-Power software [9]. Simulated effect of the valve spring preload on the valve lift curve is presented in Figure 1.

Sensor faults were added to the simulated results with Matlab [10]. Six engine cycles were used in the data, leading to the signal length of 0.96 s. The amount of signal failures was varied from 3% to 7%. The maximal failure duration was varied from 0.22 to 1.0 ms. The failure point of times during the six cycles were randomized. Due to signal losses, the lift curve starts to drift, as shown in Figure 1.

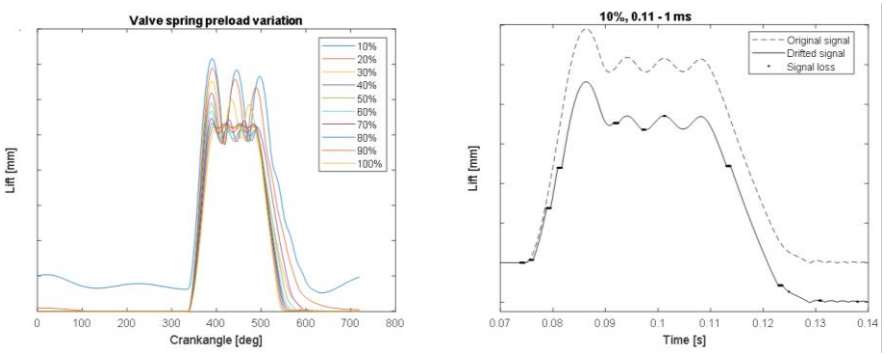

Figure 1. Effect of the valve spring preload on lift curve (left). An example of drifting due to signal loss; spring load 50%, sensor fault rate 10% and fault durations 0.11-1.0 ms (right).

15.5 Fault correction algorithm

We have implemented an algorithm that estimates valve position based on the observed position signal from the quadrature sensor. The sensor is assumed to be either healthy or faulty at any given time. Failures lead to the significant drifting of the position signal, i.e. the offset between the actual and observed position. The developed algorithm corrects drifting by detecting when the valve closes and resetting the position value.

State estimation model

The model of the valve movement is based on only basic Newtonian dynamics with three continuous state variables: the actual position x of the valve, the velocity v and the offset w between the actual position and the sensor position signal. The observed position is $x + w$. Accelerations are estimated from observations, without explicitly modelling the forces on the valve.

To model sensor failures and valve closing, we extend the system model with a discrete state variable. For technical reasons, there are seven discrete states as

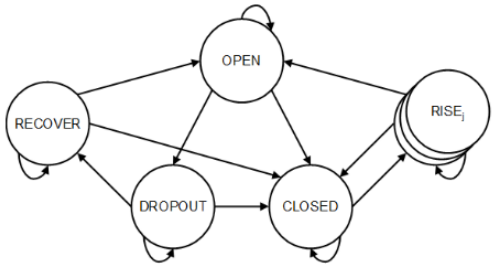

Figure 2. Discrete model states and state transitions. The OPEN and CLOSED states represent normal operation with the valve open or closed. DROPOUT represents sensor failure with the valve open. Sensor failure with the valve closed is incorporated in the CLOSED state. The RECOVER state and the three RISE$_j$ states are artificial states that enable position correction right after a sensor failure.

shown in Figure 2. When the sensor is healthy, the state changes between OPEN and CLOSED. Once a sensor failure with the valve open happens, the system enters the DROPOUT state, and after the failure passes through the artificial RECOVER state back to OPEN. Sensor failures with the valve closed are not detectable and are not modelled as such – however, if the dropout extends past the opening of the valve, there is a detectable velocity discontinuity, and we have three artificial RISE$_j$ states ($j \in \{1,2,3\}$) to model the required position correction.

In all states, the position x and velocity v follow the equations $x_{k+1} = x_k + v_k \Delta t + \frac{1}{2} a_k \, \Delta t^2$, and $v_{k+1} = v_k + a_k \, \Delta t$, where k is a time step index, Δt is the length of the time step, and the acceleration term a_k is modelled as Gaussian white noise. In discrete states other than DROPOUT, the offset stays constant with $w_{k+1} = w_k$. In the DROPOUT state, the offset w follows the equation $w_{k+1} = w_k - v_k dt - \frac{1}{2} a_k \, \Delta t^2$, keeping the observed position $x_k + w_k$ constant.

Transitions between discrete states occur otherwise at constant time intervals, but transitions to and from DROPOUT states are triggered whenever the sensor position signal changes (as the quadrature signal is discrete-valued). The transition probabilities between discrete states are modelled according to Table. In the table, the probabilities p_D, p_{DS}, p_{DR}, p_O, $p_{R,j}$, and p_{RR} are free parameters that we estimate from data. The closing probability $p_C(x, v) = \mathrm{P}(x \leq 0)\mathrm{P}(v \leq 0)$ is derived from the Gaussian distribution of state variables (w, x, v) in the origin state of the transition; this roughly approximates the probability that the estimated position is at or below closing ($x \leq 0$) and the velocity is downward ($v \leq 0$). As a special case, if the estimated mean position $x \leq 0$, transition to CLOSED state always occurs with probability 1; for simplicity this special case is not fully written out in the table. In RISE$_j$ states, only the latter mechanism is active, denoted by $p_{CR}(x)$.

On transition, the continuous state variables are not changed except in two circumstances. First, on the transition to CLOSED state, the continuous state is reset to $(s_k, 0, 0)$ where s_k is the observed sensor position. Second, on the transition to a RISE$_j$ state, the continuous state is reset to a predetermined Gaussian representing valve state early on the lift curve, as seen in Figure 3.

Table 2. Transition probabilities between discrete states. The sum of elements on each row must be 1, and the element completing the sum to 1 is indicated as $1 - \cdots$.

	To state				
From state	OPEN	DROPOUT	RECOVER	CLOSED	RISE_j
OPEN	$1 - \cdots$	$p_D(1 - p_C)$		$p_C(x, v)$	
DROPOUT		$p_{DS}(1 - p_C)$	$1 - \cdots$	$p_C(x, v)$	
RECOVER	$p_{DR}(1 - p_C)$		$1 - \cdots$	$p_C(x, v)$	
CLOSED	p_O			$1 - \cdots$	$(1 - p_O)p_{R,j}$
RISE_j	p_{RR}			$p_{CR}(x)$	$1 - \cdots$

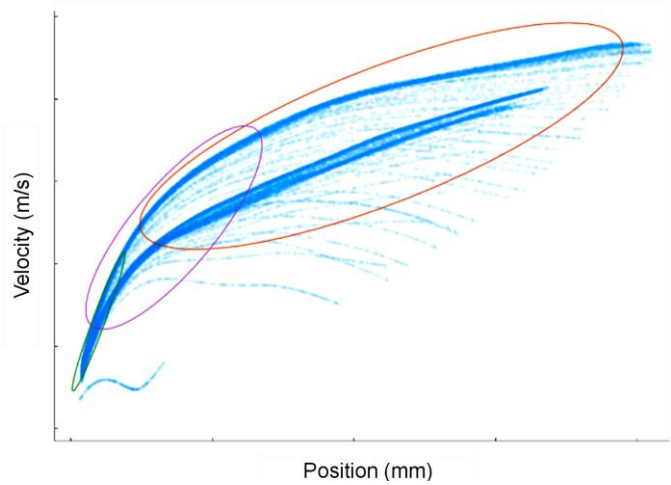

Figure 3. Measured points in position-velocity coordinates (blue), from the first 5 ms of valve lift above 0.1 mm in datasets 1 and 4. The ellipses represent a three-component Gaussian mixture model: each ellipse shows the 95% confidence interval of a bivariate Gaussian distribution. The mixture model is used as prior probabilities for position- velocity combinations when leaving CLOSED state: each RISE_j state corresponds to a separate Gaussian component.

State estimation algorithm

The continuous state variables could be estimated by a Kalman or H_∞ filter as long as the system is in a known discrete state, but there is no similar closed-form solution for estimating the discrete state transitions [11, 12]. Marginalized particle filtering is an option, but requires substantial computational effort for good accuracy [13].

In order to minimize computational requirements, we apply assumed density filtering (ADF [12, p. 658]). For each of the 7 discrete states, we maintain a single Gaussian state estimate over the continuous state variables (w, x, v). Denoting the discrete state by z, the posterior likelihood at a given time step k is of the form

$$f_k(z_k, w_k, x_k, v_k) = \sum_{i=1}^{7} \pi_k^{(i)} N_3\left((w_k, x_k, v_k)\middle|\mu_k^{(i)}, S_k^{(i)}\right),$$

where i runs over the discrete states, the weights $\pi_k^{(i)}$, means $\mu_k^{(i)}$ and covariances $S_k^{(i)}$ are estimated, and $N_3(u|\mu, S)$ is the 3-dimensional Gaussian probability density function.

For each discrete state i, the Gaussian parameters $\mu_k^{(i)}$ and $S_k^{(i)}$ are updated on each time step by a Kalman filter. In OPEN, DROPOUT and CLOSED states, we assume a one-dimensional observation $x + w$. In the CLOSED state, we apply an additional artificial observation x with fixed measurement value 0: this is a soft constraint keeping the position x near zero [14].

During sensor dropouts, the model can only project the position forward at the last known velocity, and the uncertainty of position and velocity estimates increases. To adjust the position after dropout based on velocity observations, we have augmented the system model with artificial RECOVER and RISE$_j$ states. In these states, instead of position $x + w$, the Kalman filter uses observations of velocity v, which are computed as $(s_k - s_{k-1})/\Delta t$ from observed sensor positions s_k. The velocity-based Kalman filter is not used in other discrete states, because it follows the apparent position s_k too closely to be able to distinguish dropout states.

At regular intervals, transitions between the discrete states are computed, updating the weights $\pi_k^{(i)}$ and approximating each resulting Gaussian mixture with a single Gaussian with updated parameters $\mu_k^{(i)}$ and $S_k^{(i)}$. As the desired position estimate, the algorithm outputs the expected position $\mu_k^{(i_{ML})}$ from the maximum likelihood state $i_{ML} = \mathrm{argmax}_i\, \pi_k^{(i)}$.

15.6 Computational experiments

We have performed parameter estimation for the algorithm first using only measurement data, and then using both measurement data and simulated data. The goal is to take advantage of simulated data to improve the performance of the algorithm on actual measured data sets. The data sets used for parameter estimation (training) and separately for testing are described in Table 3.

Table 3. Training data for the two cases, and separate test data.

Case	Data usage	Measured data sets	Simulated data sets
1. Measured data only	Training	1	-
2. Measured and simulated data	Training	1	Spring 60% – 100% and dropout rate 3% or 5%
Both cases	Test	3, 4, 5, 6	Spring 10% – 50% or dropout rate 7%

To estimate the transition probabilities p_D, p_{DS}, p_{DR}, p_O, and p_{RR}, we applied Bayesian optimization with the mlrMBO software package [15, 16]. The parameter optimization was based on two objectives: the primary objective is the number of time steps on which the estimated discrete state i_{ML} matches the reference data, and the secondary objective is the mean squared difference between the estimated position and the reference position (second valve in measured data sets).

15.7 Results

A summary of the results for both cases is shown in Figure 4. Individual test results from training in the data-enriched case are visualized in Figure 5.

In all measured data sets, the top of the lift curve deviated up to 19 % from the correct top height: the largest deviation occurred on measured dataset 5, which included controlled RPM variations. This was an improvement over our earlier algorithm in [8], which resulted in the deviations of up to 40 % on the same dataset.

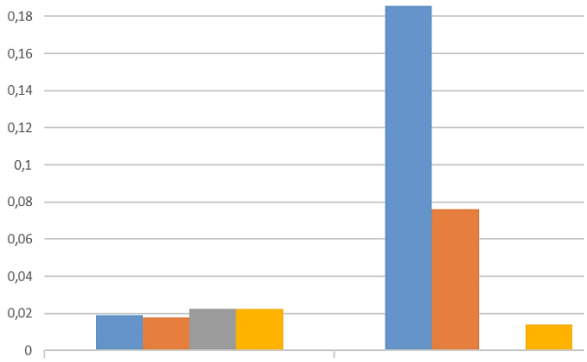

(a)

	Dropout rate		
Spring	3 %	5 %	7 %
10 %	0,15	0,25	0,21
20 %	0,10	0,11	0,13
30 %	0,07	0,11	0,12
40 %	0,02	0,03	0,03
50 %	0,02	0,03	0,02
60 %	0,01	0,02	0,02
70 %	0,01	0,02	0,04
80 %	0,01	0,02	0,02
90 %	0,01	0,01	0,03
100 %	0,01	0,01	0,02

(b)

Figure 4. a) Overall error measures after training, measured by mean position error in mm + 1000 times mean mismatch in discrete state (1 for error). Errors on measured data sets are shown on the left, and on simulated data sets on the right: case 1 testing (blue), case 2 testing (orange), case 1 training (grey), case 2 training (yellow). Note that there is no grey bar on the right, since no simulated data sets were used in case 1 training. **b)** Error measures on simulated data sets with different spring loads and dropout rates. The outlined box indicates the data sets used for training.

15.8 Discussion and conclusions

The fault correction algorithm was able to detect and correct the dropouts reasonably well, but not perfectly. Augmenting a limited amount of measurement data with simulated data in training improved the accuracy of state estimation in testing: thus, data enrichment was found useful here. However, we have found that

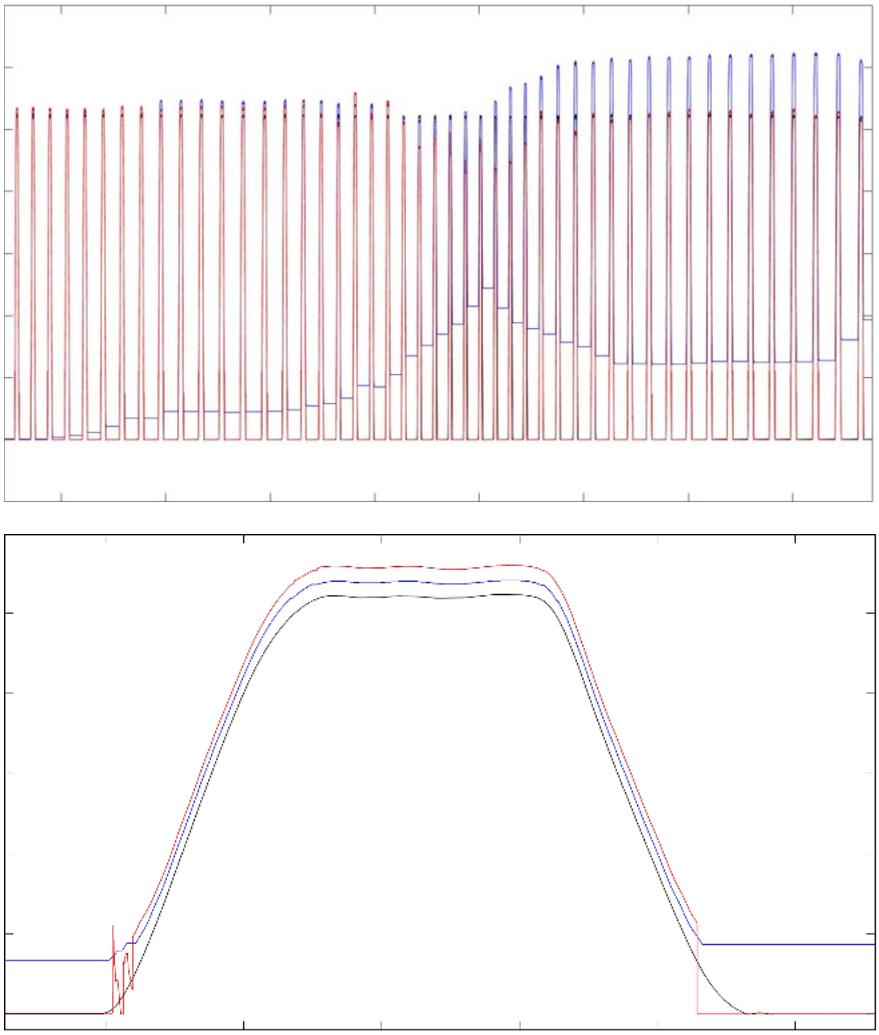

Figure 5. Overview of valve lift curves (lift in mm over time in seconds) on data set 5 (above) and an individual lift curve (below), both from case 2 (combined measured/simulated training). The figures show the estimated valve position (red) over sensor signal (blue) and reference position (black).

training with a larger subset of measurement data eliminated the advantage of data enrichment, and for now, we were unable to create more varied simulation data.

If the spring load was reduced further than the data sets included in training, the accuracy of the algorithm deteriorated. Applying a larger sensor dropout rate than found in the training data also reduced the accuracy of the algorithm, but the effect was small.

More testing and validation is needed to make the algorithm ready for production use. In particular, further work is needed to detect complete failures of either the sensor or the estimation algorithm.

References

[1] R. Isermann, Fault-diagnosis Systems, Springer, 2006.

[2] S. J. Qin, Survey on data-driven industrial process monitoring and diagnosis, Annual Reviews in Control, 36, 2012, pp. 220–234.

[3] X. Dai, and Z. Gao, From model, signal to knowledge: A data-driven perspective of fault detection and diagnosis, IEEE Transactions on Industrial Informatics, 9 (4), 2013, pp. 2226–2238.

[4] K. Tidriri, N. Chatti, S. Verron, and T. Tiplica, Bridging data-driven and modelbased approaches for process fault diagnosis and health monitoring: A review of researches and future challenges, Annual Reviews in Control, 42, 2016, pp. 63–81.

[5] S. Tripakis, Data-driven and model-based design, 2018 IEEE Industrial Cyber-Physical Systems (ICPS). IEEE, 2018.

[6] J. Flett and G.M. Bone, Fault detection and diagnosis of diesel engine valve trains, Mechanical Systems and Signal Processing, vol. 72-73,pp. 316–327, 2015.

[7] M. Herranen, Fully Variable Valve Actuation in Large Bore Diesel Engines, Doctoral thesis, Tampere University of Technology, 2014.

[8] H. Rummukainen, A. Hynninen and J. Kortelainen, Data-enriched system fault diagnostics. In Integrated Energy Solutions to Smart and Green Shipping (pp. 54-59). VTT Technical Research Centre of Finland, 2019.

[9] GT-SUITE, User's manual version v2019, Gamma Technologies, 2019.

[10] MATLAB, User's manual version R2018a, Mathworks, 2018.

[11] D.Simon. Optimal state estimation – Kalman, H_∞ and nonlinear approaches. Wiley, 2006.

[12] K. Murphy. Machine learning – a probabilistic perspective. MIT Press, 2012.

[13] F. Gustafsson. Particle filter theory and practice with positioning applications. IEEE Aerospace and Electronic Systems Magazine, 25 (7), 2010, pp. 53-82.

[14] D. Simon. Kalman filtering with state constraints: a survey of linear and nonlinear algorithms. IET Control Theory & Applications, 4 (8), 2010, pp. 1303-1318.

[15] B. Shahriari, et al. Taking the human out of the loop: a review of Bayesian optimization. Proceedings of the IEEE, 104 (1), pp.148-175, 2016.

[16] B. Bischl, et al. mlrMBO: A modular framework for model-based optimization of expensive black-box functions. URL:http://arxiv.org/abs/1703.03373, 2017.

16. Digital-twinning the engine research platform in VEBIC

Saana Hautala[1], Emma Söderäng[1], Seppo Niemi[1]
University of Vaasa

16.1 Introduction

This chapter presents important steps towards a digital twin of a hybrid power generation system. The goal is to investigate the implementation of the digital twin concept and to build a digital twin of the existing laboratory equipment in the VEBIC engine research platform. It is also beneficial to explore the twin's potential in the laboratory environment and the gained knowledge can be utilised for real ship systems later.

In order to reduce GHG emissions and meet the global goals, shipping efficiency needs to be improved. Digital twins are predicted to have an important role when moving towards a smarter and greener shipping industry. The concept may possibly offer significant benefits such as improved energy efficiency and reduced emissions. This is because a digital twin could accelerate the development and optimization of the ship power and propulsion systems as well as operational practices such as speed optimization and route planning. However, before this becomes a reality, the digital twin concept must be explored and possible challenges must be identified and resolved.

In this research, the first step was to develop the component models of the existing equipment in the VEBIC laboratory. The next step was to model the hybrid power generation system and then to convert the model into a real-time application. The electrical components were modelled with MATLAB/Simulink and the engine with GT-POWER. Simulink Real-Time was used for the real-time simulation. In order to be able to utilise the full potential of the digital twin, it is also important to investigate the connection and communication between the physical equipment and the virtual twin. A Speedgoat performance real-time target machine will be used for implementing the connection and it is designed to perform real-time simulations

[1] Contact: firstname.lastname@uva.fi

together with Simulink and Simulink Real-Time. The Speedgoat target machine in VEBIC is also responsible for the engine control system. Later on, the real-time application will be run in parallel with the real-world counterpart and then it is possible to investigate the different ways of optimizing engine design and operation, as well as the integration of technologies such as energy storages, waste heat recovery and emissions reduction.

16.2 Modelling the hybrid power generation system components

In order to model the hybrid power generation system and create a digital twin, the components in the VEBIC engine laboratory had to be modelled first. The components were divided into two main entities: the internal combustion engine and the electrical equipment connected to the engine.

16.2.1 Engine model

The engine located in VEBIC laboratory is a 4-cylinder common rail medium speed diesel engine (W4L20). At the beginning of the project, Wärtsilä provided a GT-POWER model of 4L20 engine which was used as a base model. However, the design of the 4L20 in the VEBIC laboratory is a non-commercial one, and the engine contains both marine and power plant components. Thus, time was invested in calibrating the engine model to ensure the simulations match the actual operation sufficiently and possible differences could be detected. Later, the validated engine model was used as a starting point for developing a mean value engine model.

16.2.1.1 Calibration and validation of the engine model

The engine model calibration was started with the component calibration. The charge-air-cooler (CAC), the turbocharger and the cylinder were calibrated separately against measurement data. The data used in the calibration was from previous engine experiments measured in the VEBIC engine laboratory, where the load points had been 10%, 25%, 50%, 75%, 100% and 110%, and the engine was run at the nominal speed of 1000 rpm. In the calibration, the load points of 25%, 50%, 75% and 100% were used. The components were decoupled from the engine model close to the points where temperatures and pressures are measured in the engine laboratory. These values were used as boundary conditions for the component models. In Table 1, the inputs, the calibrated parameters and the used calibration methods of the component models are presented. Before calibrating the cylinder model, the combustion profile of the engine was built. Three Pressure Analysis (TPA) method in GT-POWER was used to produce the burn rates for the combustion profile.

Table 1. Component calibration of the engine model.

Component model	Inputs	Calibrated parameter	Calibration method
CAC	Inlet and outlet pressure and temperature	CAC outlet temperature	Case dependent wall temperature (CAC)
Turbocharger	Inlet and outlet pressures and temperatures, turbine and compressor maps	Air mass flow, compressor and turbine outlet pressure and temperatures, turbocharger speed	Efficiency multiplier (turbine)
Cylinder (TPA)	Intake and exhaust pressure and temperature, cylinder pressure, injection data	Brake power, BMEP, BTE, max. cylinder pressure, air and fuel mass flow rates, volumetric efficiency	Flow area multiplier (intake valves), unburned fuel concentration (cylinder)
Cylinder	Inlet and outlet pressure and temperature, combustion profile, injection data, start of combustion	Brake power, BMEP, BTE, max. cylinder pressure, air and fuel mass flow rates, volumetric efficiency	Flow area multiplier (intake valves)

Thereafter, the entire engine model was calibrated and validated. The validation parameters for the engine model were selected to be brake thermal efficiency (BTE), brake mean effective pressure (BMEP), maximum cylinder pressure and exhaust temperature before turbine. There were some differences in simulated results when comparing to measurements.

Figure 1 presents the measured and simulated validation parameters after calibration. After flow area multiplier optimization, the simulated BTE and BMEP were close to measured values. The simulated maximum cylinder pressure appeared somewhat lower comparing to measurements. During the cylinder pressure signal processing, it was noted that the signal contained noise and spikes even after the averaging over the cylinders and cycles, thus the averaged signal was filtered. Due to averaging and filtering, some difference between the simulated and measured signal could be expected. The maximum cylinder pressure values were approved, since other cylinder results were close to the experiment data.

The most noticeable differences were in the exhaust temperature before turbine. Even though the orifice diameter and discharge coefficient of turbine's inlet pipes were decreased and the exhaust valve timing was slightly advanced, the simulated temperatures appeared lower compared to measurements. It was discovered that there were uncertainties with the temperature sensor during the measurements and

the sensors had been replaced afterwards when faults were detected. Thus, the measured temperatures cannot be considered as absolute values. However, the form of the simulated temperatures over the load points was consistent with the measurements. When the limitations set by the measurement uncertainties were considered, it was concluded that the simulations with the engine model emulated the measurements with sufficient accuracy.

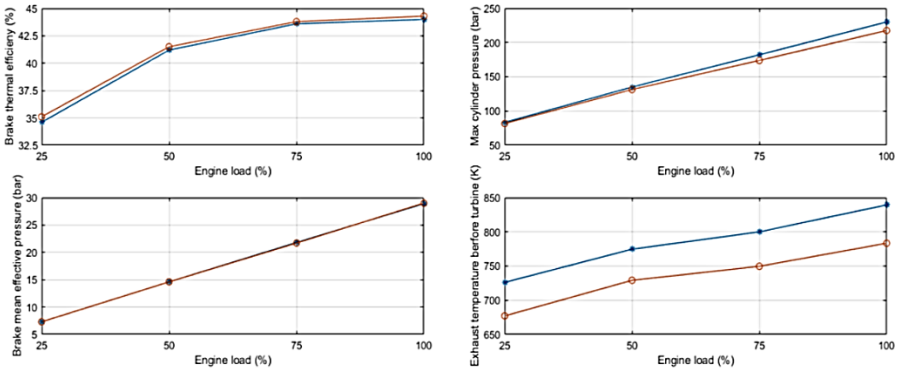

Figure 1. Measured (blue) and simulated (orange) validation parameters of the engine model.

16.2.1.2 Reduction into a mean value engine model

The process to reduce the validated engine model into a mean value (MV) engine model was needed since it is a requirement for the engine model to run in real-time. The aim was to gain lower execution time but maintain sufficient accuracy over the used load points. In MV engine model, faster execution time is achieved with map based MV cylinder model and simplified flow systems. The most important parameters for the MV cylinder were selected to be IMEP, ITE, volumetric efficiency, exhaust temperature, maximum cylinder pressure and burned mass fraction of fuel at CA50. (CA, crank angle.)

These parameters will determine the MV cylinder performance through the maps produced with Neural Network training (NNT) in GT-POWER. For the NNT, a design of experiments (DoE) was performed to produce a wide range of variables. As the experimental design method, Latin hypercube was selected since it efficiently scatters the experiment points evenly over the specified input ranges. The range of each input variable can comprise a wider range than what is required to qualify for the operating conditions of the MV model. [1] The variables that were seen to have most impact on the selected parameters were boost pressure and temperature, back pressure, injection timing and injected fuel mass. The DoE input variables and their ranges are presented in Table 2.

Table 2. DoE input variables and ranges (bTDC, before top dead centre).

Variable	Range
Boost pressure (bar)	1.3-5.0
Boost temperature (K)	330-530
Back pressure (bar)	1.3-3.9
Injection timing (deg bTDC)	14.5 - 9.0
Injected fuel mass (mg/cyl)	420-1490

As a part of the reduction, flow components were merged as simplified bigger entities and the aim was to decrease the number of volumes but to maintain the physical behaviour of the system. Later, pressure drops between the merged volumes, heat transfer and engine friction need to be calibrated and the MV engine model need to be validated against the simulations with the full engine model. Therefore, it needs to be noted that the MV engine model can only be validated for the load points used in the previous steps. This restriction was accepted due to the limited measurement data in use. In addition, since these are the most common points used in the laboratory, it was seen as the possible starting point of the DT. Nevertheless, extensive engine experiments with various load points and speed would be beneficial and could be used to increase the operating range of the model. Refinements and changes may still occur in the reduction process of the MV model as the work progresses.

16.2.2 Modelling of the electrical equipment

In the VEBIC engine laboratory, there are advanced electrical equipment that includes an induction generator (asynchronous), a frequency converter, transformers, a gen-set automation system and a data acquisition system. The toolbox Simscape and the Specialized Power Systems were used for the modelling of the electrical equipment and an example model, "Wind Farm – Synchronous Generator and Full Scale Converter (Type 4) Average Model", was used as the base model. In order to match the laboratory equipment, the base model was modified. The major changes were:

- The synchronous generator was replaced by an asynchronous generator.
- The uncontrollable diode bridge and the average DC-DC converter were replaced with a fully controllable insulated-gate bipolar transistor (IGBT) bridge that supports bidirectional power flow.
    - IGBT converter is represented as an average converter.
- A generator-side converter control system was added.
- A battery energy storage system (BESS) was added and connected to the DC-link in the converter.

Consequently, the proposed model consists of a squirrel-cage induction generator (SCIG), an averaged back-to-back converter, a BESS, a transformer and a grid. The

inputs to the SCIG are rotational speed and torque, both of which are coming from the internal combustion engine. The SCIG, converter and BESS are connected to the main ac grid via a 690 V/ 20 kV, 2 MVA transformer. The frequency converter allows the engine to run at variable speed, which can possibly offer advantages such as reduced fuel consumption, reduced emissions, reduced noise, as well as reduced engine thermal and mechanical loading [2]. The frequency converter consists of force-commutated IGBT inverters and rectifiers which are connected back-to-back with a common DC-link in between. The converter is a voltage source converter that enables bidirectional power flow, which is required for the SCIG, since a SCIG requires a magnetizing current. The back-to-back converter has two separate control systems, the grid-side converter control system and the generator-side converter control system. The grid-side converter control system could be utilized from the base model. Both control systems are implemented by the means of vector control in the arbitrary direct-quadrature (dq) reference frame. Additionally, there are filters on the grid-side in order to reduce harmonics. Only passive filters are used here, and their values are calculated based on the voltages, powers and the frequency in the grid. Due to the real-time simulation requirement, the model complexity needs to be considered. Consequently, the average converter type was used and no switching models or (pulse width modulation) PWM modulators were included. Switching requires sample times that are too small for the computational power available. The BESS does not physically exist yet, but it is included in the model in order to be able to simulate hybridization. The interest of modelling the BESS is because, in the shipping sector, the use of an energy storage can contribute to fuel consumption savings and emission reductions by reducing the load variations for the gen-set [3]. Additionally, it may also be possible to reduce installed power and the battery can act as back-up supply in case of an engine failure. However, the addition of a BESS causes additional challenges, such as the need for a control strategy that is capable of maximizing the fuel consumption reduction and emissions reduction by charging and discharging the battery at appropriate times. [2] The continuous developments in battery technology and lithium-ion technology also make battery hybrid solutions appealing. In this model, the BESS consists of a lithium-ion battery, a DC-DC converter and a battery management system (BMS). The optimization of the sizing and control for the BESS was not in the scope of this study and therefore it was implemented in a simple way at this stage. The lithium-ion battery is a built-in block from Simscape Specialized Power Systems library, and it calculates the state-of-charge (SoC). The BESS is connected to the DC link through a DC-DC converter, which is represented as an average DC-DC converter. The proposed model with control system functionalities was validated on the development computer with MATLAB/Simulink simulations. The validation showed that the different control systems operated together in the requested way.

16.3 Real-time setup and further steps towards digital twin

When the model is working on the development computer, the next step is to confirm that it is capable of real-time simulation. The real-time simulation behavior can be evaluated on the development computer first, to see if the model is likely to be real-time capable. However, the only way to ensure real-time capability is to convert the model into a real-time application and run the application on the target PC. The computational power of the target PC ultimately determines if the application is real-time viable. A real-time viable model must use a fixed-step solver and the step size needs to be adjusted according to the computational power available. The step size needs to be small enough to maintain simulation accuracy, but a too small step size will cause CPU overloading.

The real-time simulation capability validation was made for the electrical equipment model. Thus, after the model functionalities were validated, the model was converted into a real-time application and it was transferred to the target PC. In order to test the real-time capability, the application was run on the target PC for 30 hours. During this time, the average task-execution time (TET) on the target PC was 7.6×10^{-6} s while the used sample time was 5×10^{-5} s. Accordingly, the simulation did not cause CPU overloading.

As noted, the MV format is necessary for the engine model to operate in real-time and to develop the DT of the hybrid power generation system. Once the MV format is established and the engine model's run time has been reduced, changes are still needed for the model to run in real-time. However, there is specific license GT-SUITE-RT where conversion to real-time can be performed. Additional steps are not required for the electric equipment models, since they are already real-time capable. Afterwards, appropriate links are used to connect the GT-POWER engine model with Matlab/Simulink environment. These links are used to export and import data between the two software, i.e. create inputs and outputs between the models. The sequence of the steps to build the hybrid power generation system model is presented in Figure 2.

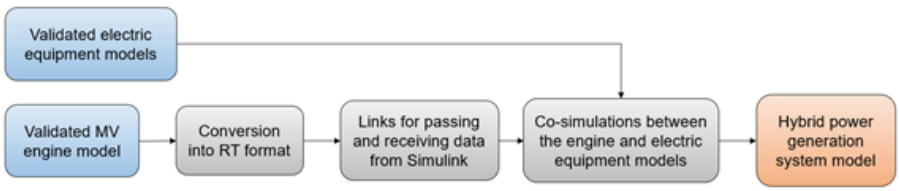

Figure 2. Planned steps to create the hybrid power generation system model.

After the engine model and the electrical equipment model are combined in Simulink, the real-time capability of this new combined model needs to be verified. When the real-time application of the hybrid power generation system is working, it can be run in parallel with the real-world equipment in VEBIC and their behaviors can be compared. The setup for establishing the connection is presented in Figure

3. In the VEBIC research platform, there is a Speedgoat Performance real-time target machine and this machine is working together with Simulink in order to perform real-time simulations. The Speedgoat machine is used for establishing the connection between the model and the physical equipment. The DT needs measured data from the physical twin. Hence, the application is running on the target PC, which is communicating with the Speedgoat target machine through MODBUS. Additionally, the software CANape will be used for monitoring signals and for changing parameter values during real-time simulations.

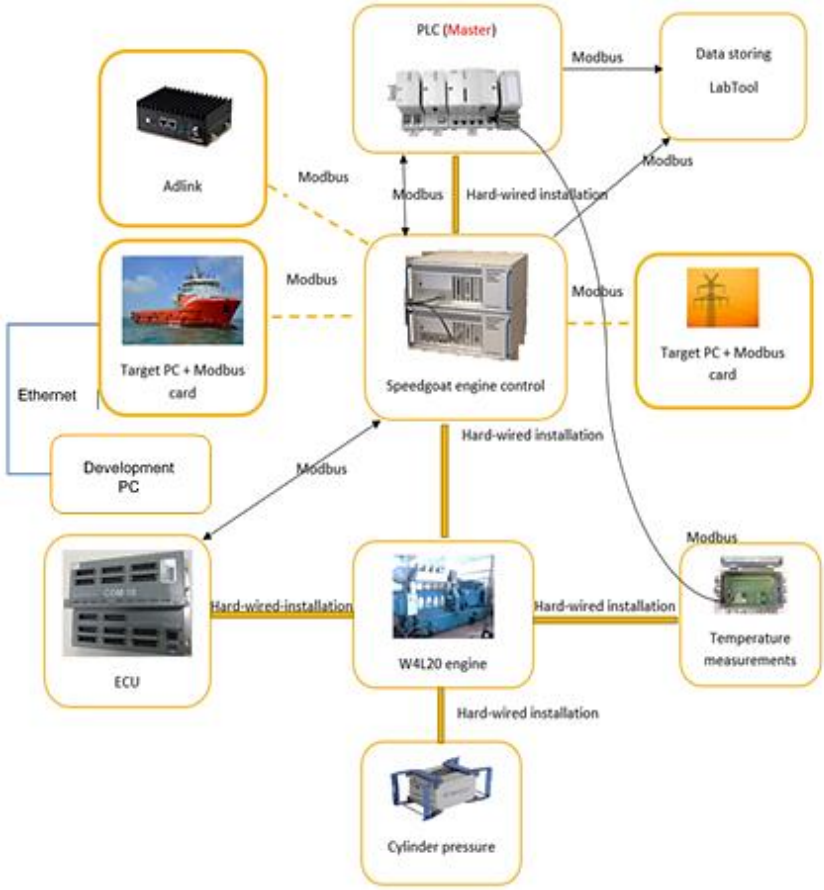

Figure 3. The connection setup in VEBIC. Modified from [4].

References

[1] E. Ko and J. Park, “Diesel Mean Value Engine Modeling Based on Thermodynamic Cycle Simulation Using Artificial Neural Network,” Energies, MDPI, Open Access Journal, vol. 12(14), pp. 1-17, July.

[2] A. Lana, K. Tikkanen, T. Lindh, J. Partanen, “Control of directly connected energy storage in diesel electric vessel drives,” IEEE, 15th International Power Electronics and Motion Control Conference, EPE-PEMC 2012 ECCE Europe, Novi Sad, Serbia. 2012 ISBN: 978-1-4673-1972-0.

[3] R.D. Geertsma, R.R. Negenborn, K. Visser, J.J. Hopman, ”Design and control of hybrid power and propulsion systems for smart ships: A review of developments,” Elsevier, Applied Energy. 2017. Vol. 194, pp. 30-54.

[4] Xiaoguo Storm, University of Vaasa, November 2019.

Series title and number

VTT Technology 380

Title	**Integrated Energy Solutions to Smart And Green Shipping** 2020 Edition
Author(s)	Zou Guangrong | Saara Hänninen (Editors)
Abstract	The decarbonization, digitalization and automation of global shipping are intensifying due to high pressure and need from the regulatory, environmental, economic and technological perspectives. The INTENS project is one of the ongoing Finnish major R&D efforts towards smart and green shipping, which is an industry-wide collaborative research and innovation action striving to advance, showcase and promote the digital transformation and collaboration in the Finnish maritime industries and beyond, especially in relation to ship energy efficiency improvement and emissions reduction. This book features a selected collection of extended abstracts of the 2020 INTENS WEEK public webinar series, also acting as the proceedings of the second INTENS project public dissemination event. It aims to give the readers a brief update on some results that have been achieved by the INTENS project partners during the second project year, specifically addressing a list of dedicated topics on novel technologies, solutions and innovations to digital, energy-efficient and low-emission shipping.
ISBN, ISSN, URN	ISBN 978-951-38-8740-7 ISSN-L 2242-1211 ISSN 2242-122X (Online) DOI: 10.32040/2242-122X.2020.T380
Date	October 2020
Language	English
Pages	128 p.
Name of the project	INTENS -Integrated Energy Solutions to Smart And Green Shipping
Commissioned by	Business Finland, Aalto University, Deltamarin Ltd, Dinex Finland Oy, LUT University, Meyer Turku Oy, NAPA Oy, Parker Hannifin Manufacturing Finland Oy, Pinja Oy (formerly Protacon technologies Oy), Vahterus Oy, University of Vaasa, Wärtsilä Oyj Abp, Åbo Akademi University, and VTT Technical Research Centre of Finland Ltd
Keywords	Smart and green shipping, ship energy systems, energy efficiency, emissions reduction, digitalization, decarbonization, collaboration
Publisher	VTT Technical Research Centre of Finland Ltd P.O. Box 1000, FI-02044 VTT, Finland, Tel. 020 722 111, https://www.vttresearch.com

Integrated Energy Solutions to Smart And Green Shipping

2020 Edition

ISBN 978-951-38-8740-7
ISSN-L 2242-1211
ISSN 2242-122X (Online)
DOI: 10.32040/2242-122X.2020.T380

VTT beyond the obvious